

## **Shock attenuation experiments using a Hopkinson bar method – summary of experimental results**

Jan Arild Teland and Stian Sksiudalen

Forsvarets forskningsinstitutt/Norwegian Defence Research Establishment (FFI)

16. mars 2009

FFI-rapport 2009/00582

1120

P: ISBN 978-82-464-1564-2

E: ISBN 978-82-464-1565-9

## **Emneord**

Sjokkdempning

Porøse materialer

Optiske tøyningsmålere

Hopkinson Bar

## **Godkjent av**

Eirik Svinsås

Prosjektleder

Jan Ivar Botnan

Avdelingssjef

## English summary

Close-in attenuation of the pressure wave from a detonation is desirable in several applications. Porous materials are often assumed to have good shock damping properties. In this report an experimental set-up using a Hopkinson bar to test the attenuation of various materials is described. Experiments with several materials have been carried out and are documented here. Analysis of the results will be presented separately in a future document.

## Sammendrag

I mange sammenhenger er det ønskelig å kunne dempe sjokkbølger. Porøse materialer antas å ha gode sjokkdempende egenskaper. I denne rapporten beskrives et eksperimentelt oppsett med en såkalt Hopkinson Bar for å teste sjokkdempningsegenskapene til forskjellige materialer. Deretter dokumenteres eksperimenter utført med dette oppsettet for en rekke materialer. Analyse av resultatene dokumenteres separat i en fremtidig rapport.

## Contents

|          |  |           |
|----------|--|-----------|
| <b>1</b> | <b>Introduction</b>                                | <b>7</b>  |
| <b>2</b> | <b>Shock attenuation experiment</b>                | <b>7</b>  |
| <b>3</b> | <b>Damping materials</b>                           | <b>8</b>  |
| 3.1      | Pumice   | 8         |
| 3.2      | LECA   | 8         |
| 3.3      | Particle board                                     | 9         |
| 3.4      | Rubber granules (Granulated rubber / Crumb rubber) | 9         |
| 3.5      | Gravel / Sand                                      | 10        |
| 3.6      | Wood shavings                                      | 11        |
| 3.7      | Sawdust  | 11        |
| 3.8      | Norway spruce (solid wood)                         | 12        |
| 3.9      | Aluminium foam                                     | 12        |
| 3.10     | Glasopor   | 13        |
| 3.11     | Siporex  | 14        |
| 3.12     | Brick  | 14        |
| <b>4</b> | <b>Experimental set-up</b>                         | <b>15</b> |
| 4.1      | Optical strain gauges and measurement chain        | 16        |
| <b>5</b> | <b>Experiments</b>                                 | <b>17</b> |
| <b>6</b> | <b>Validation</b>                                  | <b>19</b> |
| <b>7</b> | <b>Results</b>                                     | <b>20</b> |
| 7.1      | TNT location                                       | 20        |
| 7.2      | Pumice and LECA                                    | 20        |
| 7.3      | Particle board                                     | 22        |
| 7.4      | Rubber granules                                    | 22        |
| 7.5      | Gravel   | 22        |
| 7.6      | Wood shavings                                      | 24        |
| 7.7      | Sawdust  | 24        |
| 7.8      | Norway spruce                                      | 26        |
| 7.9      | Aluminium foam (100 mm)                            | 27        |
| 7.10     | Glasopor (100 mm)                                  | 28        |
| 7.11     | Siporex  | 30        |
| 7.12     | Brick  | 30        |
| 7.13     | Reference shots                                    | 32        |

|          |  |           |
|----------|--|-----------|
| <b>8</b> | <b>Comparison of amplitudes</b>              | <b>34</b> |
| <b>9</b> | <b>Summary</b>                               | <b>35</b> |
|          | <b>References</b>                            | <b>35</b> |
|          | <b>Appendix A Uniaxial stress hypothesis</b> | <b>36</b> |
|          | <b>Appendix B Measurement details</b>        | <b>38</b> |
| B.1      | February 2008                                | 38        |
| B.2      | April 2008                                   | 47        |
| B.3      | September 2008                               | 55        |
|          | <b>Appendix C Data analysis software</b>     | <b>66</b> |
| C.1      | Introduction                                 | 66        |
| C.2      | Data analysis                                | 66        |
| C.2.1    | Data conversion                              | 67        |
| C.2.2    | Analysing software; "FFIFRIMP"               | 68        |
| C.2.3    | Post processing                              | 68        |

## 1 Introduction

Close-in attenuation of the pressure wave from a detonation is desirable in several applications. One example is within an ammunition storage, where it is important to prevent an accidental detonation of a warhead (or similar) resulting in a full detonation of all the stored objects. Another application is during EOD operations, where mitigation of the blast can increase survivability for the surroundings during an accidental or provoked explosion. Several porous materials are thought to exhibit useful properties for shock attenuation.

This report documents results from one particular experimental set-up at FFI to determine the shock attenuation properties of various materials. Analysis of these and other experimental data will be published in a separate report.

## 2 Shock attenuation experiment

To examine the actual shock attenuation properties of various damping materials, an experiment involving a Hopkinson steel bar was developed. The experimental set-up is sketched in Figure 2.1.

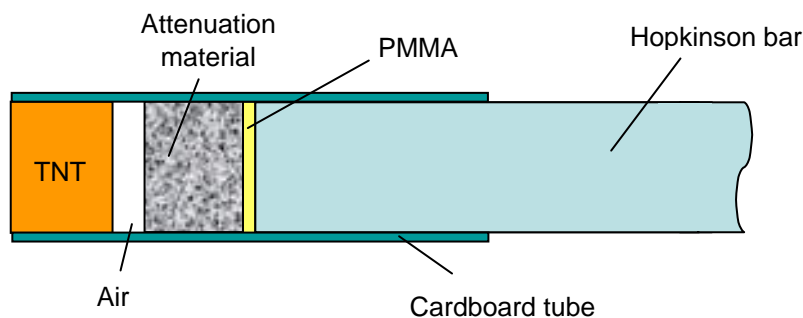


Figure 2.1 Experimental set-up.

A cylindrical explosive charge and the attenuation material are aligned carefully along the length axis of a steel Hopkinson bar. On detonation of the TNT charge, a shock wave is created. This shock wave interacts with the damping material and a protective PMMA disk before it is transmitted into the steel bar where it propagates as an elastic stress wave<sup>1</sup>. By measuring the strain in the steel bar using fibre-optical strain sensors, the transmitted stress can be calculated. More details are given in Appendix A. By comparing the stress for different materials, the idea was that their shock damping properties could be evaluated.

The small air gap was included to keep the distance between the explosive and the steel bar constant so that the thickness of damping materials could be varied.

<sup>1</sup> For a sufficiently strong pressure pulse, the stress in the steel bar would have exceeded the plastic yield limit and the wave would have been plastic. However, the TNT mass and detonation distance was chosen to deliberately avoid plasticity in the bar.

The experiment was performed for a variety of materials. The materials included different types of pumice, LECA (with various grain sizes), wood, aluminium foam, Glasopor, Siporex, brick, crumb rubber etc.

### 3 Damping materials

In this chapter we give a brief description of the tested damping materials.

#### 3.1 Pumice

Pumice is a light, porous type of igneous rock which is composed mainly of  $\text{SiO}_2$  (1). It is formed during volcanic eruptions when liquid lava is ejected into the air where it solidifies into rock. Pumice varies in density and colour, depending on the physical conditions during the volcano eruption when it was formed, but generally it is a very lightweight material with typical densities between  $300 \text{ kg/m}^3$  and  $1200 \text{ kg/m}^3$ .

In industry pumice has a variety of uses; relevant examples are as aggregate in light weight concrete, pellets for water filtration and as an abrasive in polishes and cosmetics exfoliants. It is generally available at a very low cost.

In our experiment we used pumice of several grades with density in the range  $340\text{-}500 \text{ kg/m}^3$ . The tested pumice is shown in Figure 3.1.

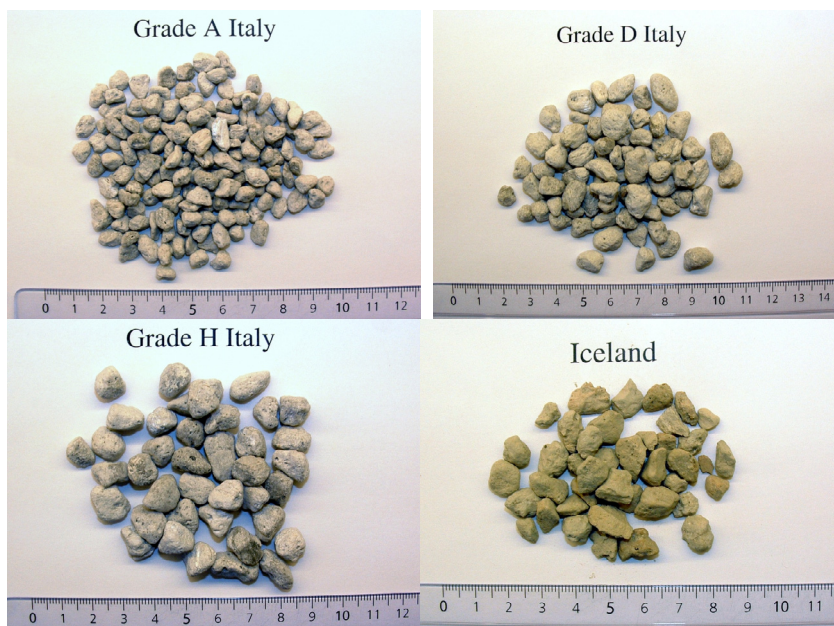


Figure 3.1 Different types of pumice.

#### 3.2 LECA

LECA stands for Light Expanded Clay Aggregate and is an industrial material (2). It consists of small bloated particles of burnt clay. During manufacturing, plastic clay is pretreated, heated and expanded in a rotary kiln and finally burnt at a high temperature. LECA is typically used as a



building material, due to its low weight and low thermal conductivity. Other uses include as a cleaning filter and in hydrocultural applications. LECA is widely available at a very low cost.

Two of the tested LECA types are shown in Figure 3.2. The density was in the range 320-400 kg/m<sup>3</sup>.



Figure 3.2 Coarse and fine LECA used in the damping experiments.

### 3.3 Particle board

Particle board is an engineered wood product manufactured from wood particles, such as wood chips, sawmill shavings and even saw dust, and a synthetic resin or other suitable binder, which is pressed and extruded (3). Particle board is cheap and readily available.

The particle board used in the test is shown in Figure 3.3. The density was around 500 kg/m<sup>3</sup>.

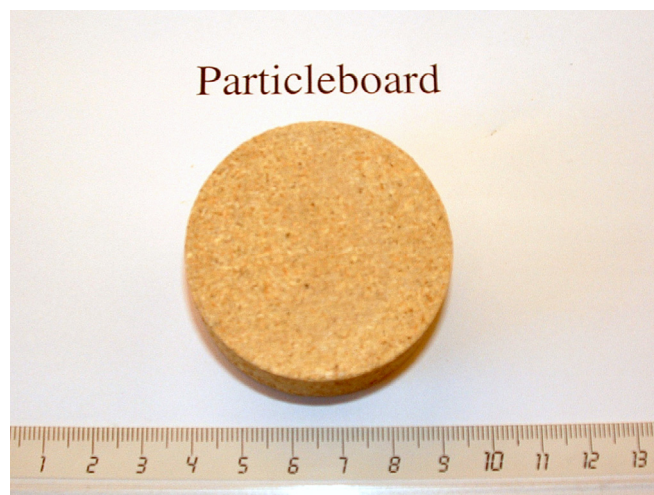


Figure 3.3 Particle board.

### 3.4 Rubber granules (Granulated rubber / Crumb rubber)

Rubber granules (also known as granulated rubber and crumb rubber) are recycled rubber, usually from automotive and truck scrap tires (4). During the recycling process steel and fluff is removed, leaving tire rubber with a granulate consistency. Continued processing with a granulator and/or cracker mill, possibly with the aid of cryogenics, reduces the size of the

particles even further. Rubberized asphalt is the largest market for crumb rubber, but it is also used as ground cover under playground equipment and as surface material for running tracks and athletic fields.

In our case, the rubber comes from isolation material used in electric cables (5). The rubber granules used in the test are shown in Figure 3.4. The density was around  $460 \text{ kg/m}^3$ .



Figure 3.4 Rubber granules (Granulated rubber / Crumb rubber).

### 3.5 Gravel / Sand

Sand is a naturally occurring granular material composed of finely divided rock and mineral particles (6). The composition of sand is highly variable depending on local rock sources and conditions. Gravel is rock that is of a specific particle size range (7).

Gravel and sand are very cheap and easily available. In our tests we used different types of gravel as shown in Figure 3.5. The density was in the range  $710 \text{ kg/m}^3$  to  $960 \text{ kg/m}^3$ .



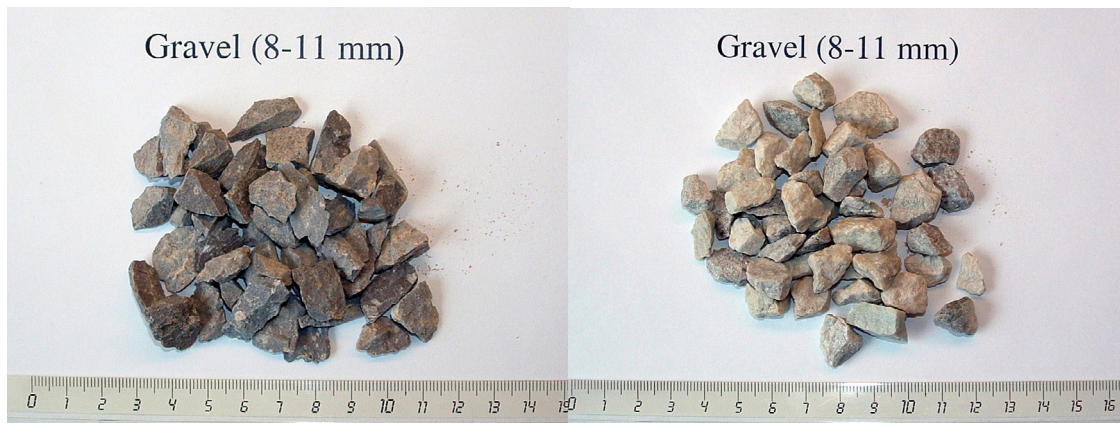


Figure 3.5 Different types of gravel / sand used in the tests.

### 3.6 Wood shavings

Wood shavings are thin pieces of wood left over after applying a plane or similar tool to the surface of a wooden material. The properties of the wood shavings will depend somewhat on the source of the material. Wood shavings are cheap and easily obtained.

The wood shavings used in our tests are shown in Figure 3.6. The sample density was in the range 165-170 kg/m<sup>3</sup>.



Figure 3.6 Wood shavings.

### 3.7 Sawdust

Sawdust is composed of fine particles of wood, produced from cutting with a saw. It has a large variety of practical uses from mulch, cat litter, fuel or in the production of particle board (8). It is cheap and easily available.

The sawdust used in our tests is shown in Figure 3.7. The sample density was in the range 185-195 kg/m<sup>3</sup>.



*Figure 3.7 Sawdust.*

### **3.8 Norway spruce (solid wood)**

As an example of solid wood, we used Norway spruce. This is a species of spruce native to Europe. It is evergreen and can typically grow 35-55 meters high with a trunk diameter of 1.0-1.5 meters (9). This type of wood is easily available in Europe (and wood in general is available in most places).

A sample of Norway spruce for our tests is shown in Figure 3.8. The density was in the range 260-273 kg/m<sup>3</sup>.



*Figure 3.8 Norway spruce.*

### **3.9 Aluminium foam**

Aluminium foam is a cellular structure consisting of solid aluminium containing a large volume fraction of gas-filled pores (10). It is used in some applications within the automotive industry.

Since a sample of the material mostly consists of empty space, aluminium foam has a very high porosity. The density of a typical sample is usually in the range 100-500 kg/m<sup>3</sup>.

One of our aluminium foam samples is shown in Figure 3.9. The density is in the range of 236-240 kg/m<sup>3</sup>.



Figure 3.9 Aluminium foam.

### 3.10 Glasopor

Glasopor aerated glass is an insulation material produced from recycled glass. It consists of 20% glass and 80% air. It is made from recycled glass which is first grounded to a powder (11). A catalysing material is added and it is passed through a furnace and melted at a temperature of more than 900 degrees C.

Some of the different Glasopor samples used in our experiments are shown in Figure 3.10. The density varied from 143 kg/m<sup>3</sup> to 478 kg/m<sup>3</sup> since the (0-4 mm) samples can be packed much tighter than the (14-22 mm) samples.





Figure 3.10 Various types of Glasopor.

### 3.11 Siporex

Siporex is a lightweight autoclaved aerated concrete which is completely cured, inert and stable form of calcium silicate hydrate (12). It is a structural material, approximately 25% of the weight of conventional concrete.

A Siporex sample used in our tests is shown in Figure 3.11. The density was around 630-640 kg/m<sup>3</sup>.

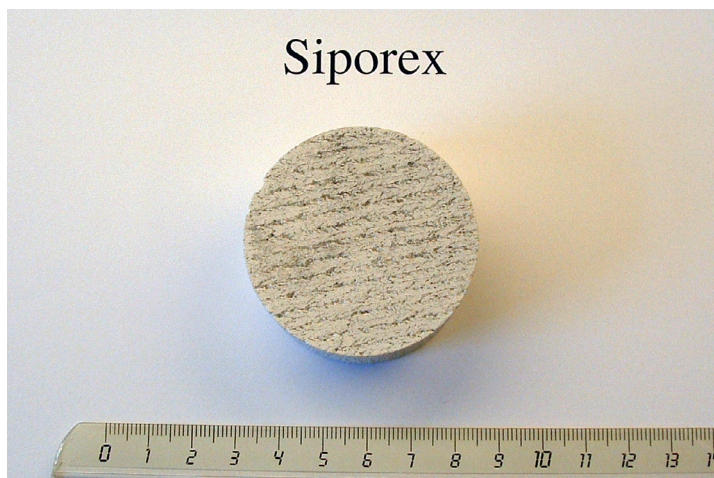


Figure 3.11 Siporex.

### 3.12 Brick

A brick is a block of ceramic material, used in masonry construction, laid using mortar (13). Unlike most of the other materials tested, it is not a lightweight material.

A brick sample used in our experiments is shown in Figure 3.12. The density was in the range 1850-2050 kg/m<sup>3</sup>.



Figure 3.12 Brick.

## 4 Experimental set-up

The experimental set-up is shown in Figure 4.1. As previously indicated in Figure 2.1, the pellets, grains or solid samples of the damping material were confined in a cardboard tube, and kept in place by two internal membranes also made of cardboard (and the explosive charge itself). This assembly was then mounted onto the steel bar, which was protected by a 10 mm thick disk of PMMA in the “active” end.

The detonator was centred at the end of the TNT charge using a PVC disk of equal diameter, and with a hole in the middle corresponding to the diameter of the detonator.



Figure 4.1 The experimental set-up, showing the cardboard tube containing the explosive charge and the damping material fitted onto the steel bar.

#### 4.1 Optical strain gauges and measurement chain

The strain measurements were based on a technique using optical fibres and fibre Bragg gratings. Bragg gratings are characterized by a grating periodicity and reflect a wavelength of light corresponding to the grating period. When the gratings are stretched or compressed (i.e. undergoing strain), the periodicity changes, which again causes a shift in the reflected wavelength. It can be shown that the shift in the wavelength is proportional to the strain, hence a measurement of reflected wavelength is equivalent to a measurement of strain.

Figure 4.2 outlines the measurement chain, which consists of Bragg gratings, a fibre Bragg grating analyzer, a conventional data acquisition system and analysis software. Table 4.1 gives details on the specific equipment used.

| Component               | Type   |
|-------------------------|--|
| Bragg gratings          | Single FBG, polyimide fibre with polyimide recoating, JC Optronics Ltd   |
| Optical fibres          | Single mode optical fibre with FC/APCR socket, Foss AS   |
| Adhesive                | M-bond AE-10, Vishay Micro-Measurements  |
| Grating Analyzer        | Fibre Bragg grating analyzer, Light Structures AS  |
| Data acquisition system | FFI registration number 109455 <ul style="list-style-type: none"> <li>• NI PXI-1031 4-Slot 3U Chassis (S/N 12B26A0)</li> <li>• NI PXI-8106 Core 2 Duo 2.16 GHz Controller with Windows XP and LabVIEW version 8.2.1.</li> <li>• NI PXI-6133 32MS Memory Series Multifunction DAQ, 8 Channels, 2.5MS/s sampling rate</li> </ul> |
| Analysis software       | FRIMP analysis software v1.0, Light Structures AS  |

Table 4.1 Equipment for strain measurements.

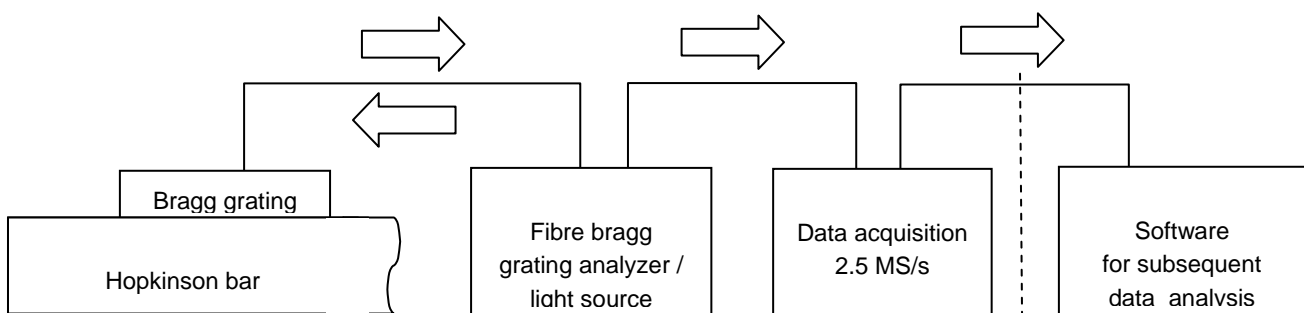


Figure 4.2 Schematic outline of the signal flow during the experiment.. Note that the size of the grating has been enormously exaggerated for illustration purposes.

In total four gratings with active length 11 mm were mounted halfway along the 3 m long steel bar, with azimuth angles  $0^\circ$ ,  $90^\circ$ ,  $180^\circ$  and  $270^\circ$ . All the sensors should thus yield the same values in an experiment with perfect cylindrical symmetry. As with conventional strain sensors, it is crucial that strain is transferred from the object to the sensor in a reliable way, and this is even more important in highly dynamic experiments. To fix the optical fibres to the steel bar, an



epoxy based adhesive was carefully applied. Numerical simulations with the AUTODYN hydrocode indicated that the response of the sensor system (adhesive layer and fibre/grating) was satisfactory. For more details, see (14).

On two of the four gratings the protective polyimide layer had been stripped prior to mounting, since there was some doubt as to whether sliding would occur between the grating and polyimide layer. During the experiments, however, no such problems were seen.

The grating analyzer contains both a broad spectrum light source and a sensing device. Light is emitted from the source through optical fibres, and certain wavelengths are reflected by the Bragg gratings mounted on the steel bar. The sensing device translates the wavelength of the reflected light to electrical signals (voltage), which are sampled at 2.5 MS/s. They are later analysed by a numerical code, converting them into strain data. This software is described more thoroughly in Appendix C.

## 5 Experiments

The firings were carried out in three separate sessions during 2008, in February (18 shots including two reference shots without damping material), April (18 shots including 2 reference shots and 3 failures) and September (22 shots including 6 reference shots). In total, 46 successful firings with damping material and 9 successful reference shots without damping material were conducted. The details of the experiments are shown in Tables 5.1-5.3. Some results from shots #1-18 (February 2008) have earlier been reported in (15), but are included here for completeness.

The optical properties of the Bragg gratings were tested statically at regular intervals between the firings. No problems were discovered.

Table 5.1 Experiments February 2008.

| Shot # | Material    | Mass[g] | Thickness [mm] | TNT charge [g] | Configuration |
|--------|-------------|---------|----------------|----------------|---------------|
| 1      | LECA fine   | 30,0    | 39,0           | 128,7          | A             |
| 2      | LECA fine   | 30,0    | 38,5           | 128,8          | B             |
| 3      | LECA fine   | 30,0    | 39,0           | 128,7          | A             |
| 4      | LECA fine   | 30,0    | 40,5           | 128,7          | B             |
| 5      | LECA fine   | 56,9    | 69,5           | 128,8          | A             |
| 6      | LECA fine   | 47,3    | 61,0           | 128,8          | A             |
| 7      | LECA fine   | 15,9    | 21,0           | 128,9          | A             |
| 8      | LECA fine   | 53,2    | 70,0           | 128,8          | A             |
| 9      | LECA fine   | 46,9    | 60,0           | 128,8          | A             |
| 10     | LECA fine   | 16,3    | 21,0           | 128,8          | A             |
| 11     | Italy       | 30,0    | 35,0           | 128,9          | A             |
| 12     | Iceland     | 30,0    | 52,0           | 128,9          | A             |
| 13     | LECA coarse | 30,0    | 50,0           | 128,9          | A             |

|    |             |      |      |       |   |
|----|-------------|------|------|-------|---|
| 14 | Italy       | 30,0 | 35,0 | 128,9 | A |
| 15 | Iceland     | 30,0 | 50,0 | 128,9 | A |
| 16 | LECA coarse | 30,0 | 49,0 | 128,9 | A |
| 17 | None        | -    | -    | 128,9 | 0 |
| 18 | None        | -    | -    | 128,9 | 0 |

Table 5.2 Experiments April 2008 (only successful shots).

| Shot # | Material         | Mass[g] | Thickness [mm] | TNT charge [g] | Configuration |
|--------|------------------|---------|----------------|----------------|---------------|
| 19     | Particle board   | 30,92   | 23,4           | 128,9          | A             |
| 20     | Particle board   | 30,33   | 23             | 129,0          | A             |
| 21     | Crumbed rubber   | 30,00   | 25             | 128,8          | A             |
| 22     | Gravel (0-4 mm)  | 30,02   | 12             | 128,8          | A             |
| 23     | Gravel (0-8 mm)  | 30,02   | 13             | 129,0          | A             |
| 24     | Gravel (0-8 mm)  | 30,01   | 13             | 128,8          | A             |
| 25     | Gravel (8-11 mm) | 29,97   | 16             | 128,9          | A             |
| 26     | Gravel (8-11 mm) | 29,95   | 14             | 129,0          | A             |
| 27     | Gravel (8-11 mm) | 30,01   | 15             | 128,9          | A (NCC)       |
| 28     | Gravel (8-11 mm) | 30,00   | 14             | 128,9          | A (NCC)       |
| 29     | Wood shavings    | 30,02   | 69             | 129,0          | A             |
| 30     | Wood shavings    | 30,02   | 68             | 129,0          | A             |
| 31     | Sawdust          | 30,03   | 61             | 129,0          | A             |
| 32     | Sawdust          | 29,97   | 60             | 128,9          | A             |
| 33     | None             |         |                | 128,9          | 0             |

Table 5.3 Experiments September 2008.

| Shot # | Material            | Mass[g] | Thickness [mm] | TNT charge [g] | Configuration |
|--------|---------------------|---------|----------------|----------------|---------------|
| 34     | Norway spruce       | 30,00   | 44             | 128,9          | A (100 mm)    |
| 35     | Norway spruce       | 29,94   | 44             | 129,0          | A (100 mm)    |
| 36     | Norway spruce       | 30,04   | 43             | 128,9          | A             |
| 37     | Norway spruce       | 30,03   | 42             | 128,9          | A             |
| 38     | Alum. foam          | 29,92   | 87             | 128,9          | A (100 mm)    |
| 39     | Alum. foam          | 30,00   | 86             | 128,8          | A (100 mm)    |
| 40     | Glasopor (0-4 mm)   | 30,01   | 25             | 129,0          | A (100 mm)    |
| 41     | Glasopor (0-4 mm)   | 30,00   | 24             | 129,0          | A (100 mm)    |
| 42     | Glasopor (4-14 mm)  | 30,05   | 71             | 128,9          | A (100 mm)    |
| 43     | Glasopor (4-14 mm)  | 30,02   | 72             | 129,0          | A (100 mm)    |
| 44     | Glasopor (14-22 mm) | 30,02   | 80             | 129,0          | A (100 mm)    |
| 45     | Glasopor (14-22 mm) | 30,03   | 79             | 128,9          | A (100 mm)    |
| 46     | Siporex             | 30,00   | 25,7           | 128,8          | A             |
| 47     | Siporex             | 30,13   | 27,7           | 129,0          | A             |

|    |                     |       |     |       |            |
|----|---------------------|-------|-----|-------|------------|
| 48 | Brick               | 29,93 | 8,2 | 129,0 | A          |
| 49 | Brick               | 30,65 | 8,6 | 129,2 | A          |
| 50 | None                |       |     | 128,9 | 0 (100 mm) |
| 51 | None                |       |     | 129,0 | 0 (100 mm) |
| 52 | None                |       |     | 128,9 | 0 (100 mm) |
| 53 | None                |       |     | 128,7 | 0 (100 mm) |
| 54 | None (no cardboard) |       |     | 129,0 | 0 (140 mm) |
| 55 | None                |       |     | 127,9 | 0 (140 mm) |

Accuracies: Mass  $\pm 0,1$  g, Thickness  $\pm 0,5$  mm, TNT charge mass  $\pm 0,1$  g

Configurations: A Damping material close to the Hopkinson Bar  
 B Damping material close to the TNT charge  
 0 No damping material

## 6 Validation

The four strain gauges produced very consistent results throughout the tests, thus reinforcing our belief in the viability of this experimental method. This is shown in Figure 6.1 where the strains measured by the four different gauges are plotted together for Shot #17 (no damping material). Results from the other shots are similar. We have therefore used the mean strain of the four gauges in the subsequent data analysis.

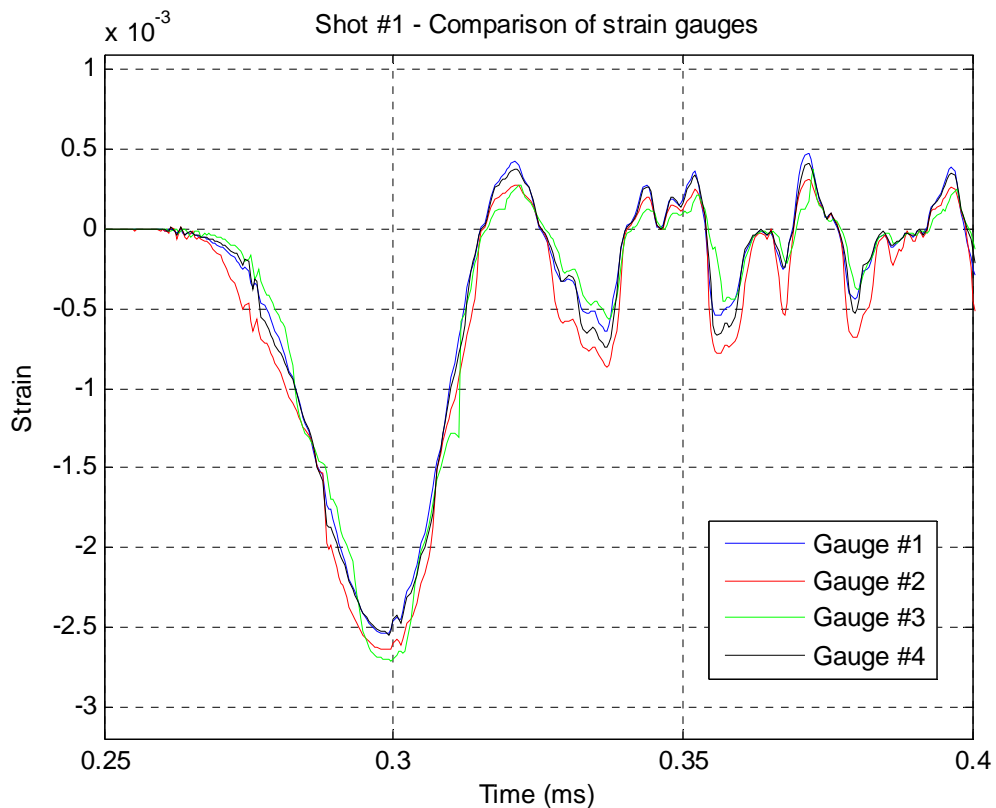


Figure 6.1 Measured strain for Shot #17. The results from the four different gauges are plotted together for comparison.

## 7 Results

In this chapter we present some of the experimental results.

### 7.1 TNT location

In Figure 7.1 we have compared Shots 1-4, where the fine LECA damping material was either close to the bar or close to the charge. We note that when the damping material was close to the charge, we obtained a significantly smaller first pulse. This may indicate that it is more effective for shock mitigation to have the damping material as close to the charge as possible.

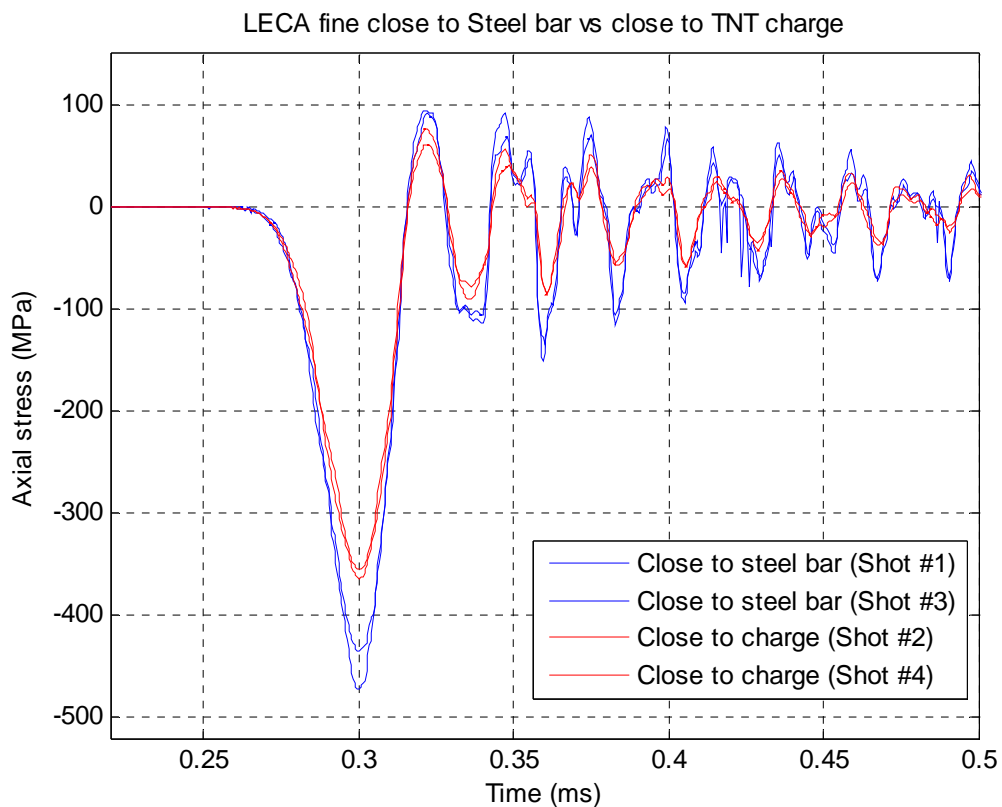


Figure 7.1 Comparison of damping when the damping material is either close to the bar or to the charge.

### 7.2 Pumice and LECA

In Figure 7.2 we have compared the damping properties for the same mass (30 g) for the different materials. From this test, it may appear that Italian pumice is the best damping material, followed by coarse LECA and Italian pumice. Fine LECA was thus seen to have the poorest damping qualities, which is in contrast to the results obtained in (16) where experiments indicated that fine LECA was the most effective shock attenuator.

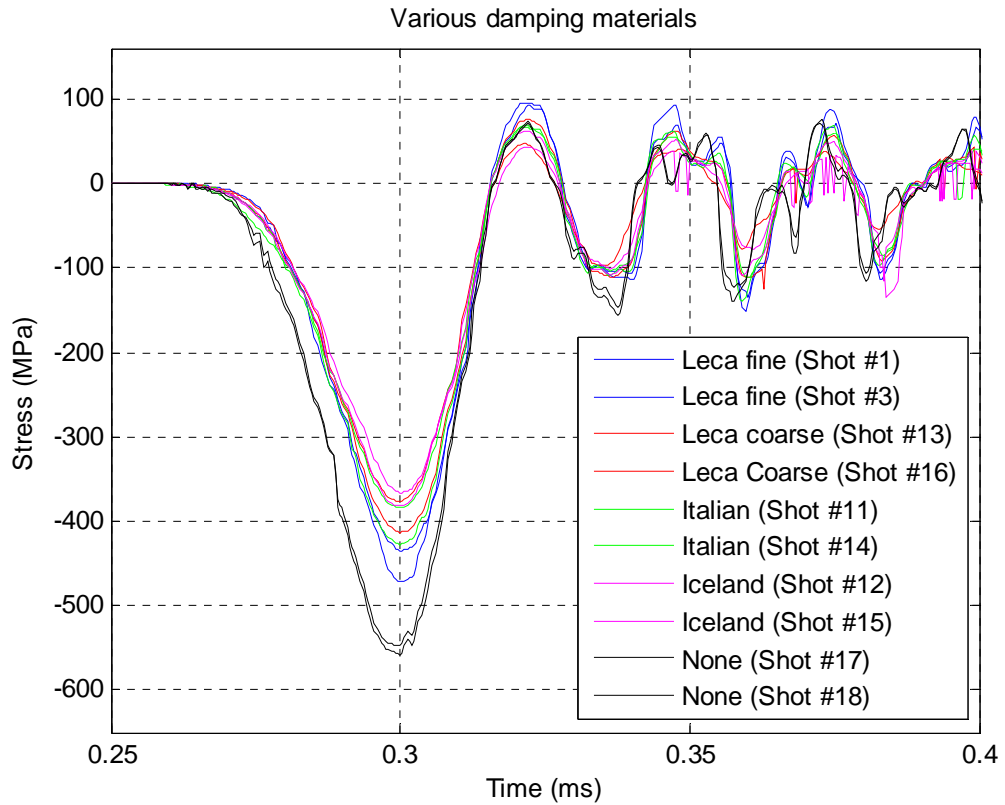


Figure 7.2 Comparison of the damping achieved with 30 g of the various damping materials.

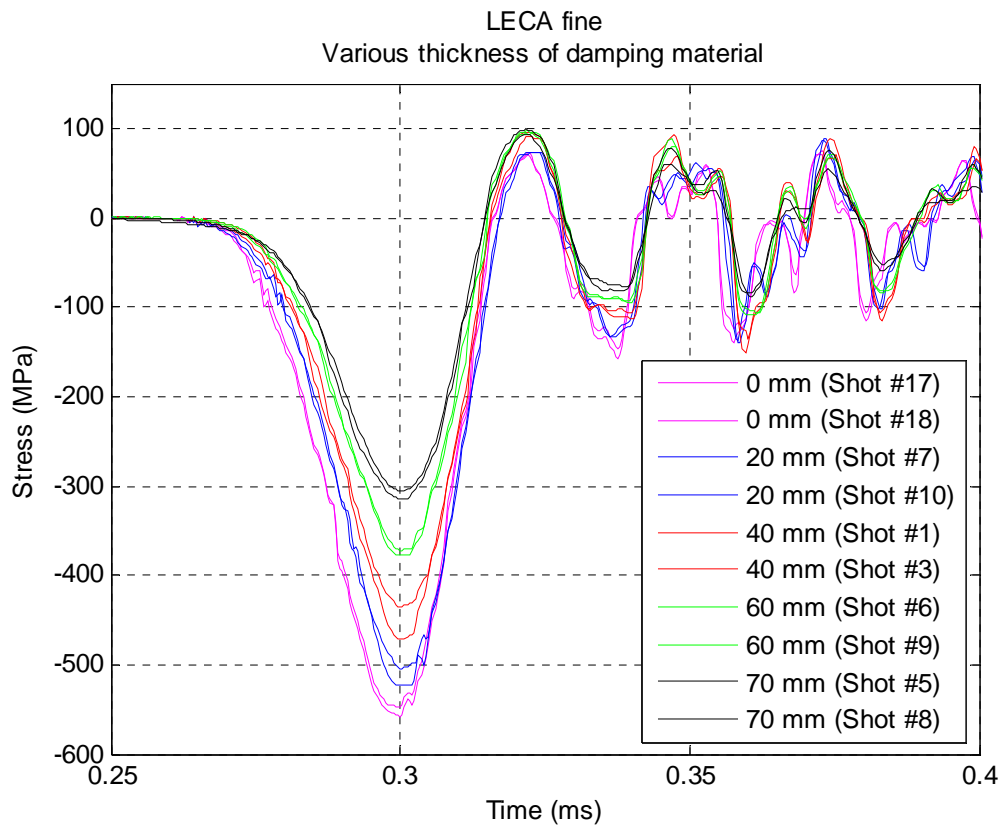


Figure 7.3 The stress wave for various material thicknesses, measured for LECA fine.

In Figure 7.3 we have focused on the material LECA fine and have compared the stress waves for different material thicknesses. As expected, the attenuation increases with increasing thickness. For 70 mm, the attenuation is approximately 40% for the amplitude of the first pulse.

### 7.3 Particle board

Figure 7.4 shows the results for particle board. The attenuation appears to be roughly similar to LECA and pumice.

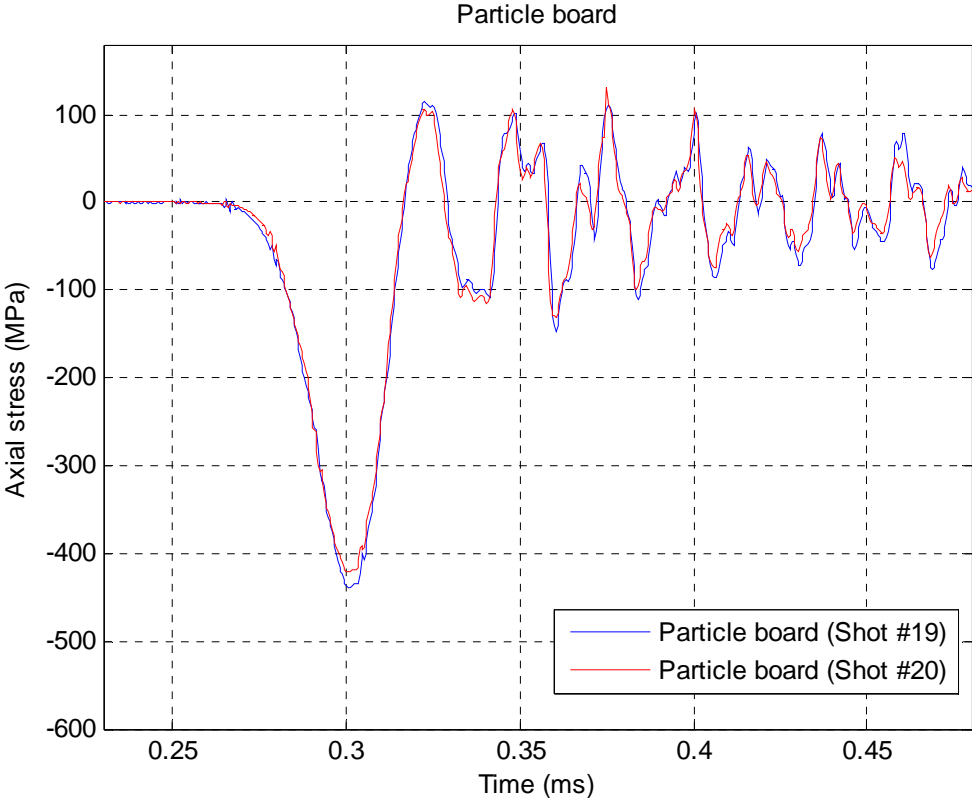


Figure 7.4 The measured stress wave for particle board damping material.

### 7.4 Rubber granules

For rubber granules, we have unfortunately, only one successful shot. This is shown in Figure 7.5, where again the damping properties appear relatively similar to LECA and pumice.

### 7.5 Gravel

Figures 7.6 and 7.7 contain results for various types of gravel. We note that in general the damping properties appear to be slightly worse than for pumice and LECA.

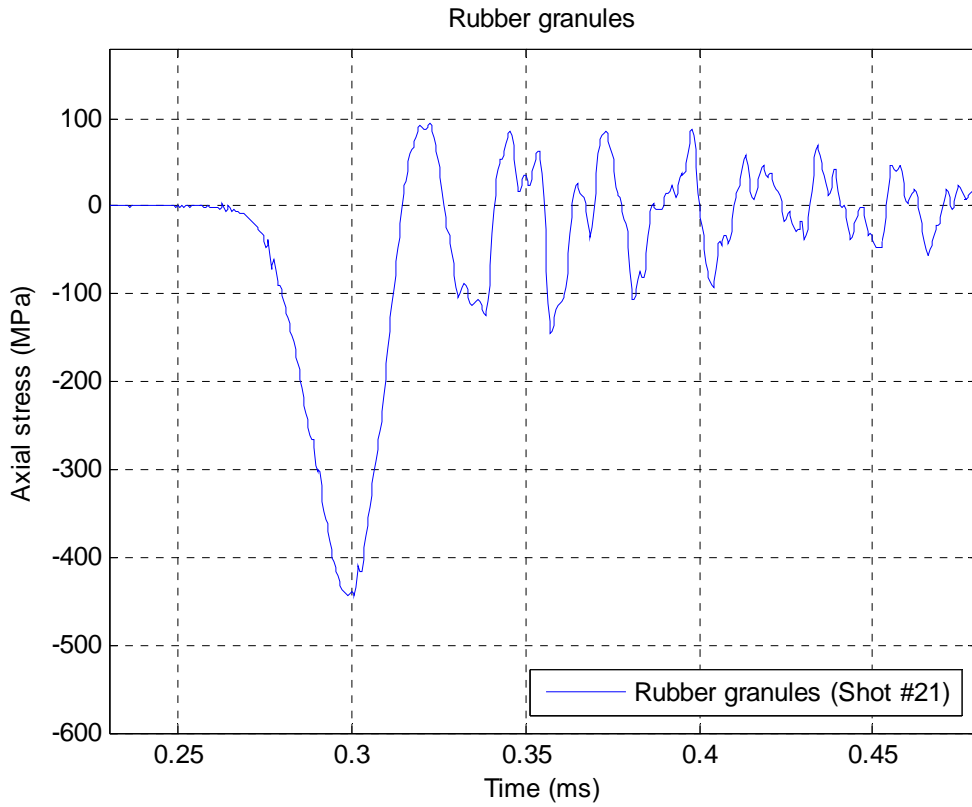


Figure 7.5 The measured stress wave for rubber granules damping material.

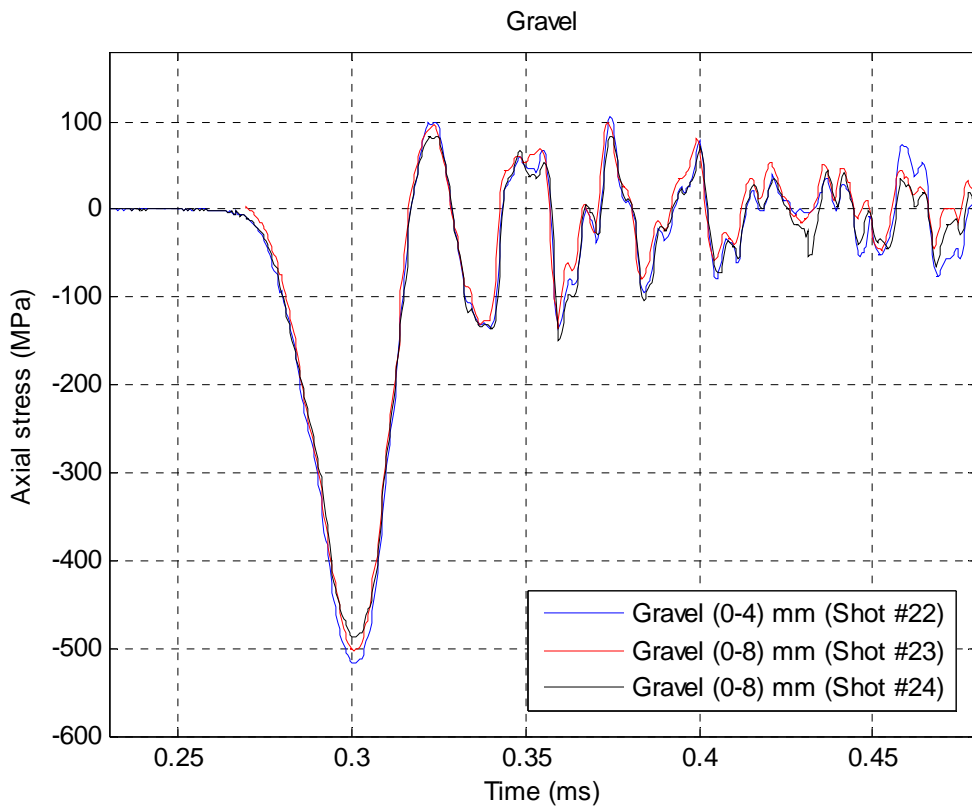


Figure 7.6 The measured stress wave for fine gravel damping material.

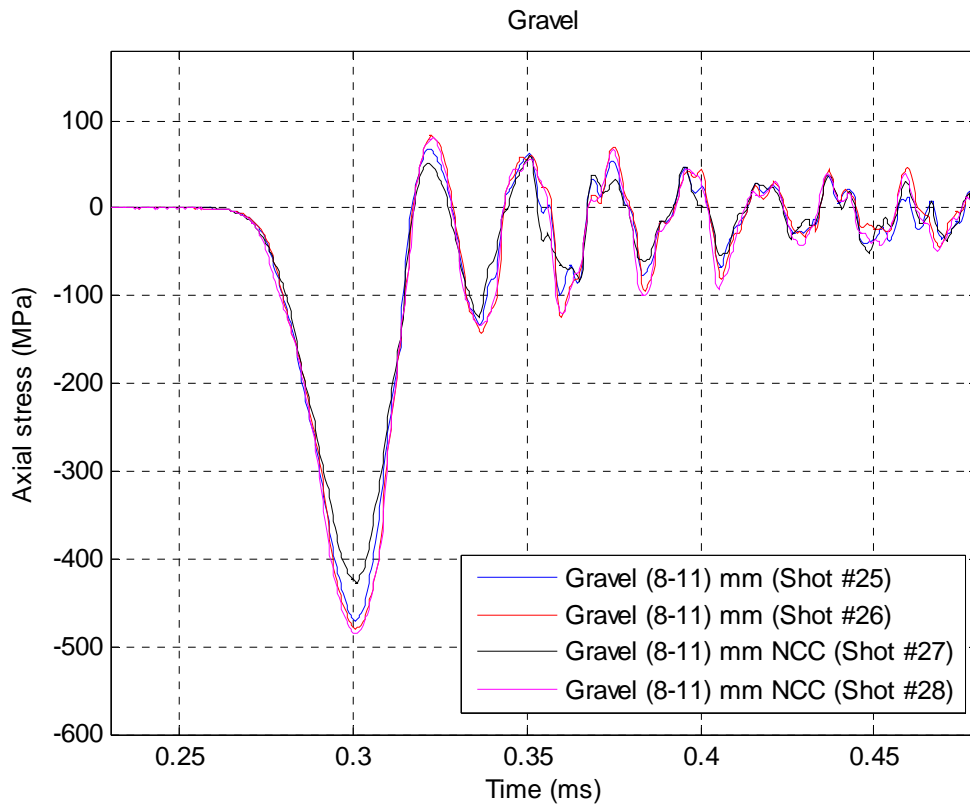


Figure 7.7 The measured stress wave for coarse gravel damping material.

## 7.6 Wood shavings

Figure 7.8 shows the results for wood shavings, which appears to be an excellent damping material.

## 7.7 Sawdust

In Figure 7.9 we have plotted the results for sawdust. We note that, perhaps somewhat surprisingly, it appears to be a less effective attenuator than wood shavings.



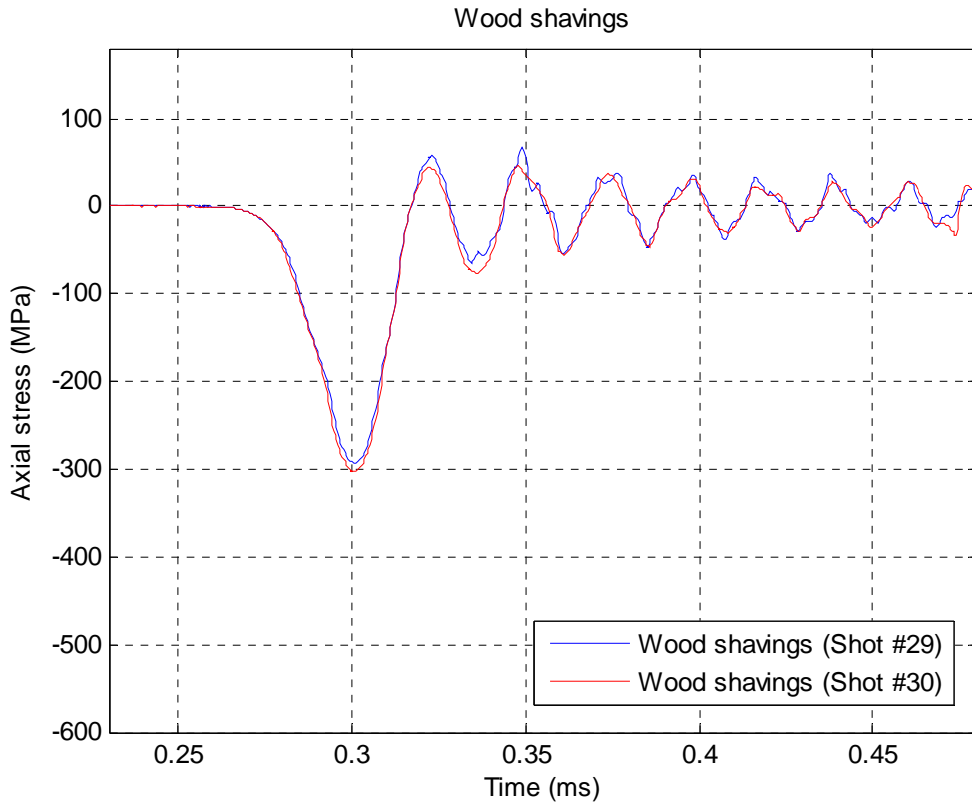


Figure 7.8 The measured stress wave for wood shavings damping material.

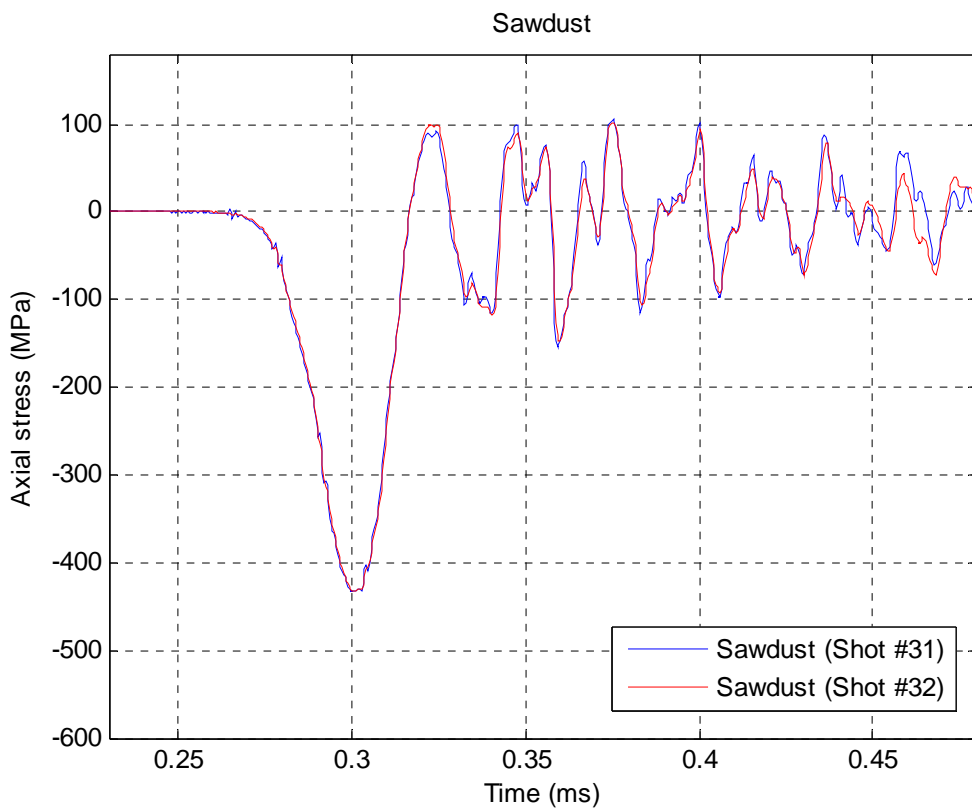


Figure 7.9 The measured stress wave for sawdust damping material.

## 7.8 Norway spruce

In Figures 7.10 and 7.11 we have plotted the results for the solid wood material, Norway spruce, for two different charge distances. We see that the attenuation properties of solid wood appear to be about the same as sawdust, but inferior to wood shavings. Further, the different charge distances do not seem to influence the results very much.

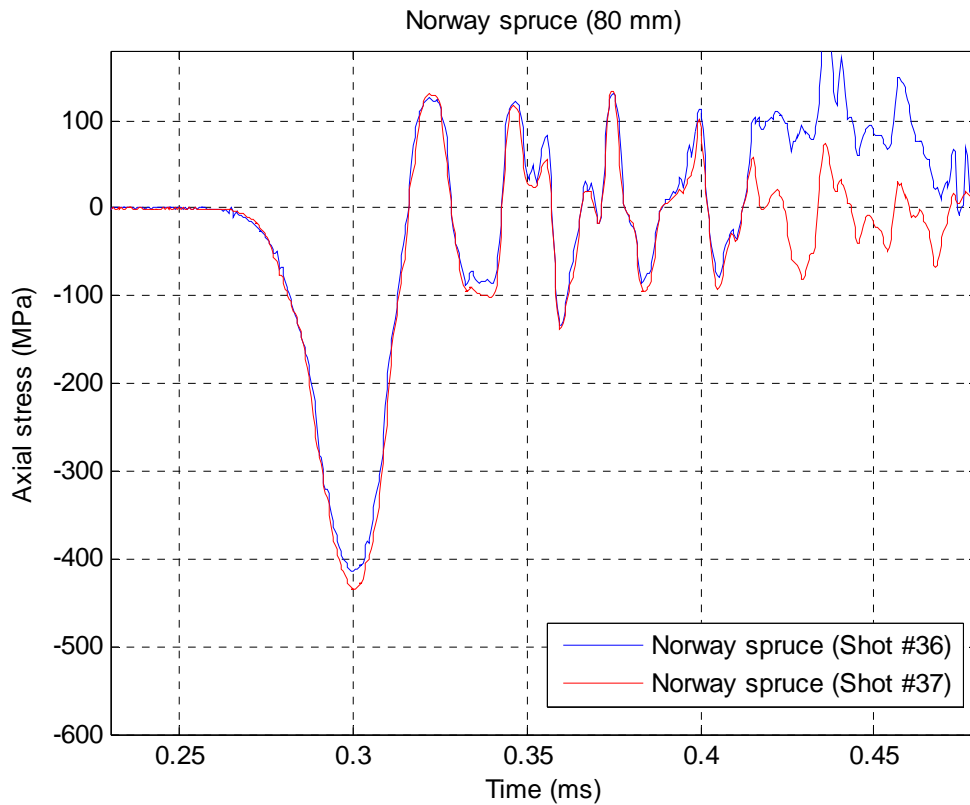


Figure 7.10 The measured stress wave for Norway spruce damping material.

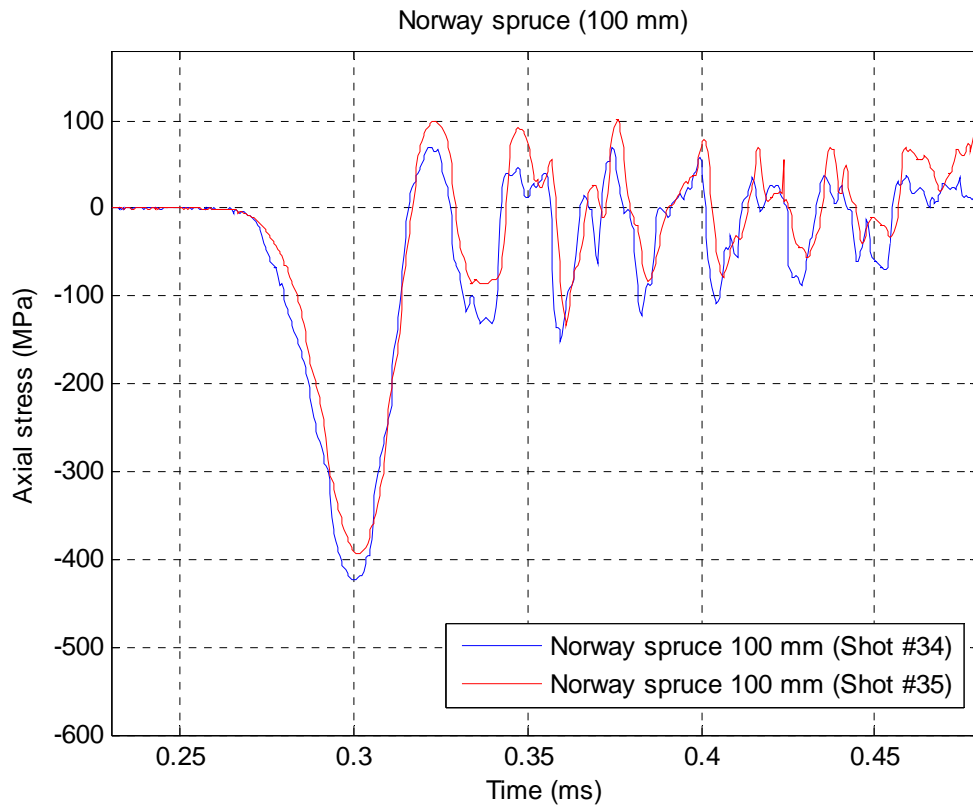


Figure 7.11 The measured stress wave for Norway spruce damping material (100 mm).

### 7.9 Aluminium foam (100 mm)

Aluminium foam appears to be the best damping material yet. This is illustrated in Figure 7.12, where we see that the damping seems to be more than 50%. Note that there appears to have been a problem with triggering for shot #39, so only data for the first reflection of the pulse was captured. (The stress has been inverted in Figure 7.12 to enable easier comparison between shots #38 and #39).

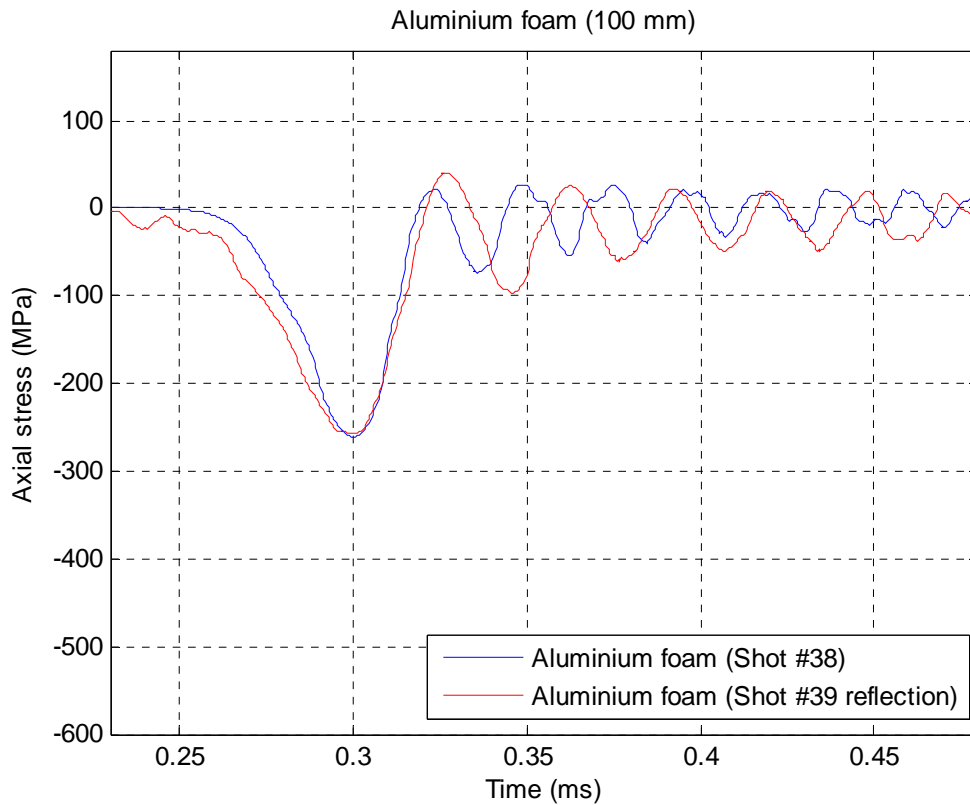


Figure 7.12 The measured stress wave for aluminium foam damping material (100 mm).

### 7.10 Glasopor (100 mm)

In Figures 7.13-7.15 we have plotted the results for the various types of Glasopor. It is seen that apart from the (0-4 mm) sample, Glasopor also appears to be a very good attenuator, although not quite as good as Aluminium foam.

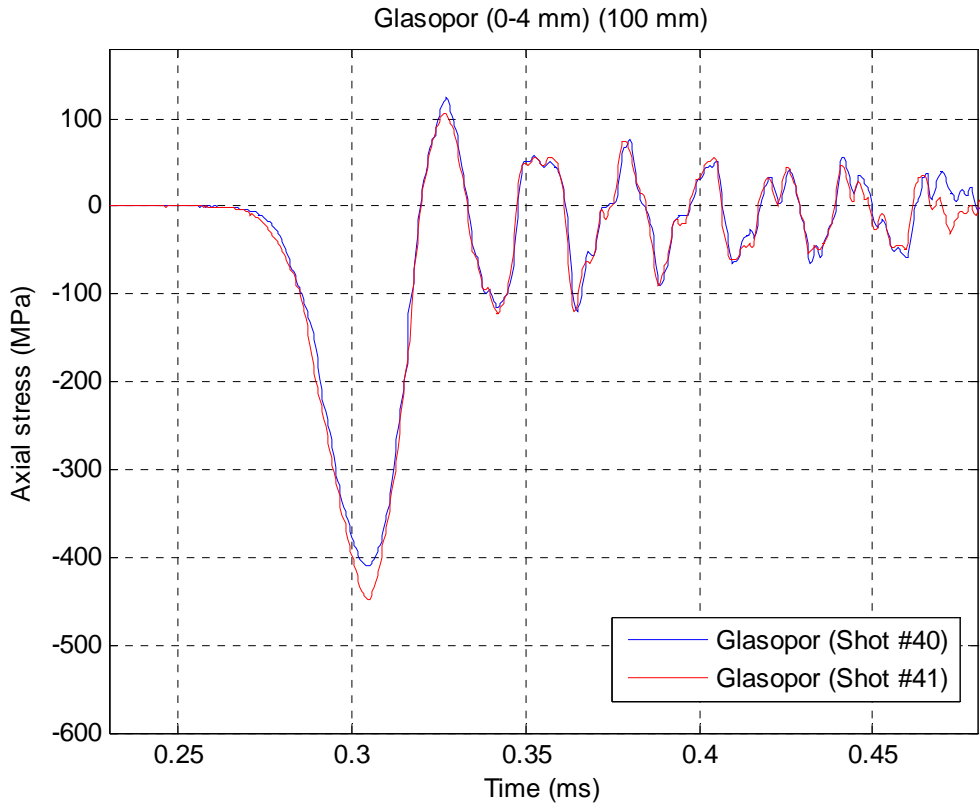


Figure 7.13 The measured stress wave for Glasopor (0-4 mm) damping material (100 mm).

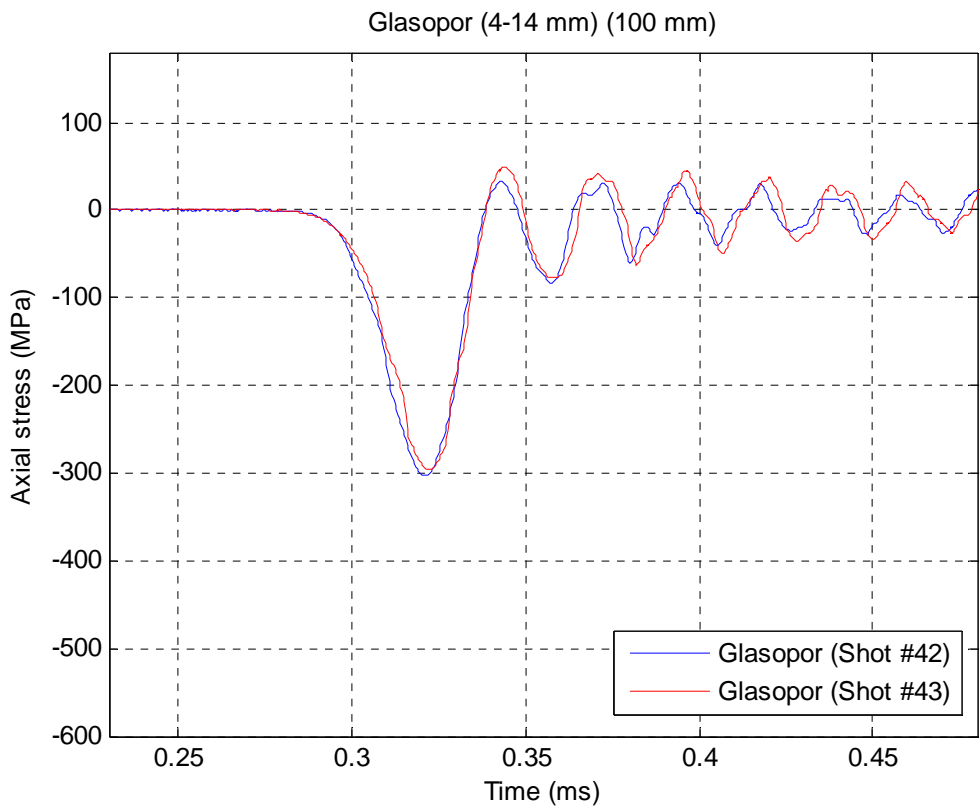


Figure 7.14 The measured stress wave for Glasopor (4-14 mm) damping material (100 mm).

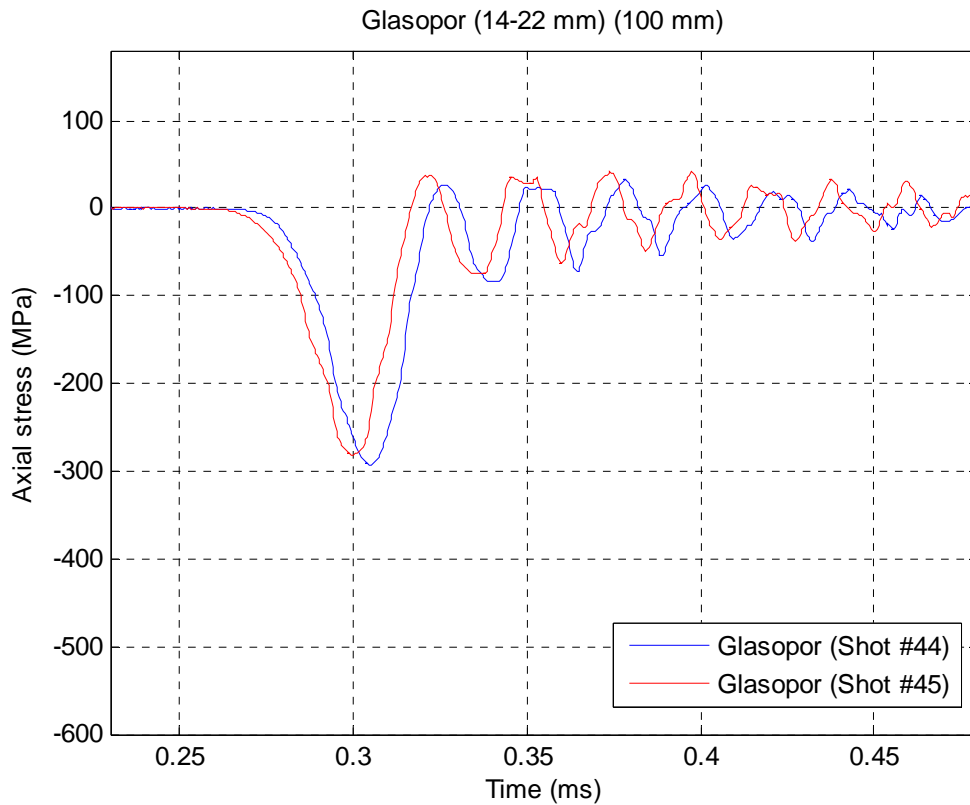


Figure 7.15 The measured stress wave for Glasopor (14-22 mm) damping material (100 mm).

### 7.11 Siporex

The results for Siporex are shown in Figure 7.16. It does not appear to be a very good shock mitigator.

### 7.12 Brick

Finally, the results for brick are shown in Figure 7.17. It appears not to cause any shock damping at all.

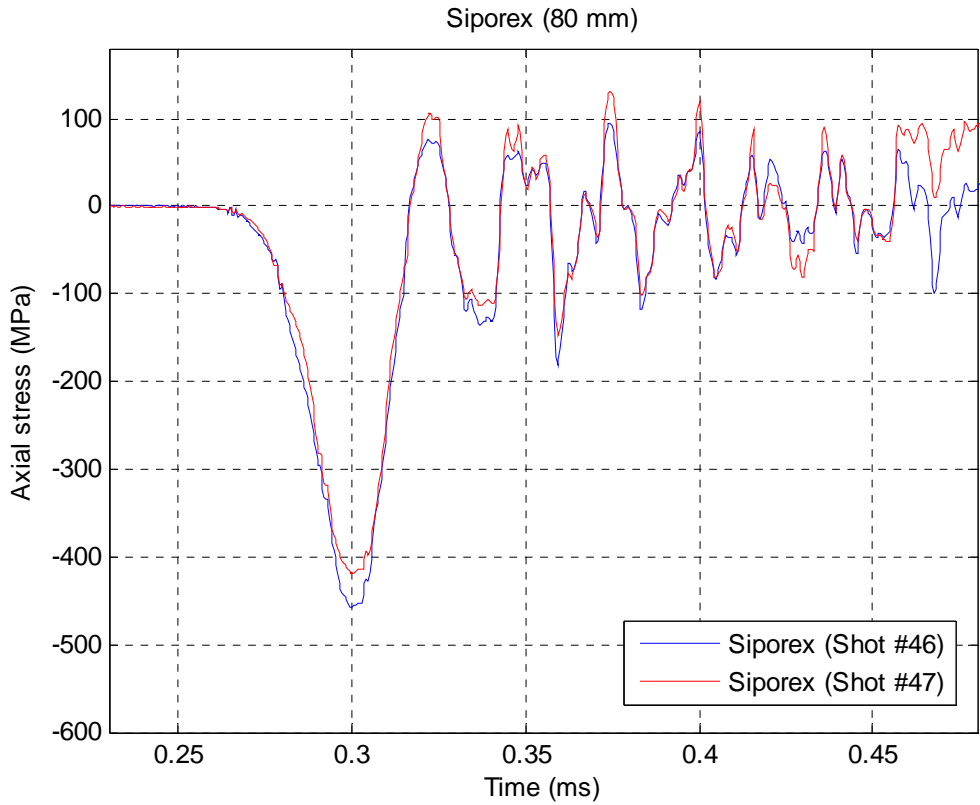


Figure 7.16 The measured stress wave for Siporex damping material.

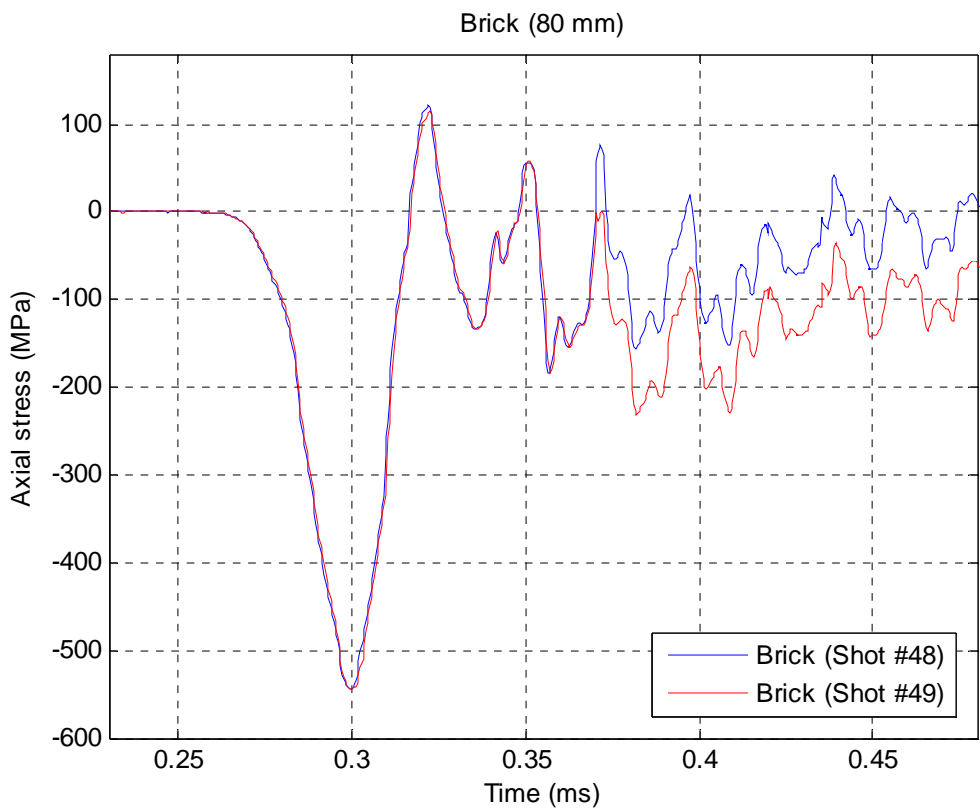


Figure 7.17 The measured stress wave for brick damping material.

### 7.13 Reference shots

The results for the reference shots without damping material, but with different distances between the TNT charge and the Hopkinson bar are shown in Figures 7.18-7.20. Interestingly, there appears to be relatively little sensitivity to the charge distance. This will be investigated more closely in a separate report.

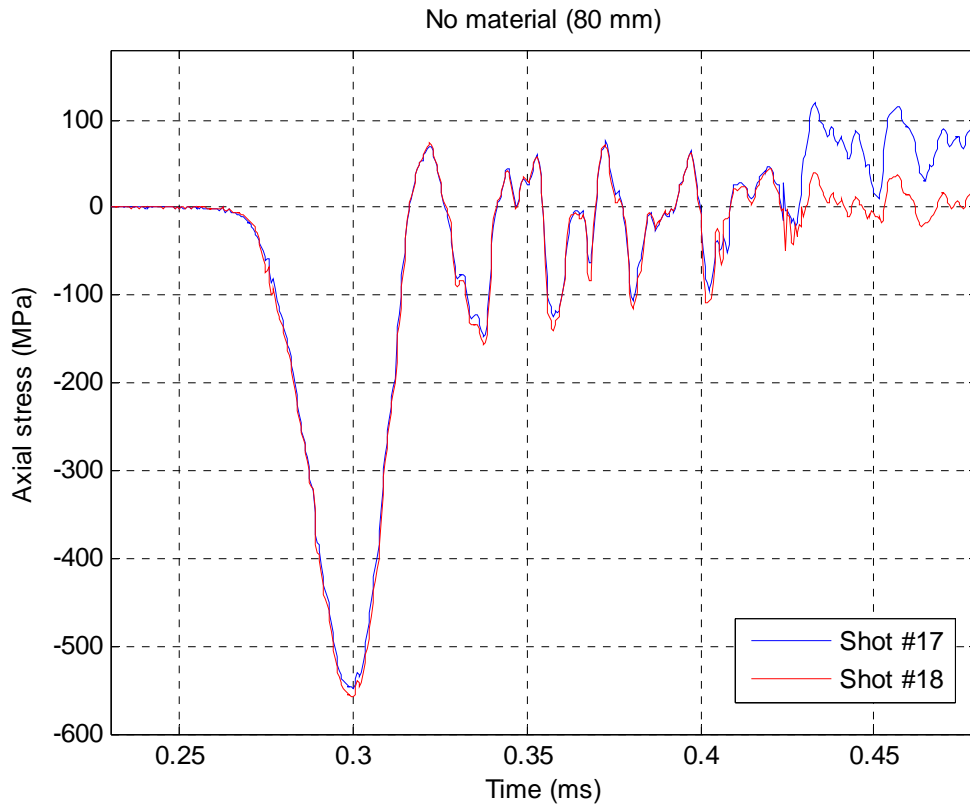


Figure 7.18 The measured stress wave for no damping material (80 mm).



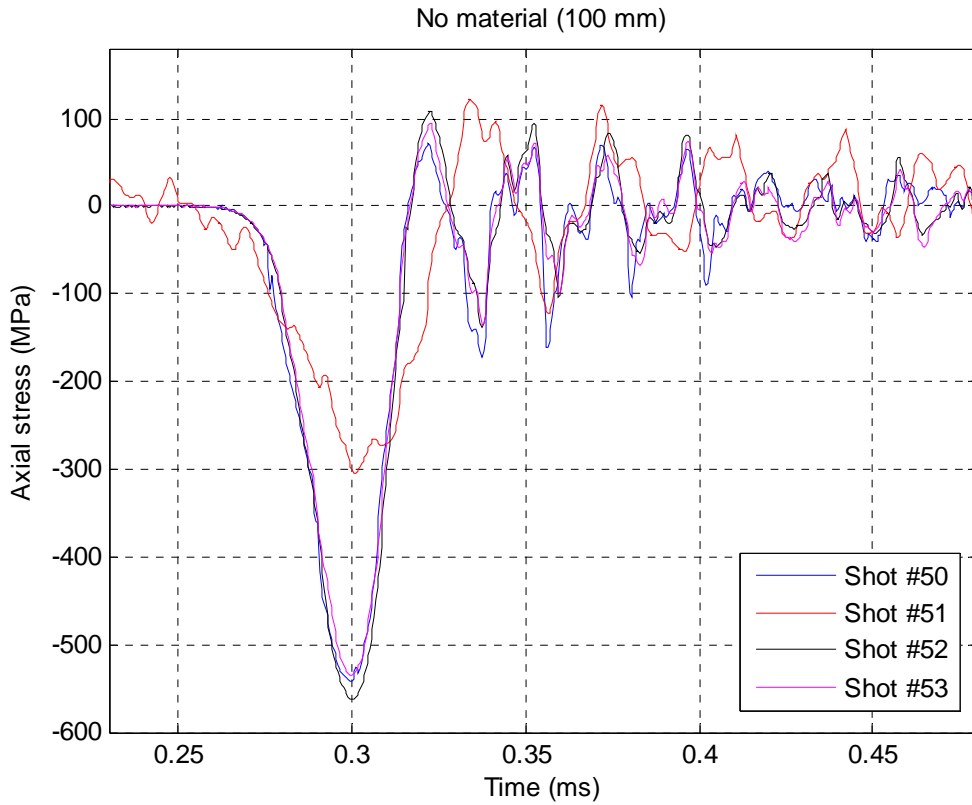


Figure 7.19 The measured stress wave for no damping material (100 mm).

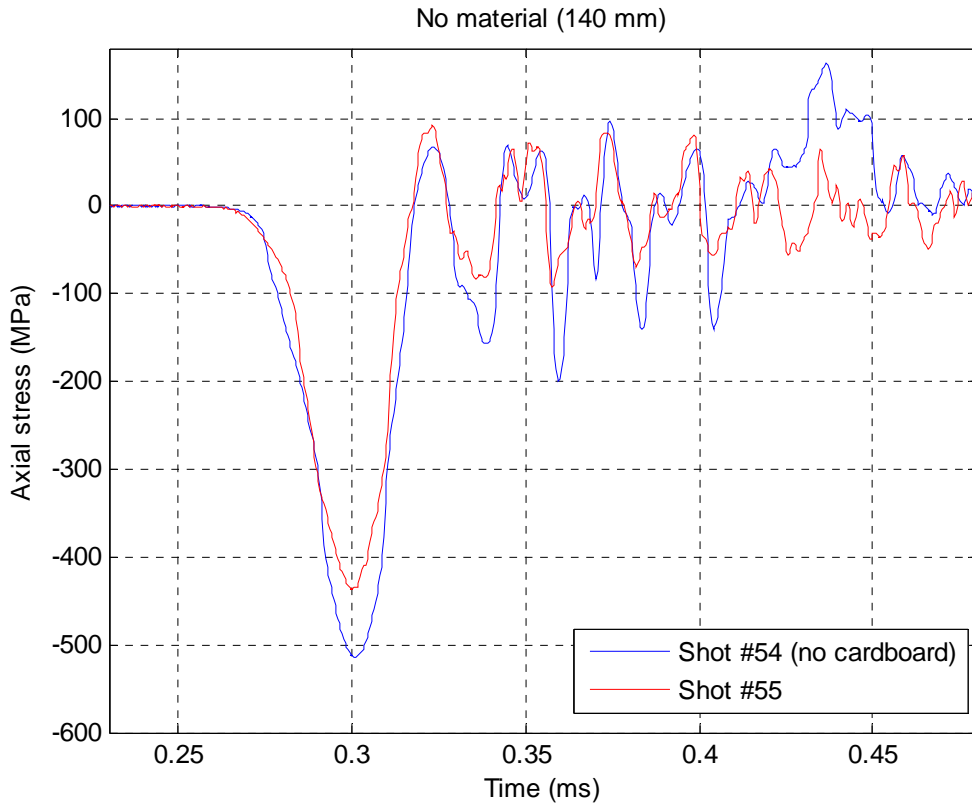


Figure 7.18 The measured stress wave for no damping material (140 mm).

## 8 Comparison of amplitudes

In Table 8.1 we have summarised the maximum stress amplitudes for all shots for different materials. As already noted LECA fine, wood shavings, aluminium foam and Glasopor appear to give most damping in this experiment.

| Material             | Distance charge-bar (mm) | Thickness (mm) | Mass (g) | Stress amplitudes (MPa) | Average amplitude (MPa) | Ratio |
|----------------------|--------------------------|----------------|----------|-------------------------|-------------------------|-------|
| Reference            | 80                       | -              | -        | 559, 548, 549           | 552.0                   | 1.00  |
| Reference            | 100                      | -              | -        | 563, 542, 535, (297)    | 546.7                   | 0.99  |
| Reference            | 140                      | -              | -        | 437, 515                | 476.0                   | 0.86  |
| LECA fine            | 80                       | 21.0           | 16.1     | 523, 504                | 513.5                   | 0.93  |
| LECA fine            | 80                       | 39.0           | 30.0     | 472, 435                | 453.5                   | 0.82  |
| LECA fine (B)        | 80                       | 39.5           | 30.0     | 364, 355                | 359.5                   | 0.65  |
| LECA fine            | 80                       | 60.5           | 47.1     | 378, 372                | 375.0                   | 0.68  |
| LECA fine            | 80                       | 69.8           | 55.0     | 315, 306                | 310.5                   | 0.56  |
| LECA coarse          | 80                       | 49.5           | 30.0     | 413, 376                | 394.5                   | 0.72  |
| Pumice (Italy)       | 80                       | 35.0           | 30.0     | 427, 382                | 404.5                   | 0.73  |
| Pumice (Iceland)     | 80                       | 51.0           | 30.0     | 366, 382                | 374.0                   | 0.68  |
| Particle board       | 80                       | 23.2           | 30.6     | 439, 421                | 430.0                   | 0.78  |
| Rubber granules      | 80                       | 25.0           | 30.0     | 443                     | 443.0                   | 0.80  |
| Gravel (0-4 mm)      | 80                       | 12.0           | 30.0     | 517                     | 517.0                   | 0.94  |
| Gravel (0-8 mm)      | 80                       | 13.0           | 30.0     | 502, 487                | 494.5                   | 0.90  |
| Gravel (8-11 mm)     | 80                       | 14.8           | 30.0     | 470, 479                | 474.5                   | 0.86  |
| Gravel (8-11 mm NCC) | 80                       | 14.5           | 30.0     | 485, 428                | 461.5                   | 0.84  |
| Wood shavings        | 80                       | 68.5           | 30.0     | 303, 294                | 298.5                   | 0.54  |
| Sawdust              | 80                       | 60.5           | 30.0     | 433, 432                | 432.5                   | 0.78  |
| Norway spruce        | 80                       | 42.5           | 30.0     | 434, 414                | 424.0                   | 0.77  |
| Norway spruce        | 100                      | 44.0           | 30.0     | 424, 395                | 409.5                   | 0.74  |
| Aluminium foam       | 100                      | 86.5           | 30.0     | 261, 256                | 258.5                   | 0.47  |
| Glasopor (0-4 mm)    | 100                      | 24.5           | 30.0     | 448, 410                | 429.0                   | 0.78  |
| Glasopor (4-14 mm)   | 100                      | 71.5           | 30.0     | 303, 296                | 299.5                   | 0.54  |
| Glasopor (14-22 mm)  | 100                      | 79.5           | 30.0     | 283, 293                | 288.0                   | 0.52  |
| Siporex              | 80                       | 26.7           | 30.1     | 420, 458                | 439.0                   | 0.80  |
| Brick                | 80                       | 8.4            | 30.3     | 544, 544                | 544.0                   | 0.99  |

Table 8.1 The measured stress amplitudes for all the damping materials.

## 9 Summary

Results from shock attenuation experiments have been presented. However, it is not yet quite clear which conclusions can be drawn from these experiments. This will be discussed in a separate report.

## References

- (1) <http://en.wikipedia.org/wiki/Pumice> (March 16, 2009)
- (2) <http://www.maxit.no/> (March 16, 2009)
- (3) [http://en.wikipedia.org/wiki/Particle\\_board](http://en.wikipedia.org/wiki/Particle_board) (March 16, 2009)
- (4) [http://en.wikipedia.org/wiki/Crumb\\_rubber](http://en.wikipedia.org/wiki/Crumb_rubber) (March 16, 2009)
- (5) Fykse H, Private communication
- (6) <http://en.wikipedia.org/wiki/Sand> (March 16, 2009)
- (7) <http://en.wikipedia.org/wiki/Gravel> (March 16, 2009)
- (8) <http://en.wikipedia.org/wiki/Sawdust> (March 16, 2009)
- (9) [http://en.wikipedia.org/wiki/Norway\\_Spruce](http://en.wikipedia.org/wiki/Norway_Spruce) (March 16, 2009)
- (10) [http://en.wikipedia.org/wiki/Aluminium\\_foam](http://en.wikipedia.org/wiki/Aluminium_foam) (March 16, 2009)
- (11) <http://www.glasopor.no/> (March 16, 2009)
- (12) <http://www.lccsiporex.com> (March 16, 2009)
- (13) <http://en.wikipedia.org/wiki/Brick> (March 16, 2009)
- (14) Skriudalen S, "Bonding of optical fibre on a steel bar using a two component epoxy based adhesive", FFI/NOTAT – 2009/00475
- (15) Teland J A, Skriudalen S, Sagvolden G, Svinsås E, Experimental investigation of shock attenuation properties of various protective materials, Proceedings of the European Survivability Workshop 2008, Great Malvern, UK, 15-17 april 2008
- (16) Teland J A, Svinsås E, Frøyland Ø, Porous geological material for shock attenuation, Proceedings of 3<sup>rd</sup> European Survivability Workshop, Toulouse, Frankrike 16-19 mai 2008
- (17) Teland J A, A review of analytical penetration mechanics, FFI/RAPPORT-99/01264

## Appendix A Uniaxial stress hypothesis

The experiment relies on our ability to calculate the stress in the steel bar from measurements of strain. According to Hooke's law there is a definite relationship between stress  $\sigma_{ij}$  and strain  $\varepsilon_{ij}$  in an elastic material:

$$\sigma_{ij} = \frac{E}{1+\nu} \left( \varepsilon_{ij} + \frac{\nu}{1-2\nu} \varepsilon_{kk} \delta_{ij} \right) \quad (\text{A.1})$$

Here  $E$  is the Young's modulus,  $\nu$  is Poisson's ratio and we have applied Einstein's summation convention. For waves propagating along a thin<sup>2</sup> bar, the situation is close to uniaxial stress, i.e. the stress in the axial direction is large compared to the other stress components. Stress propagation is discussed in detail in (17). In our case, Equation (A.1) is then reduced to the familiar simple relation:

$$\sigma_{xx} = E \varepsilon_{xx} \quad (\text{A.2})$$

The gauges will measure the strain at the the surface of the bar. We can use an AUTODYN simulation to examine whether the stress is actually close to uniaxial in this experiment. For this to be true, it should be possible to approximate the axial stress  $\sigma_{xx}$  at the symmetry axis (actually for any radial distance from the boundary) by using Equation (A.2) with strain values from the boundary. Such a comparison is shown in Figure A.1 and we note that there is good agreement for the main pulse. It therefore seems entirely justified to use Equation (A.2), together with the measured strain value at the boundary, to calculate a single representative stress value for the entire cross section of the bar.

---

<sup>2</sup> Thin means that the diameter of the bar is small compared to the wavelength of the propagating wave. For more details, see (17).

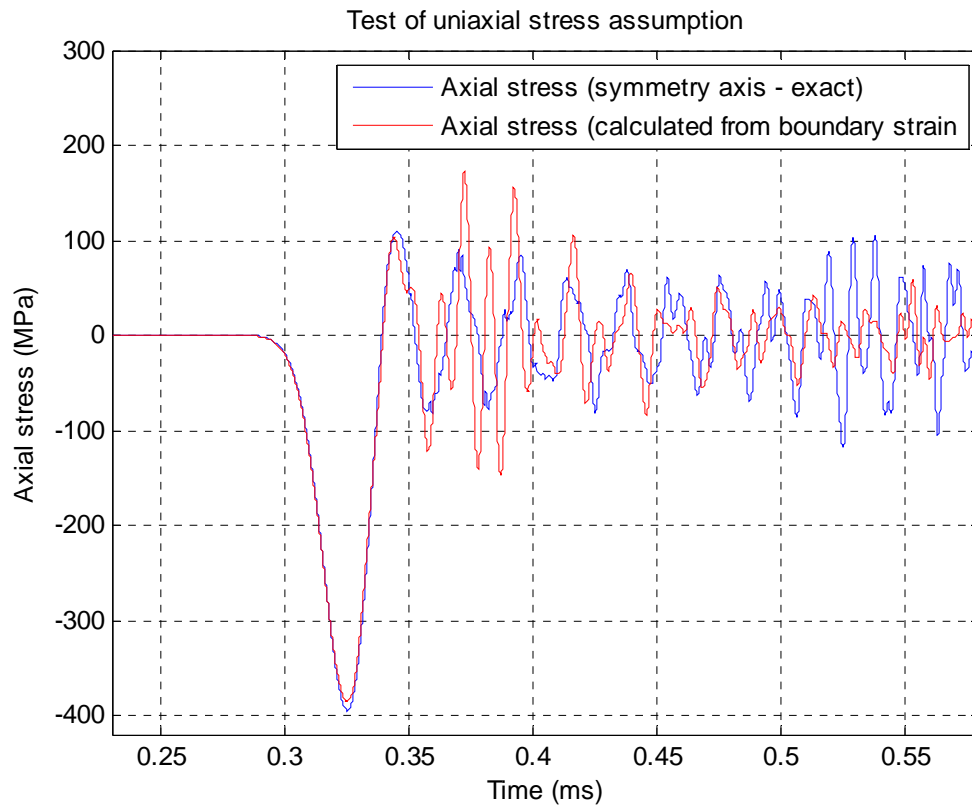
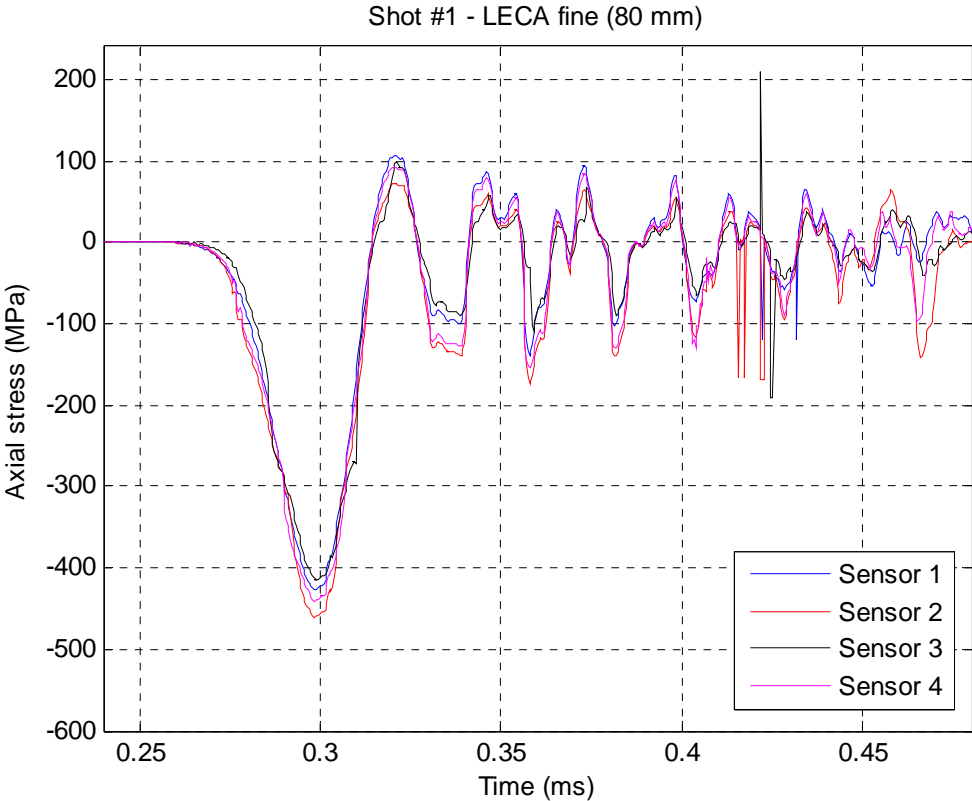


Figure A.1 Comparison of the exact axial stress with the approximate axial stress calculated using Equation (A.2).

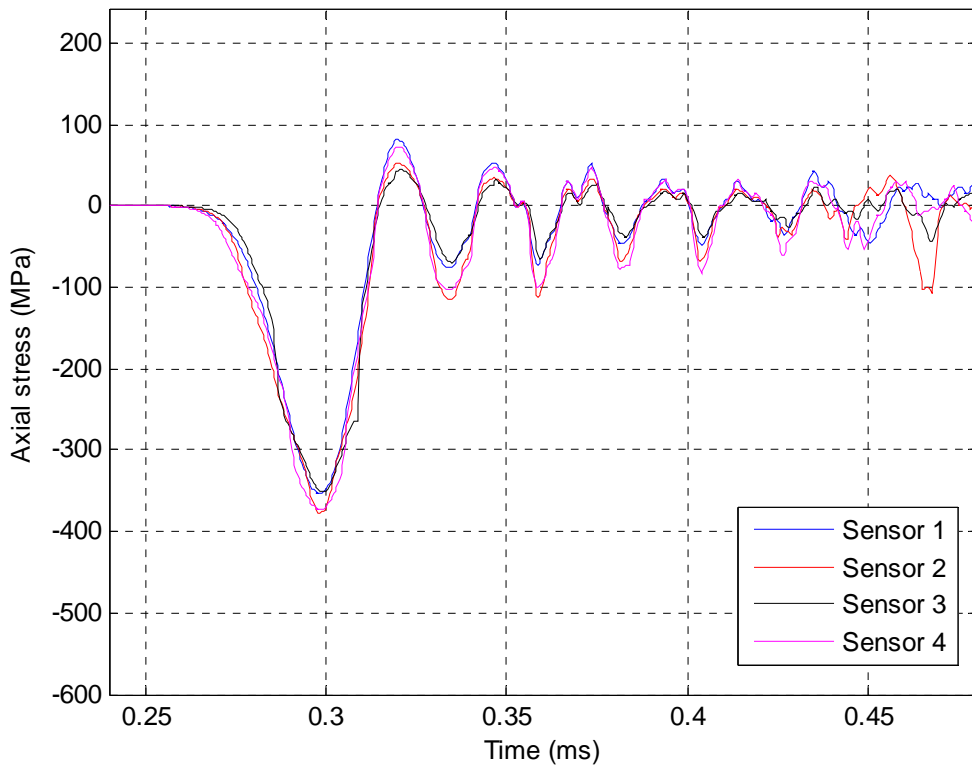
# Appendix B Measurement details

For completeness, in this section we reproduce the results of each individual sensor in each test.

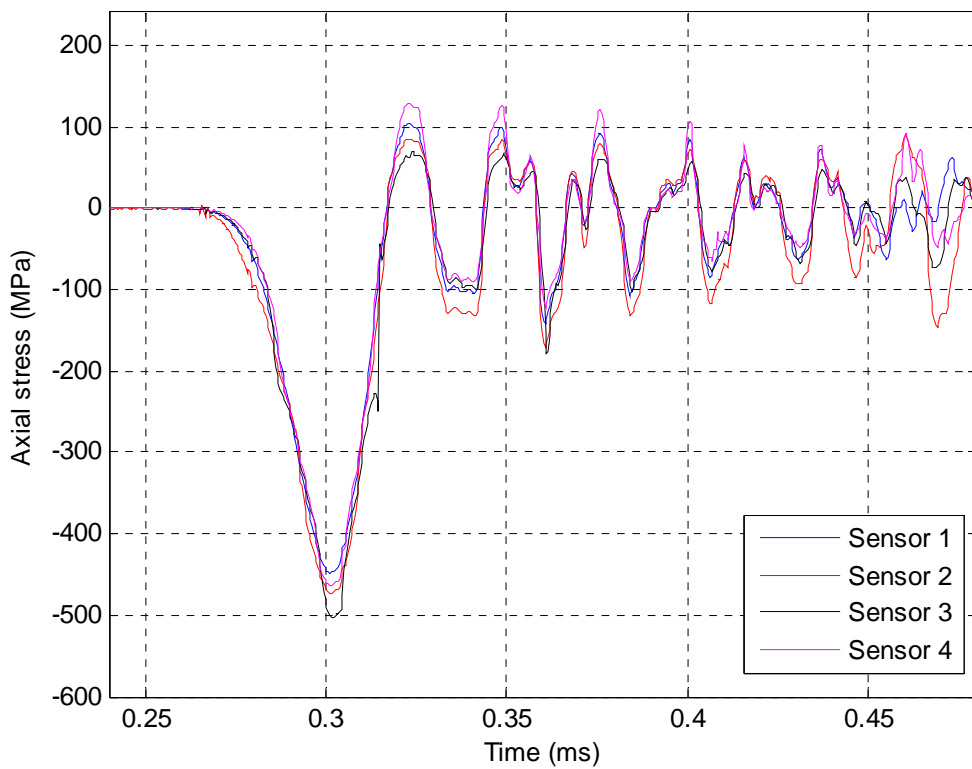
## B.1 February 2008



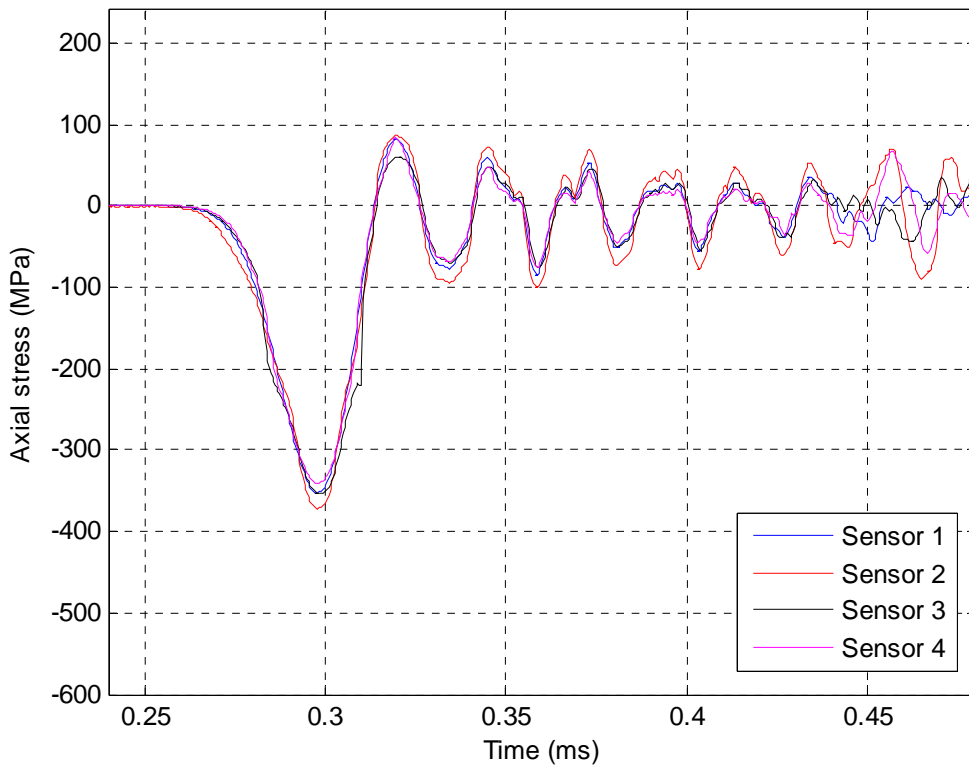
Shot #2 - LECA fine (near explosive) (80 mm)



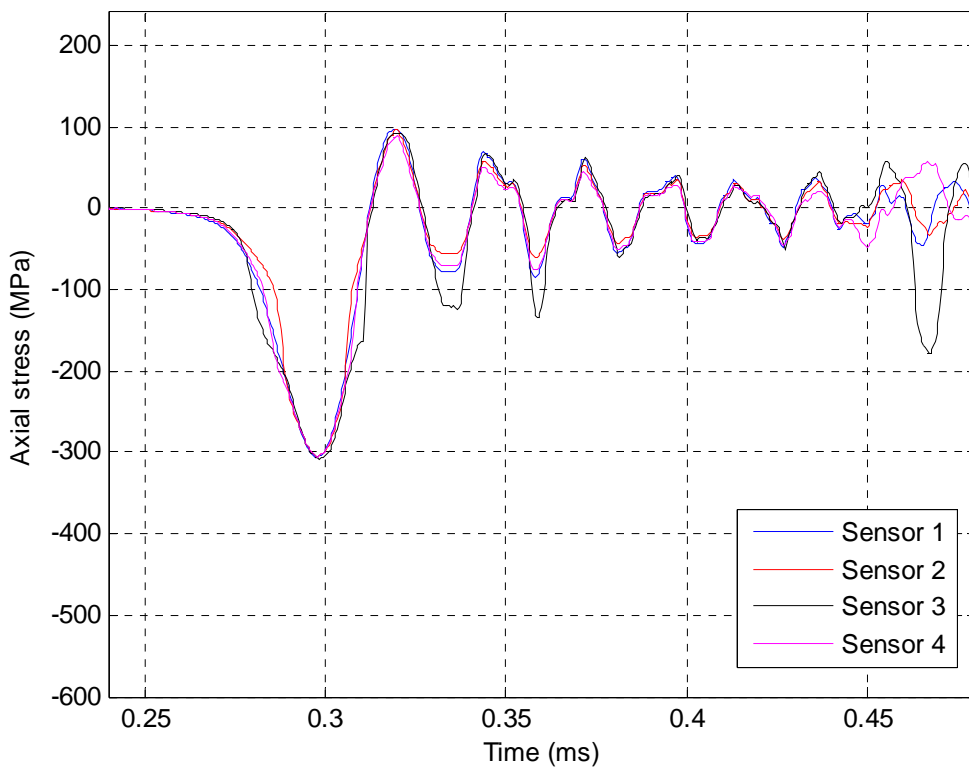
Shot #3 - LECA fine (80 mm)



Shot #4 - LECA fine (near explosive) (80 mm)

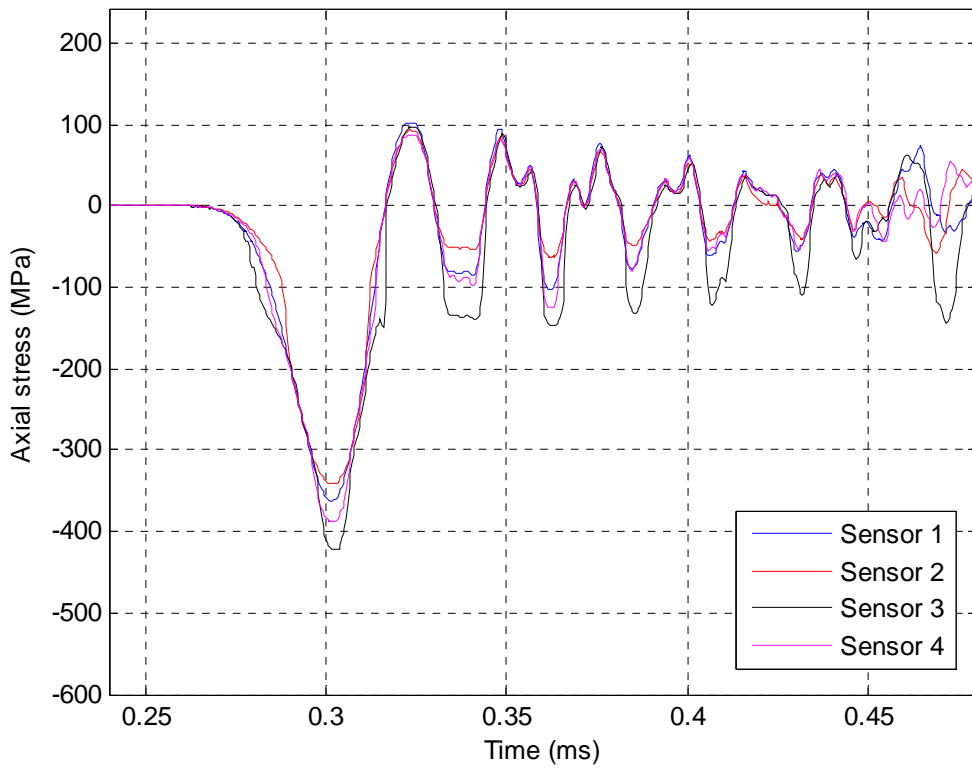


Shot #5 - LECA fine (69.5 mm thickness)

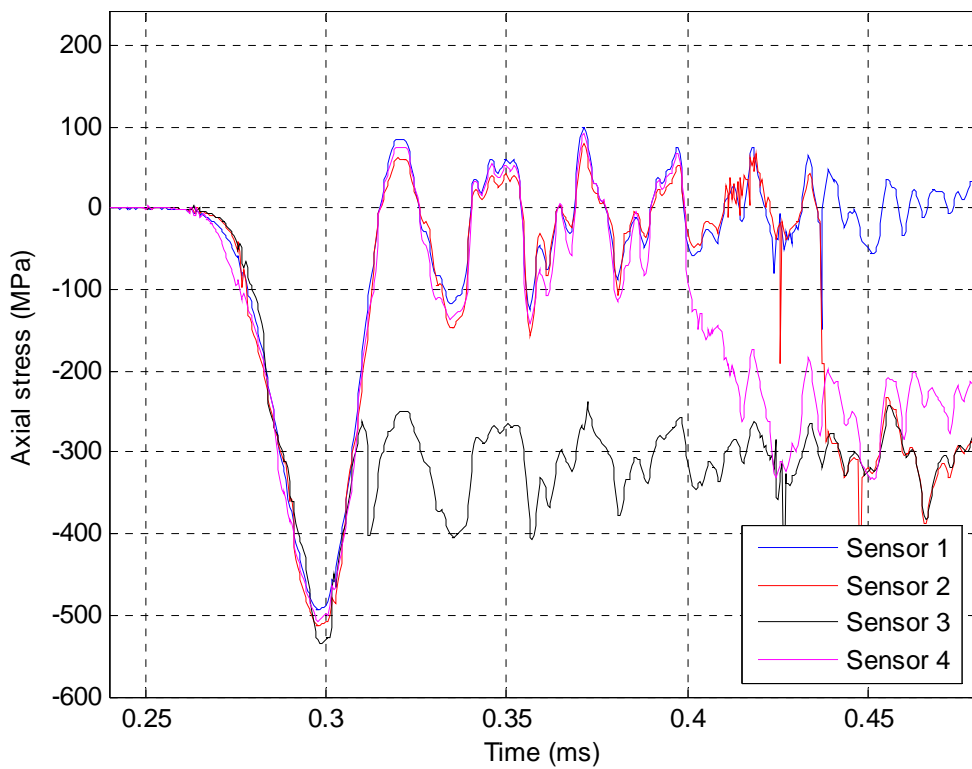




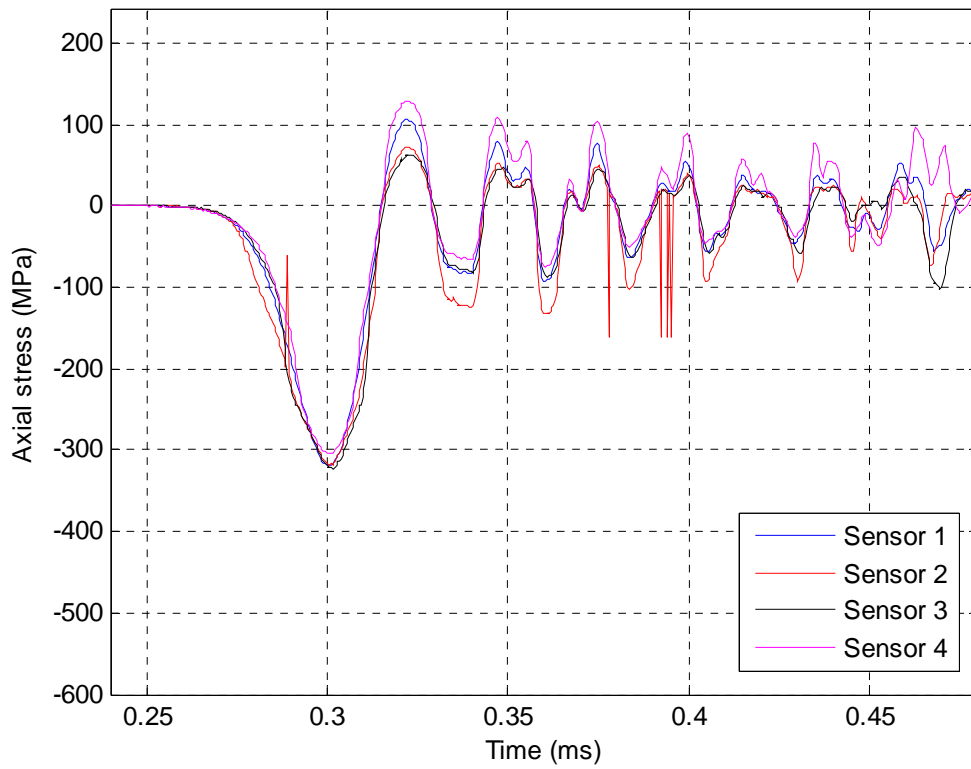
Shot #6 - LECA fine (61.0 mm thickness)



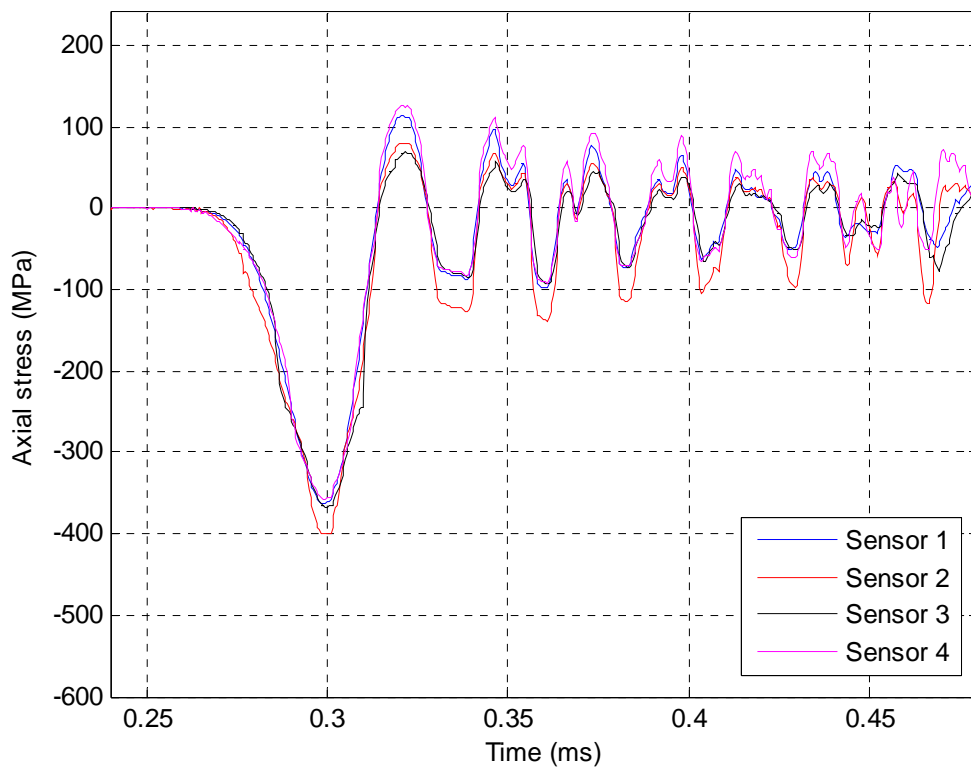
Shot #7 - LECA fine (21.0 mm thickness)



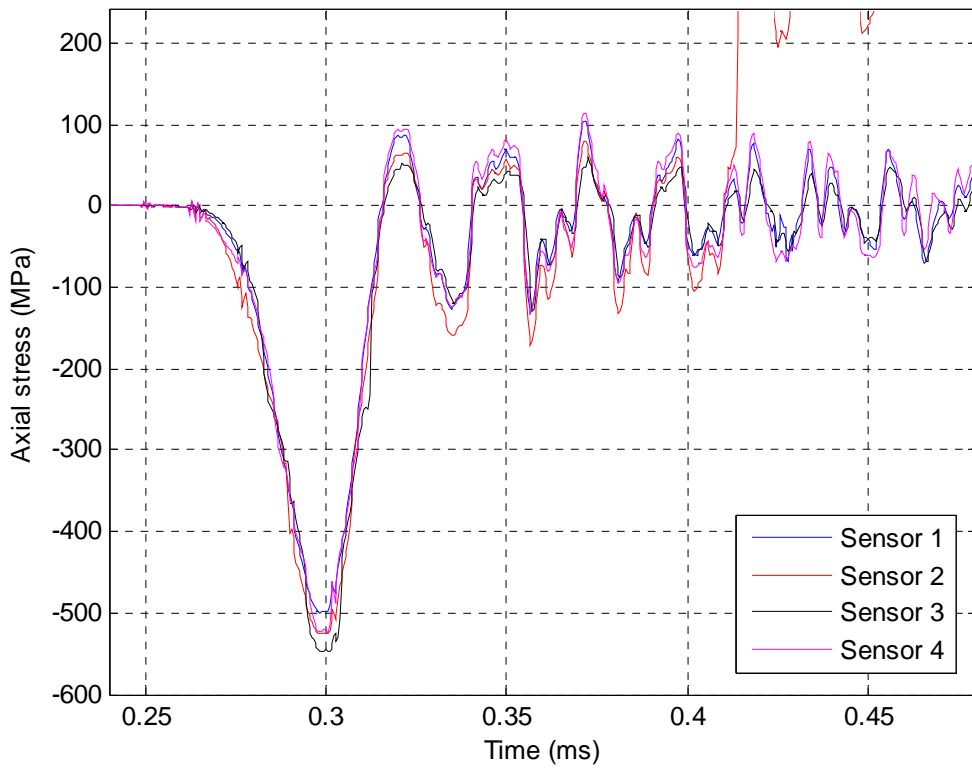
Shot #8 - LECA fine (70.0 mm thickness)



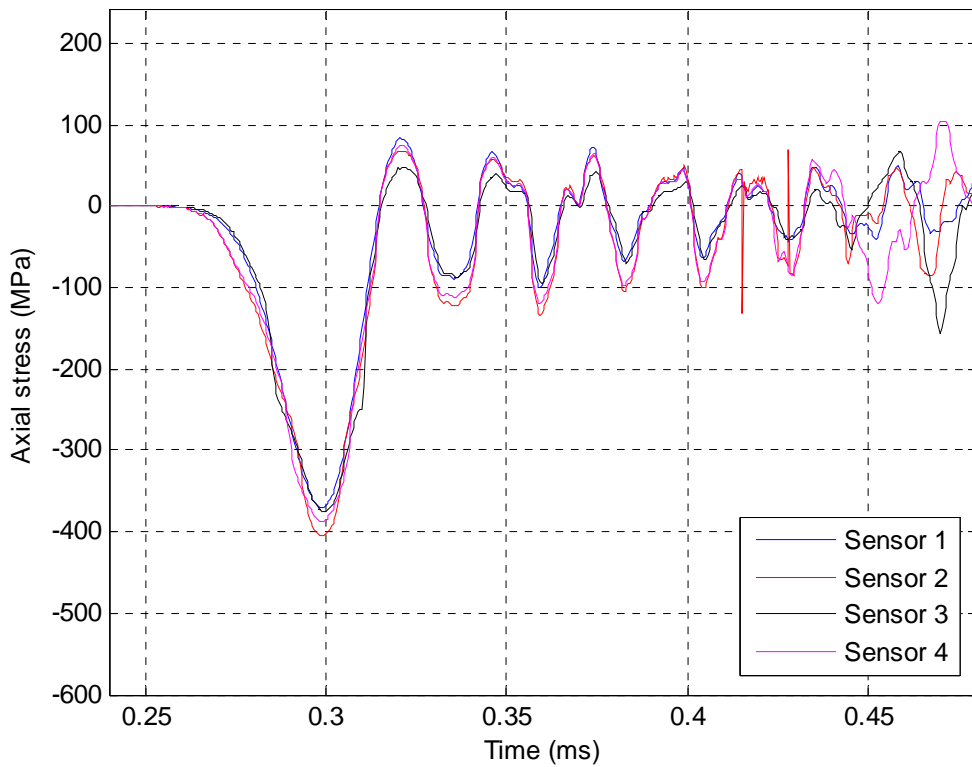
Shot #9 - LECA fine (60.0 mm thickness)



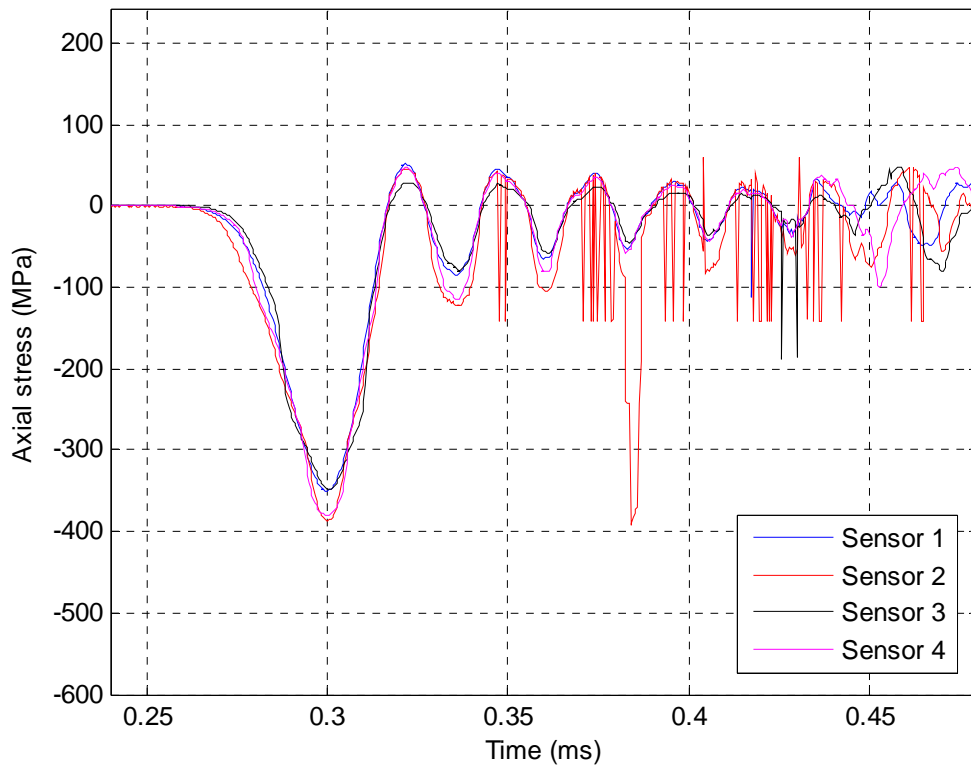
Shot #10 - LECA fine (21.0 mm thickness)



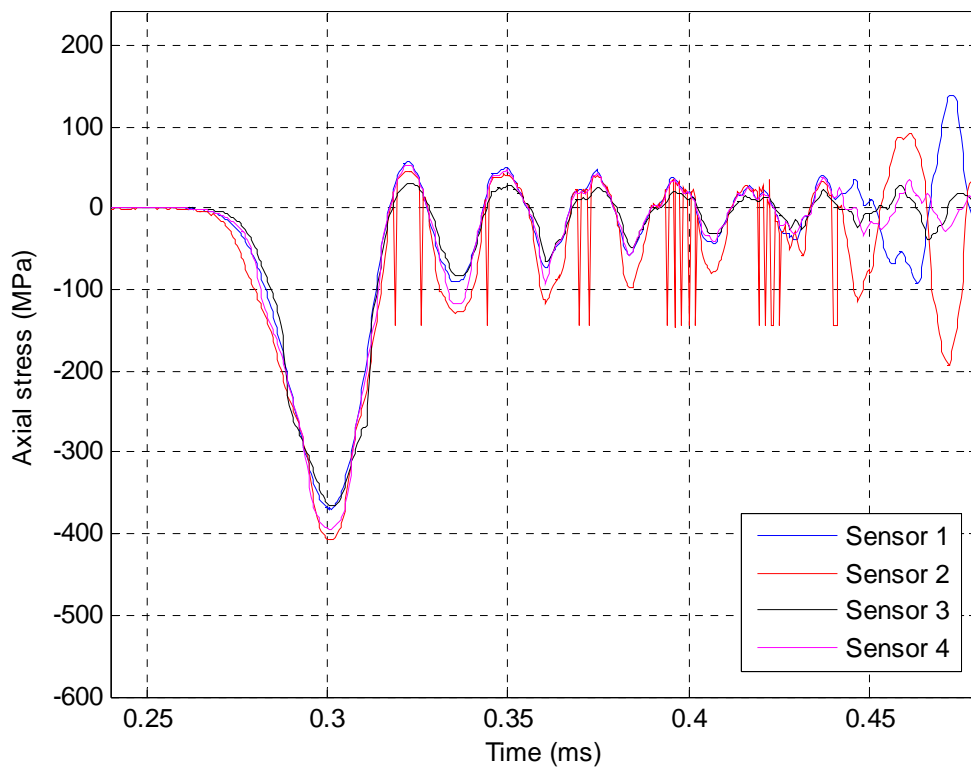
Shot #11 - Italian pumice (35.0 mm thickness)



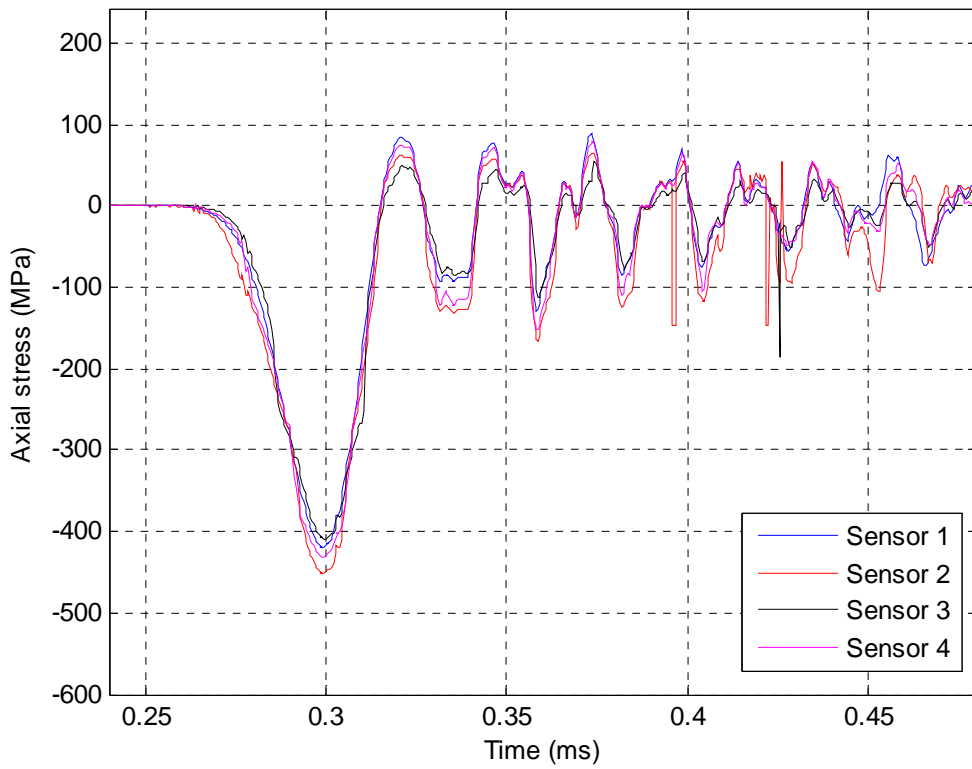
Shot #12 - Icelandic pumice (52.0 mm thickness)



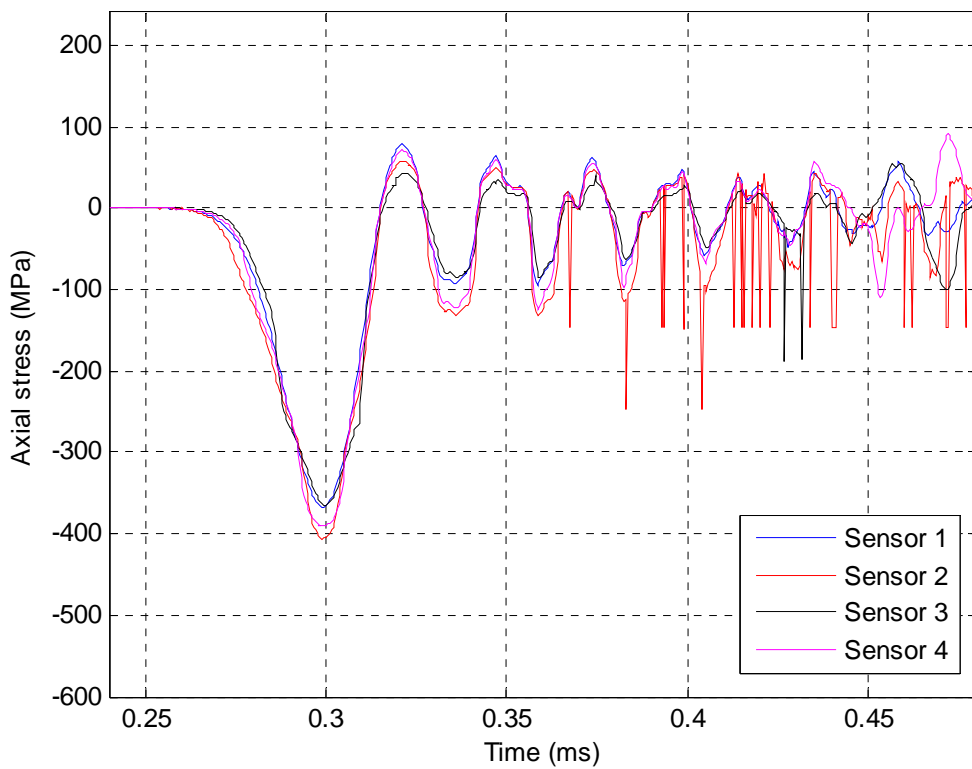
Shot #13 - LECA coarse (50.0 mm thickness)



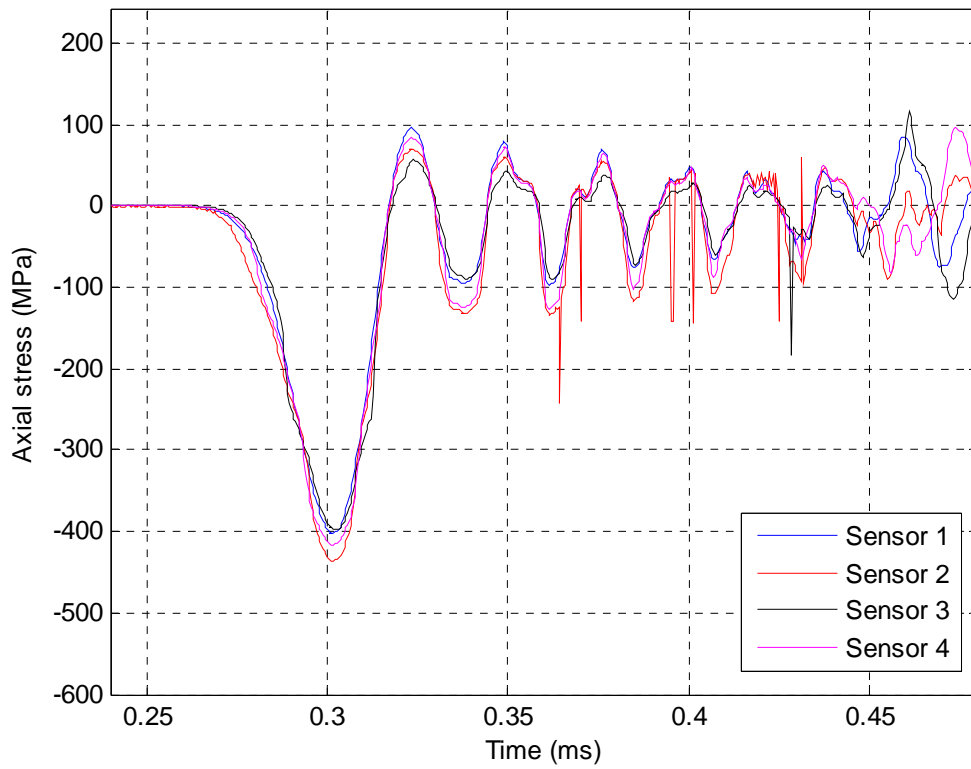
Shot #14 - Italian pumice (35.0 mm thickness)



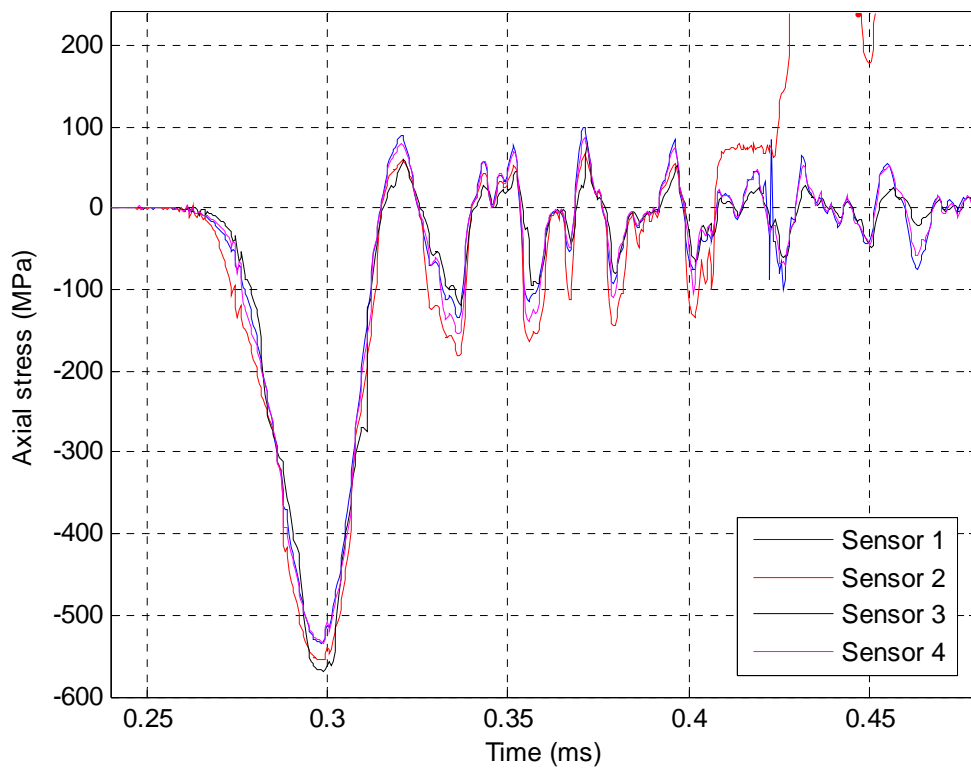
Shot #15 - Icelandic pumice (50.0 mm thickness)



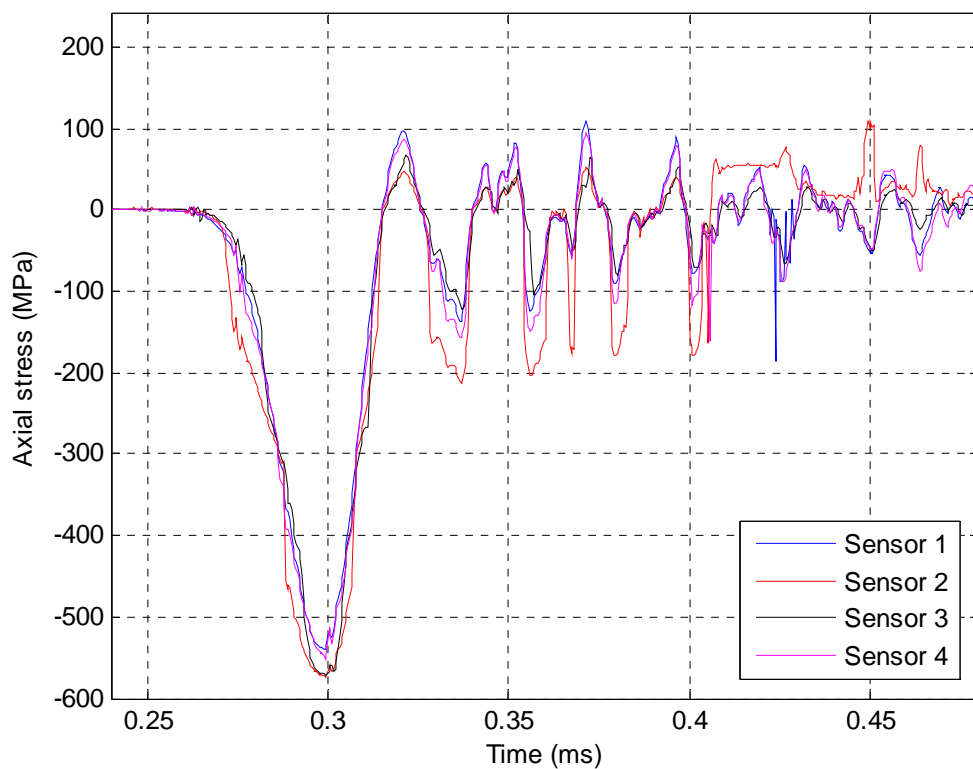
Shot #16 - LECA coarse (49.0 mm thickness)



Shot #17 - No material

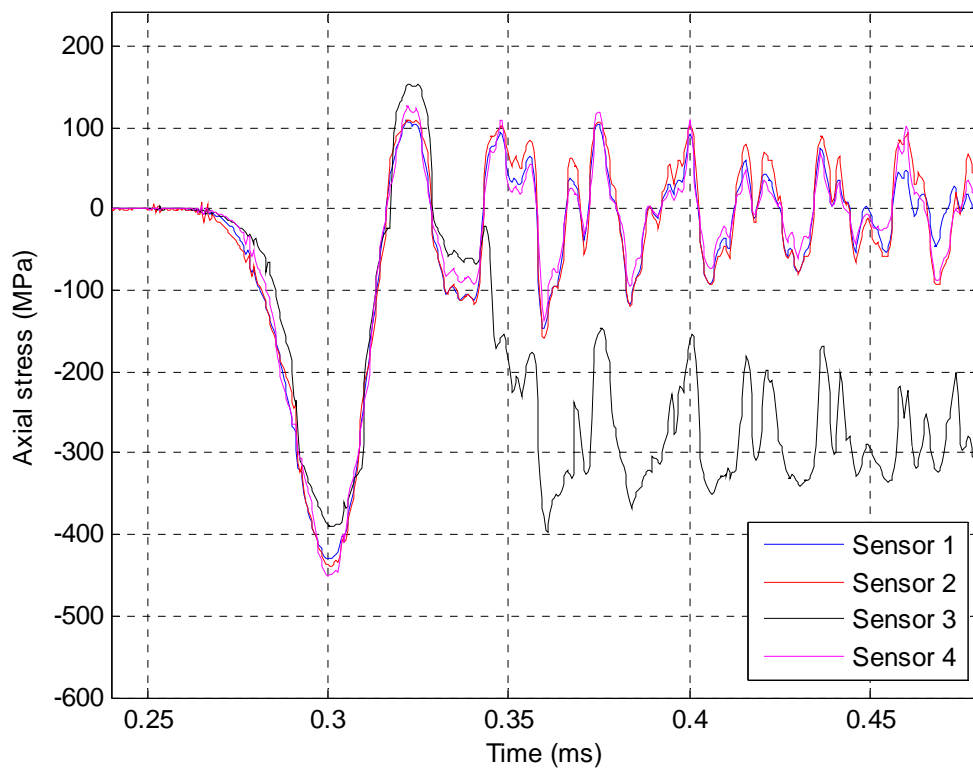


Shot #18 - No material

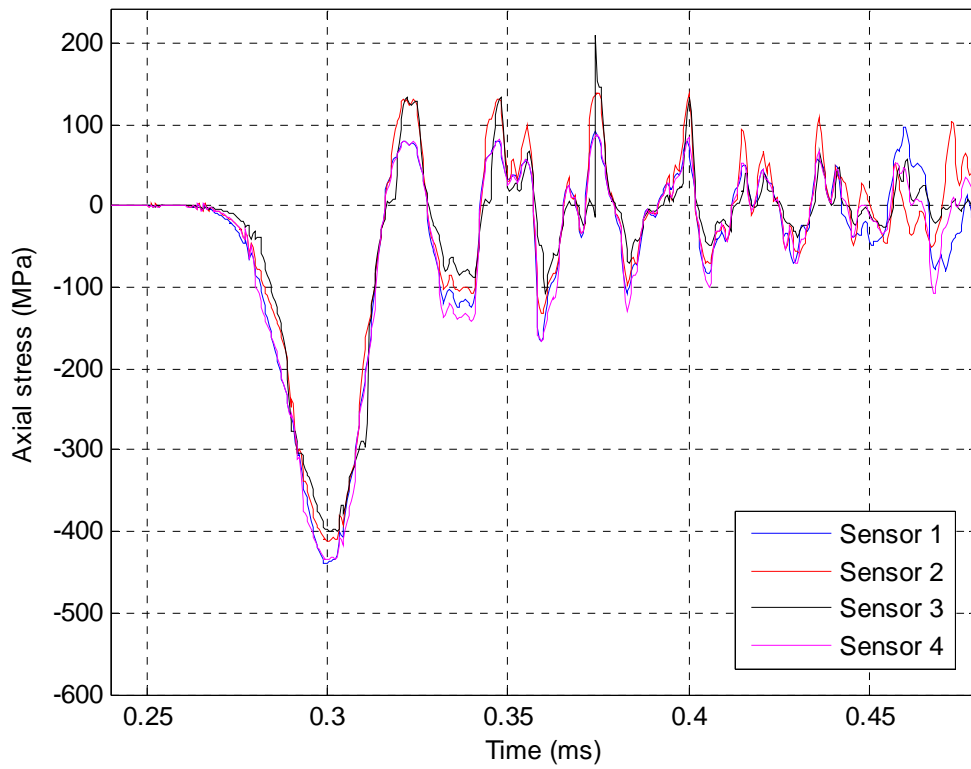


## B.2 April 2008

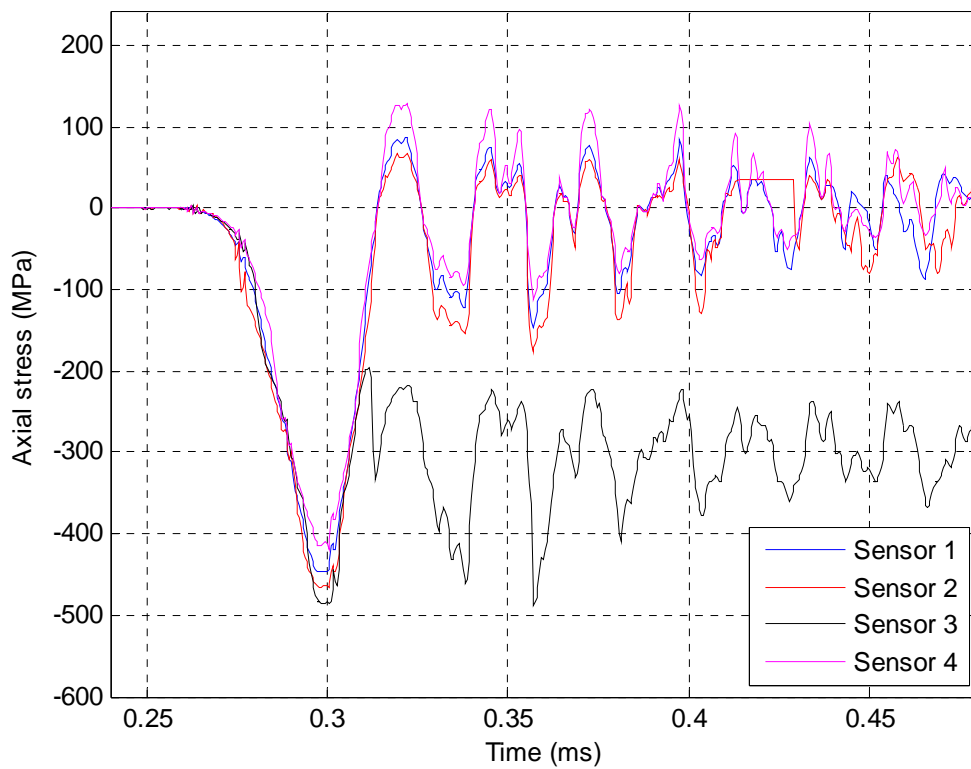
Shot #19 - Particle board (80 mm)



Shot #20 - Particle board (80 mm)

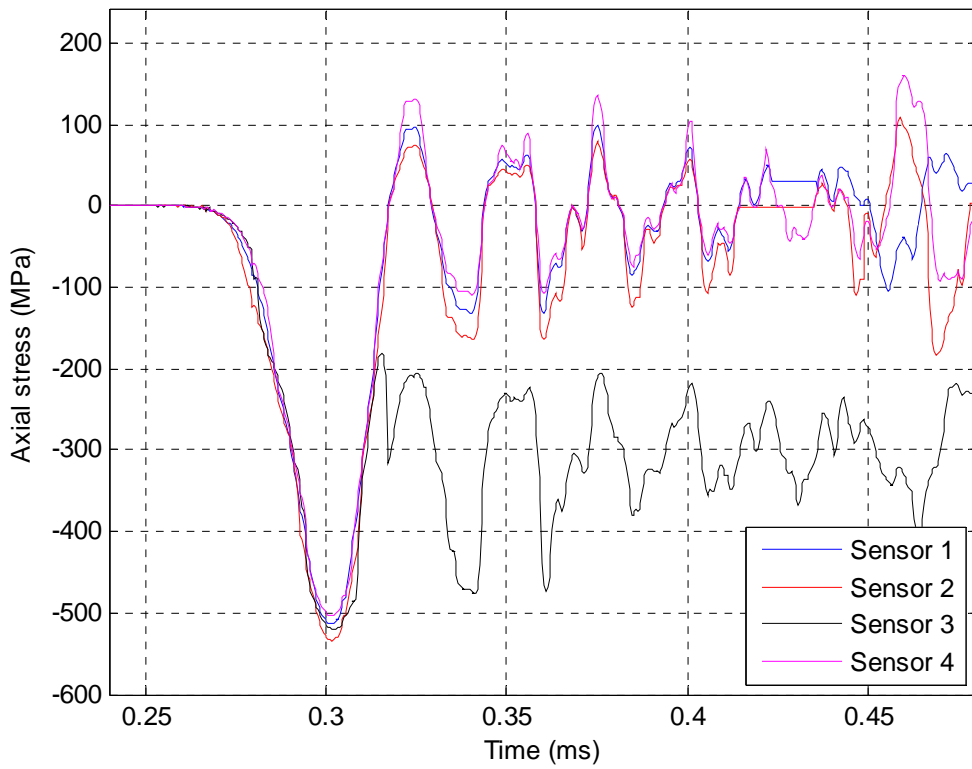


Shot #21 - Rubber granules (80 mm)

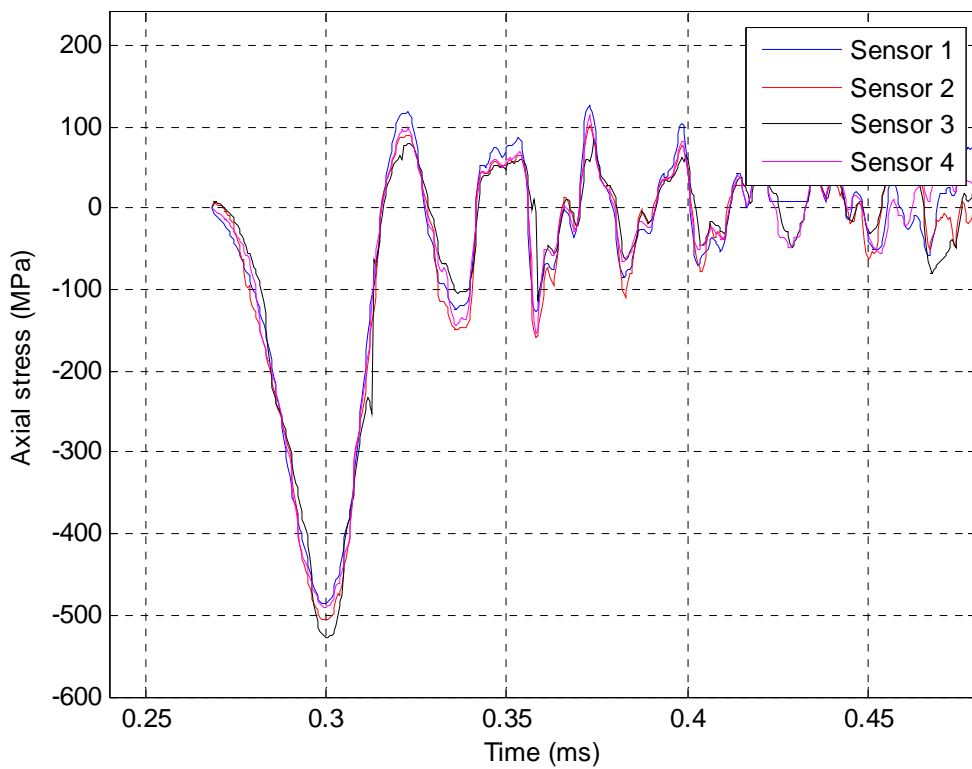




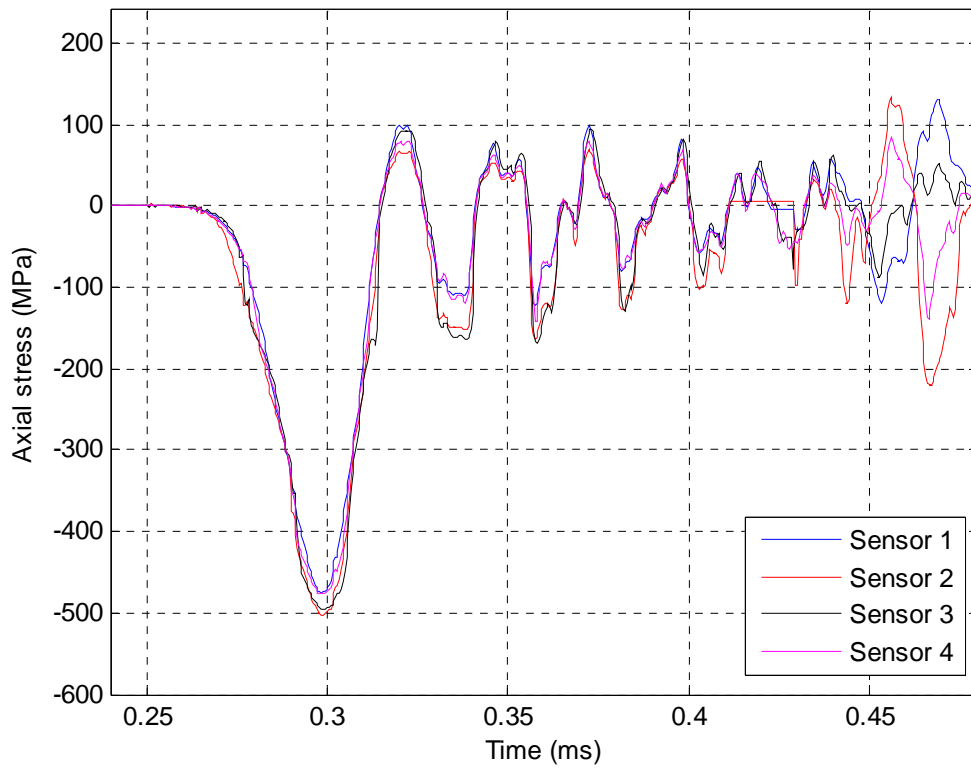
Shot #22 - Gravel (0-4 mm) (80 mm)



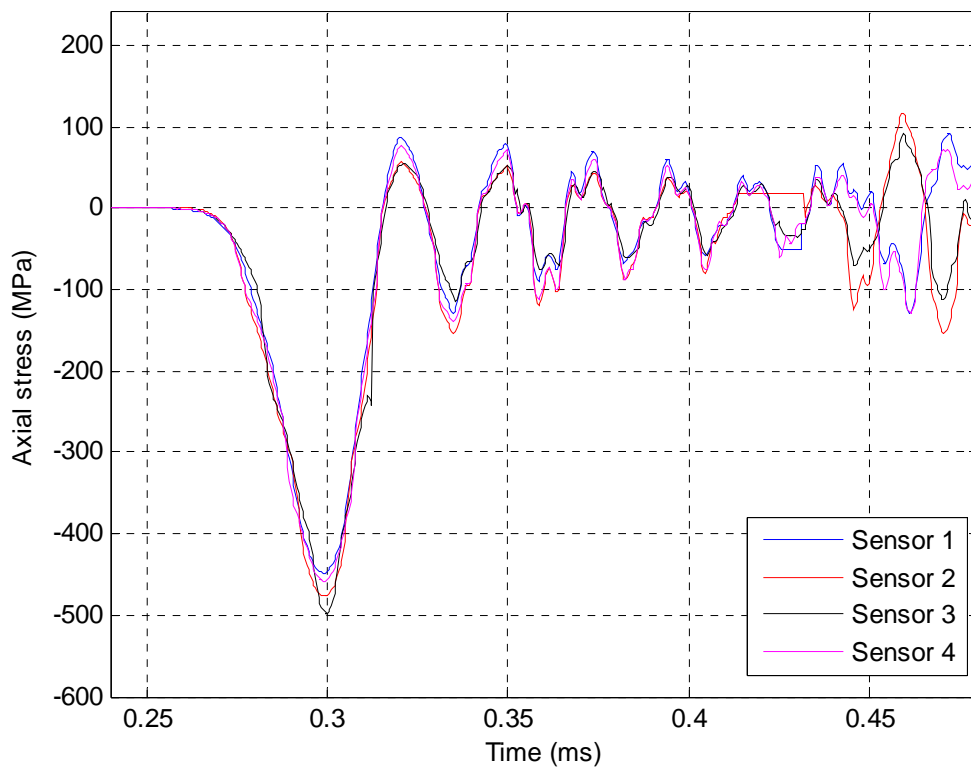
Shot #23 - Gravel (0-8 mm) (80 mm)



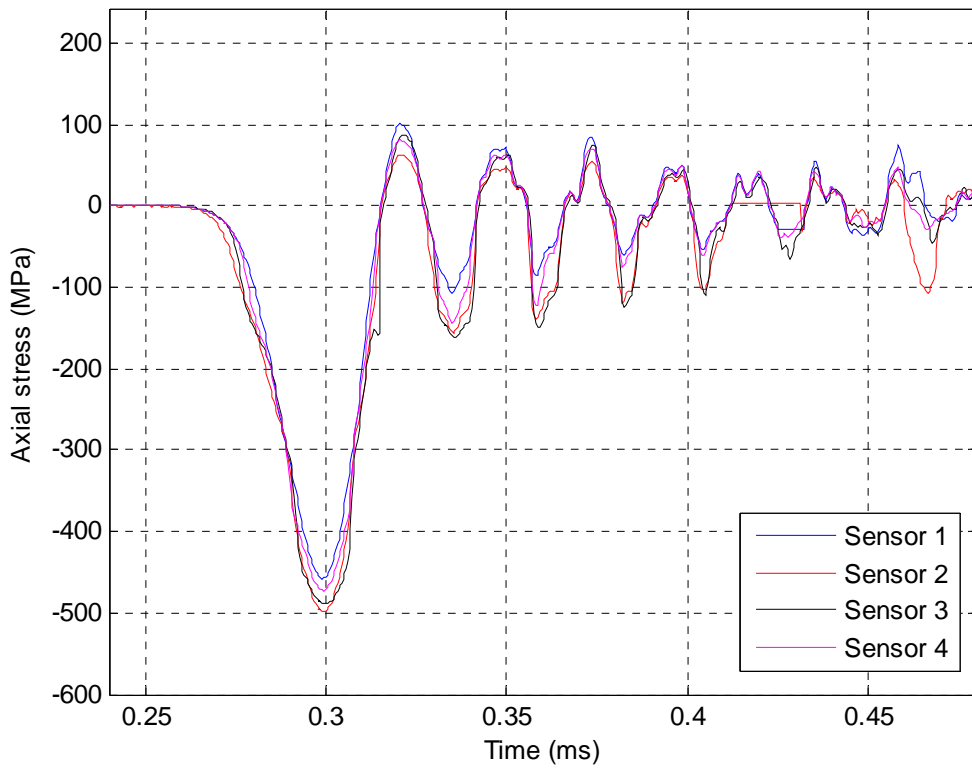
Shot #24 - Gravel (0-8 mm) (80 mm)



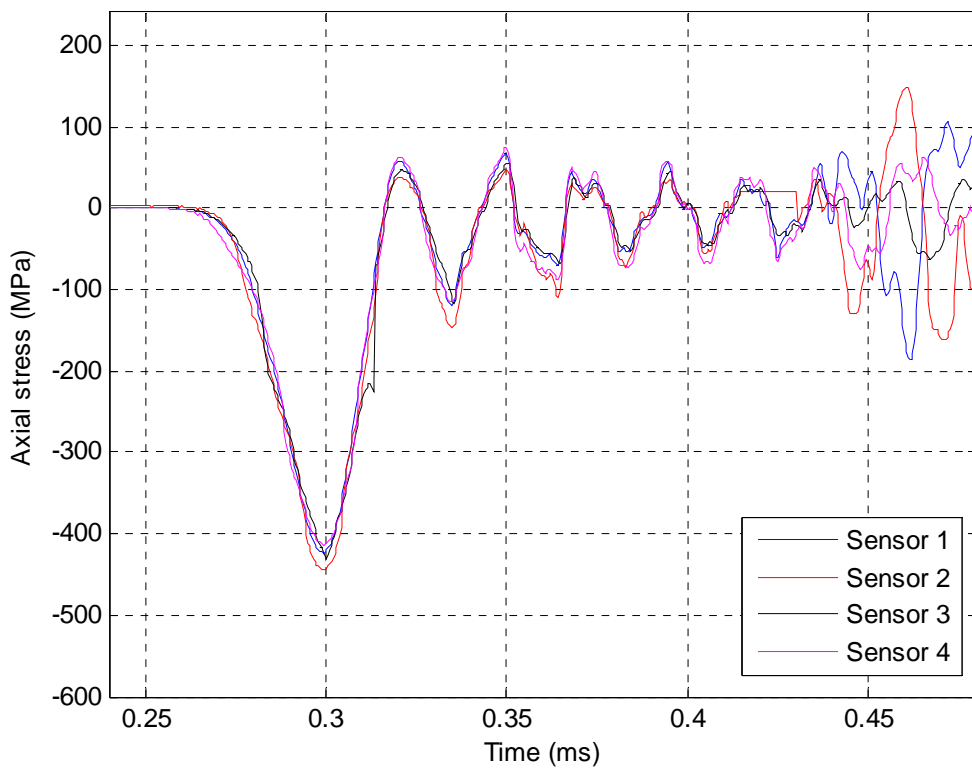
Shot #25 - Gravel (8-11 mm) (80 mm)



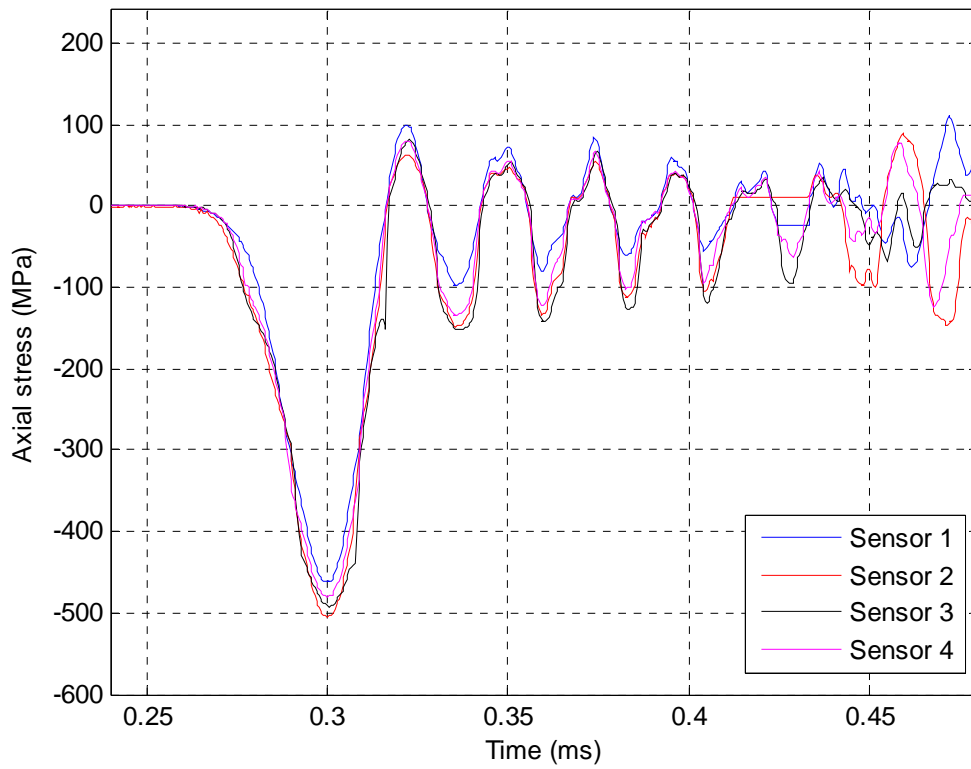
Shot #26 - Gravel (8-11 mm) (80 mm)



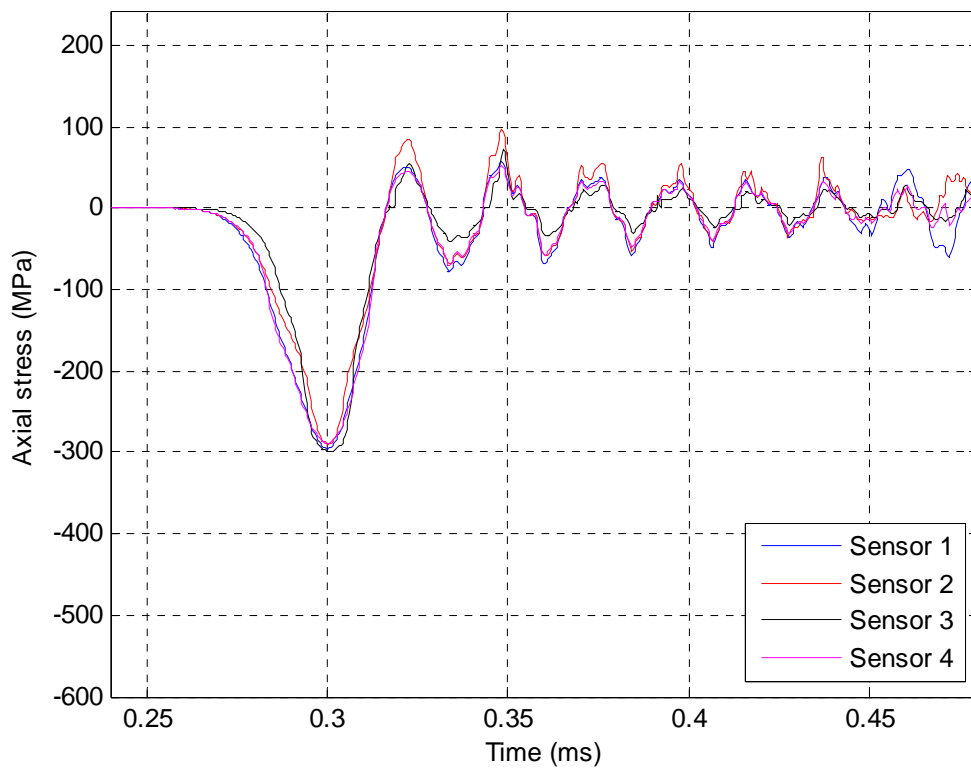
Shot #27 - Gravel (8-11 mm) NCC (80 mm)



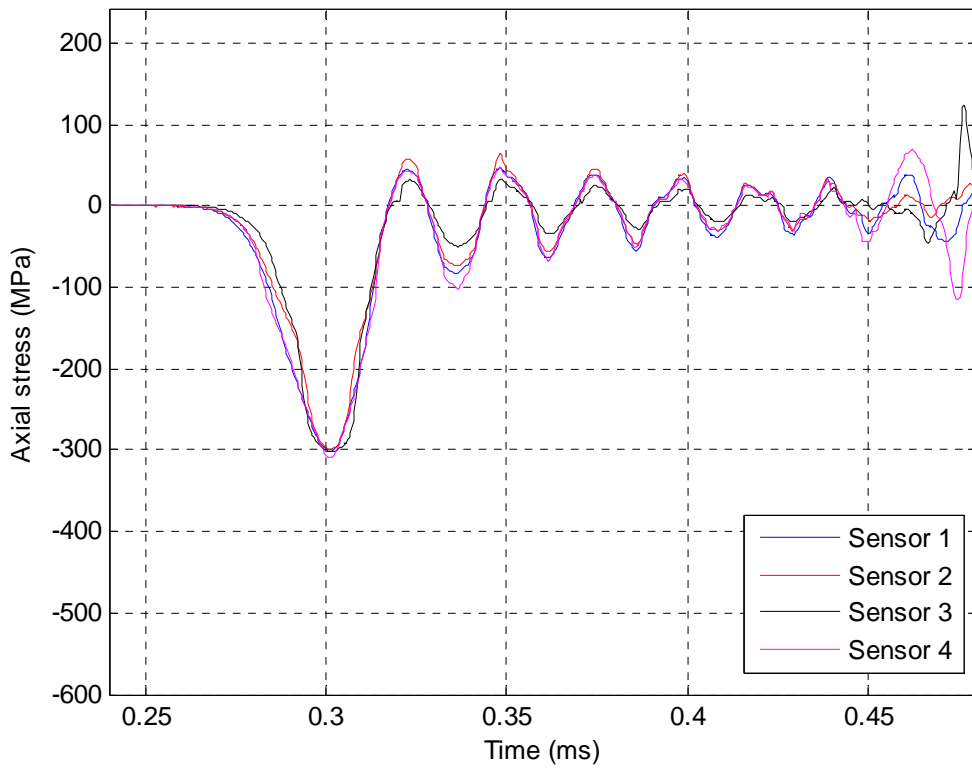
Shot #28 - Gravel (8-11 mm) NCC (80 mm)



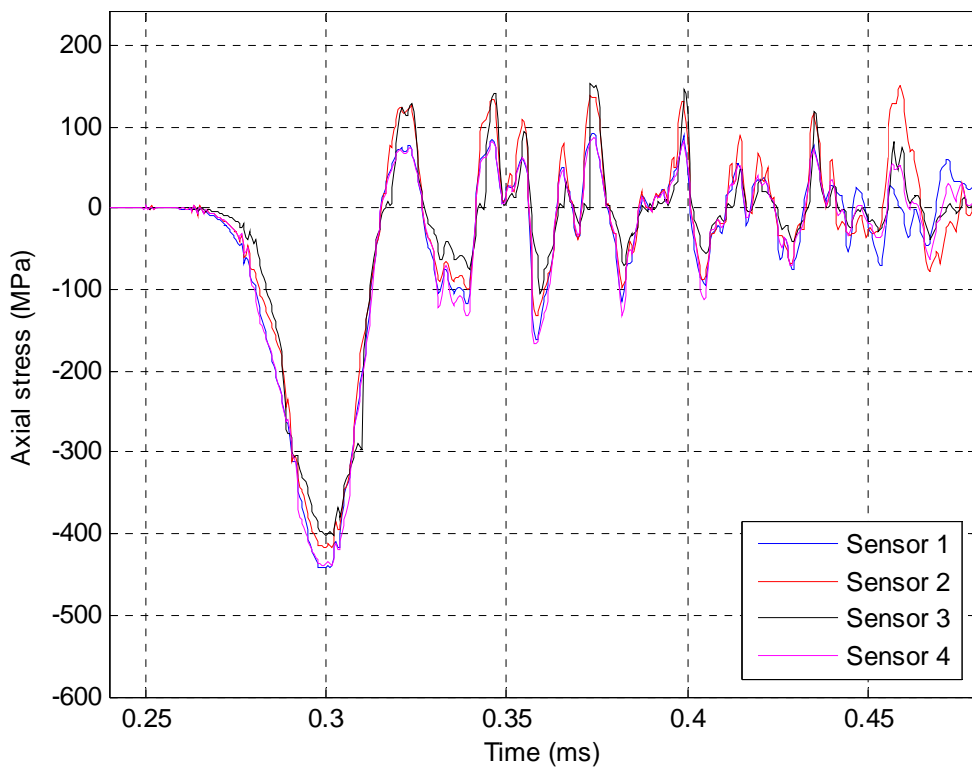
Shot #29 - Wood shavings (80 mm)



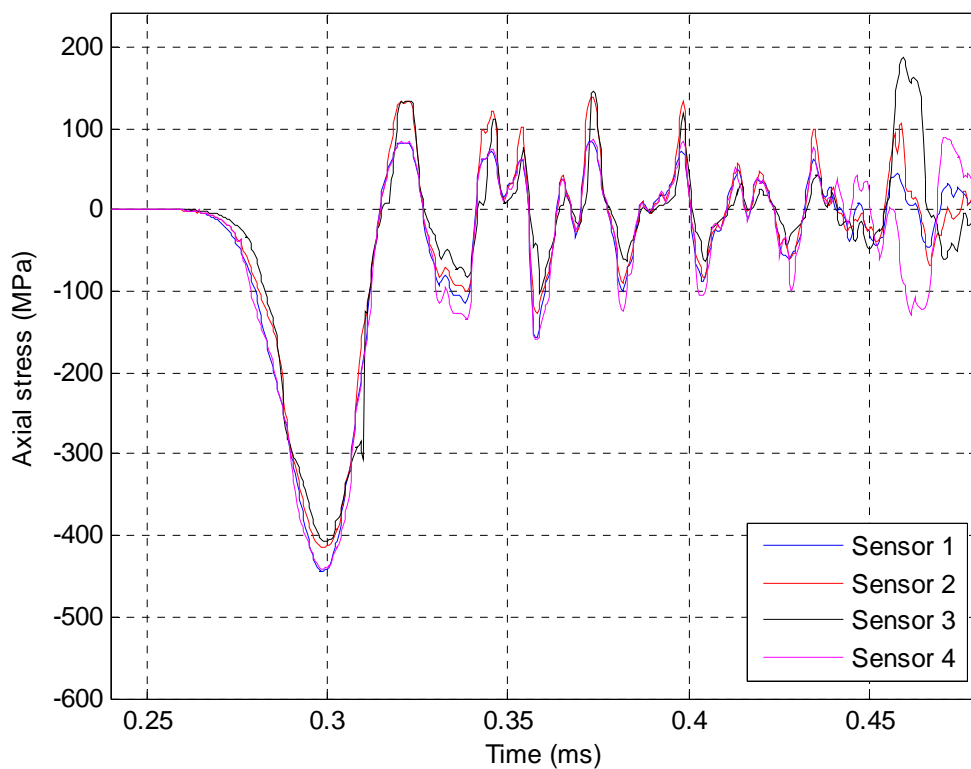
Shot #30 - Wood shavings (80 mm)



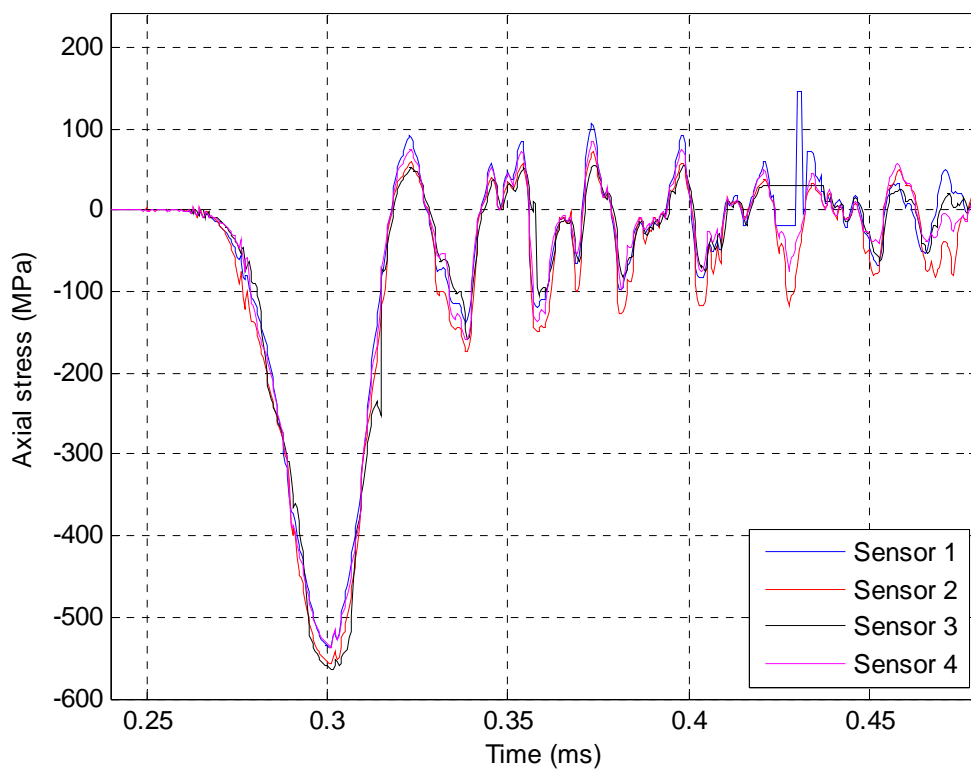
Shot #31 - Sawdust (80 mm)



Shot #32 - Sawdust (80 mm)

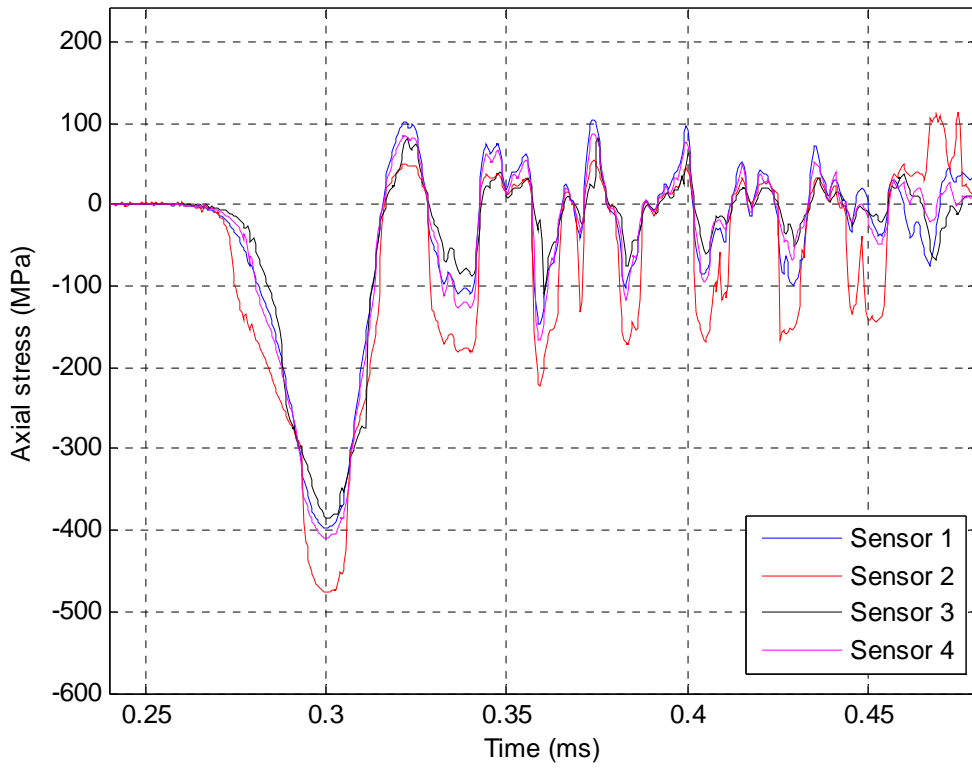


Shot #33 - No material (80 mm)

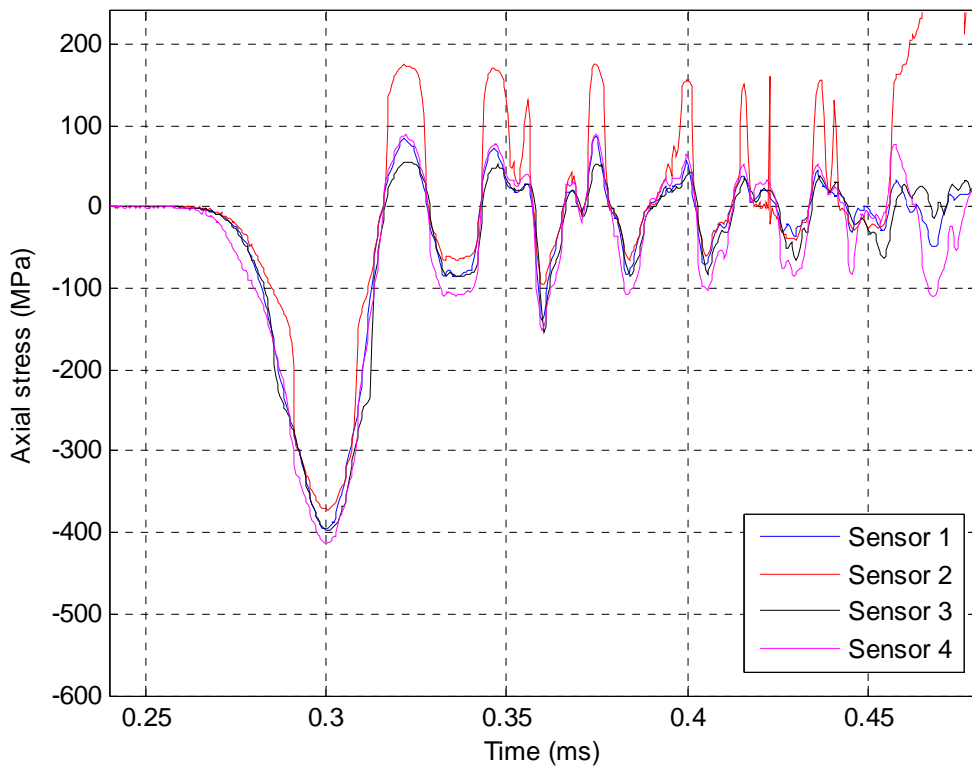


**B.3 September 2008**

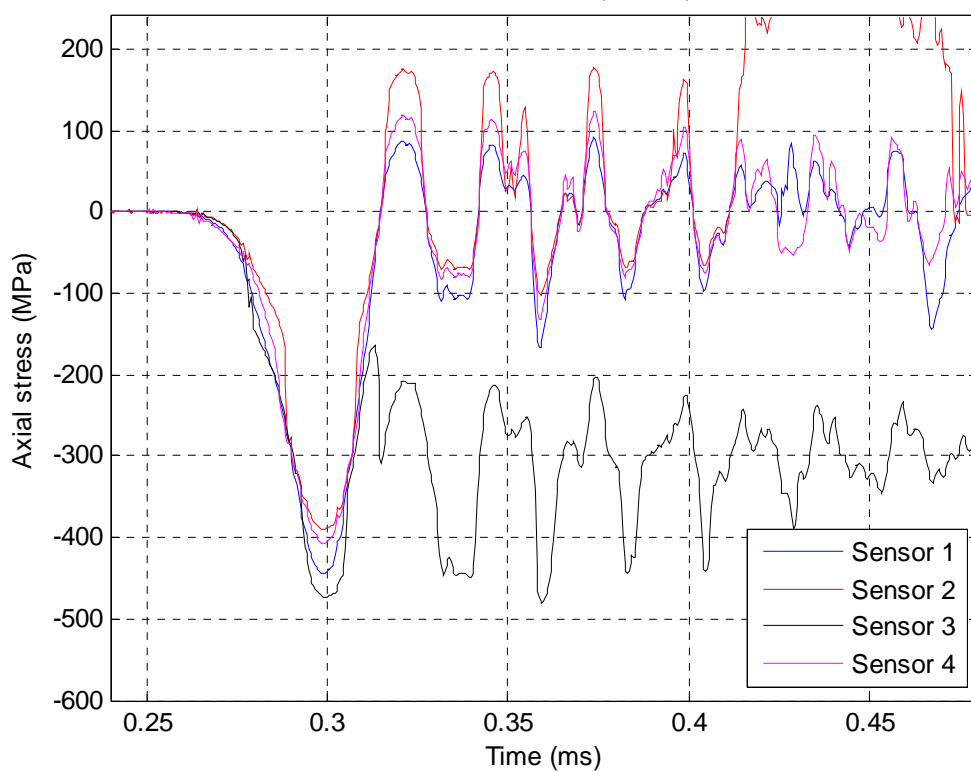
Shot #34 - Wood (100 mm)



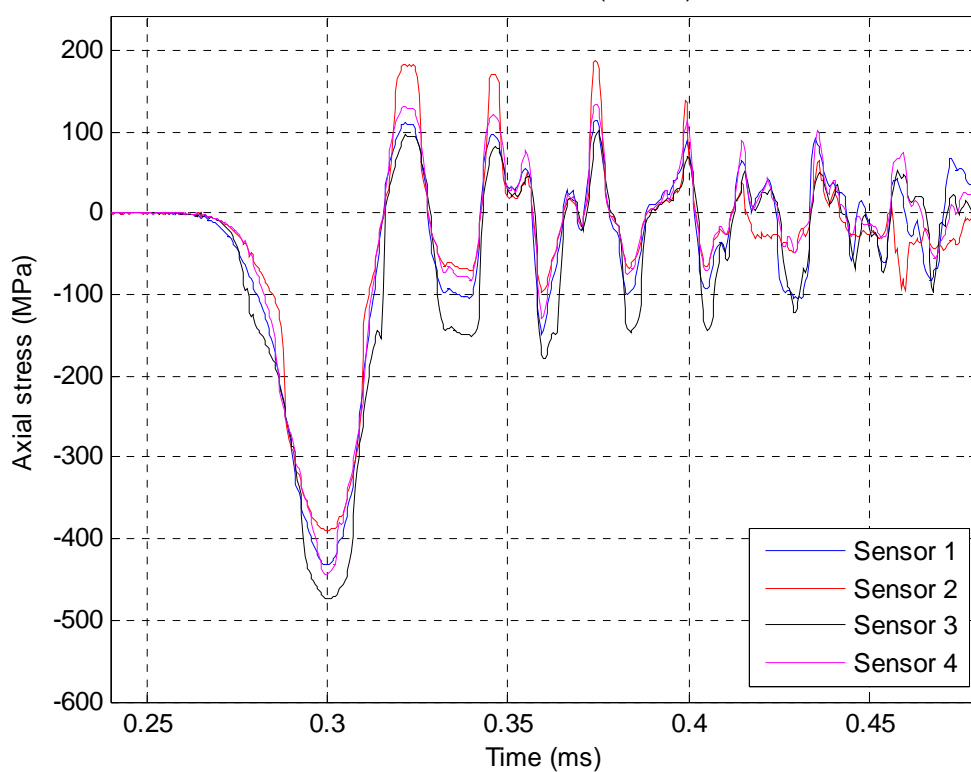
Shot #35 - Wood (100 mm)



Shot #36 - Wood (80 mm)

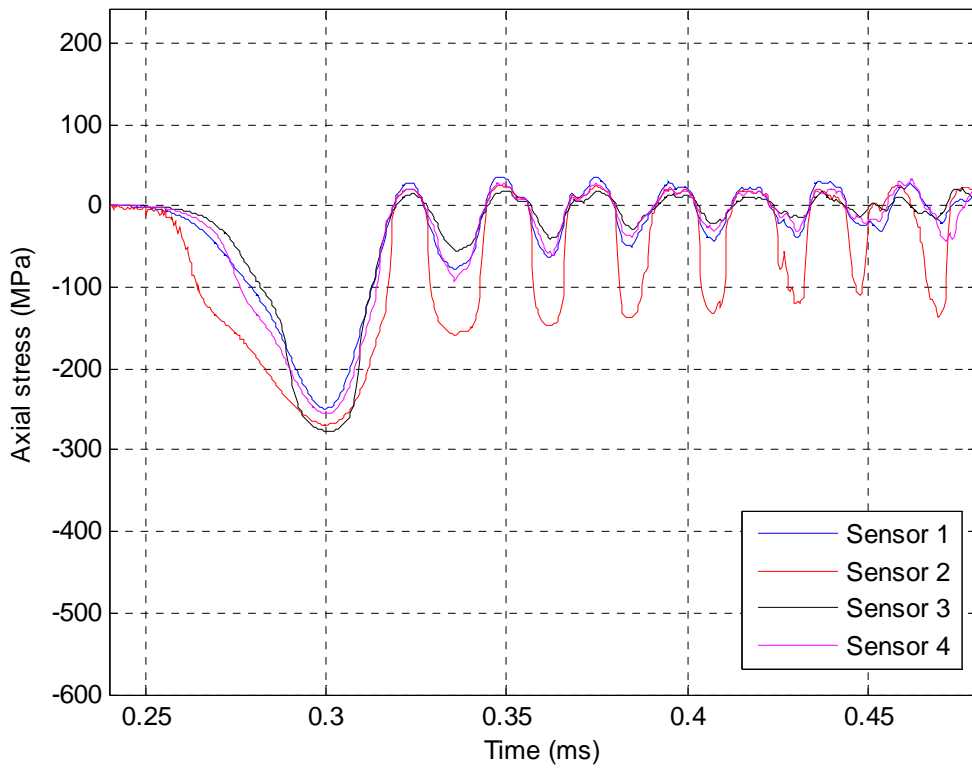


Shot #37 - Wood (80 mm)

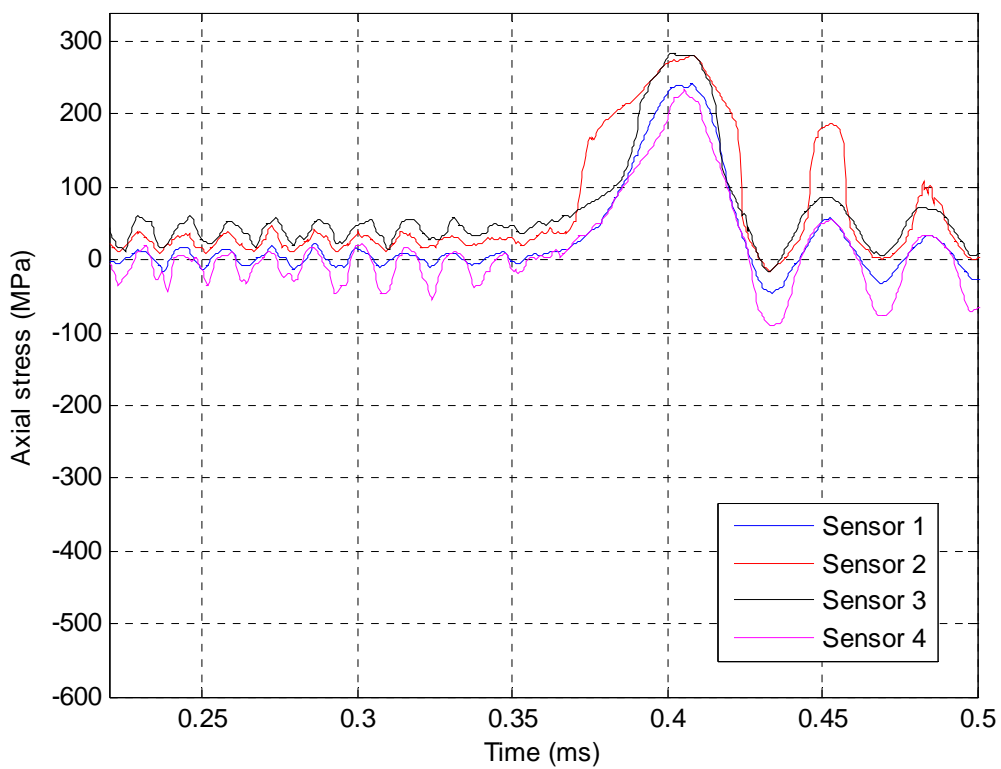




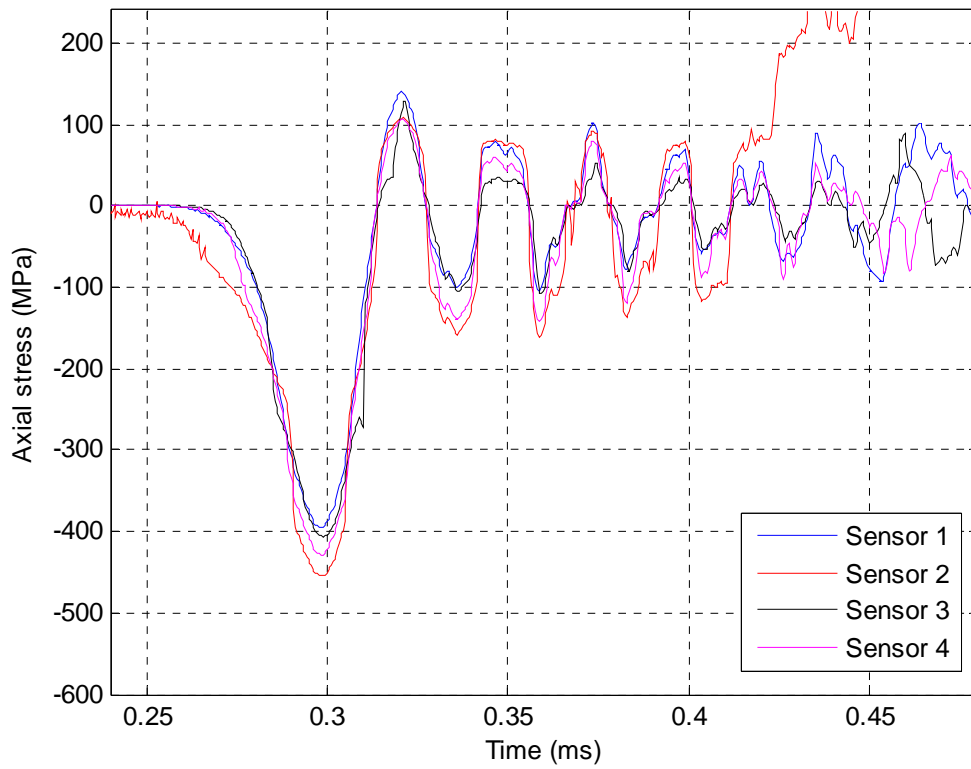
Shot #38 - Aluminium foam (100 mm)



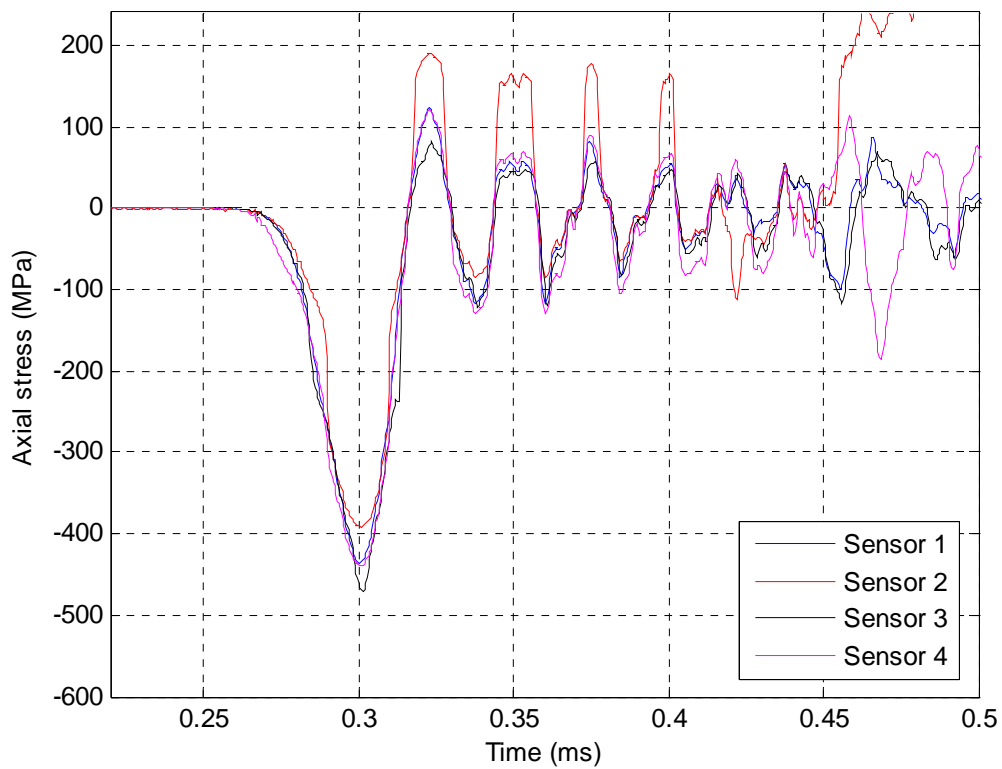
Shot #39 - Aluminium foam (100 mm)



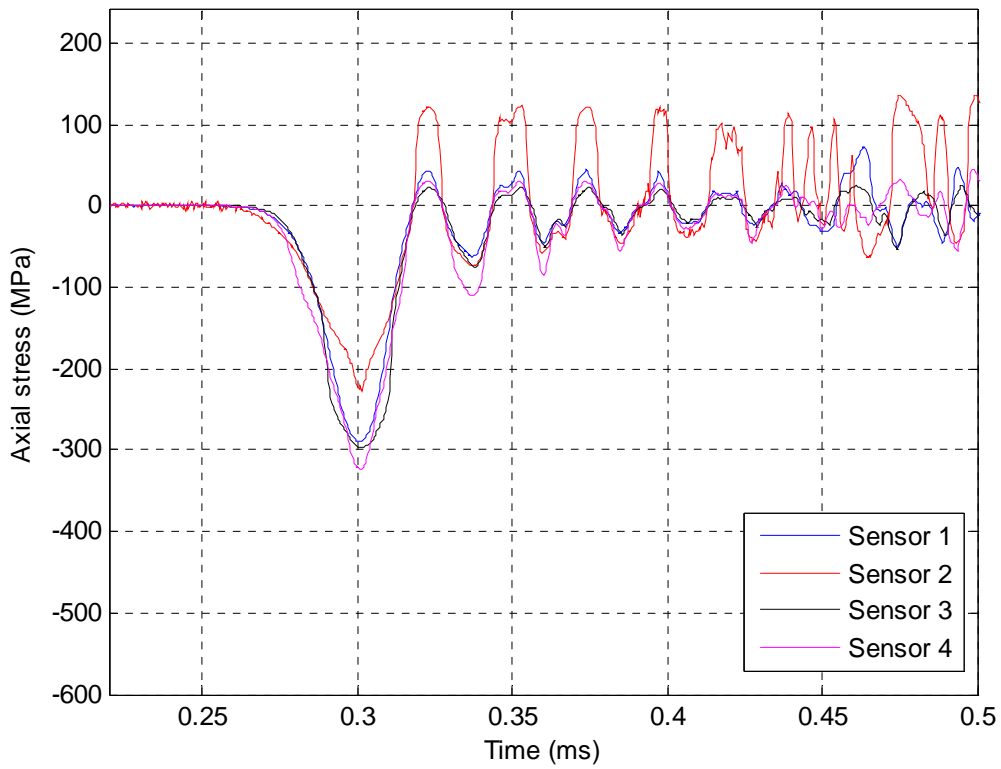
Shot #40 - Glasopor (0-4 mm) (100 mm)



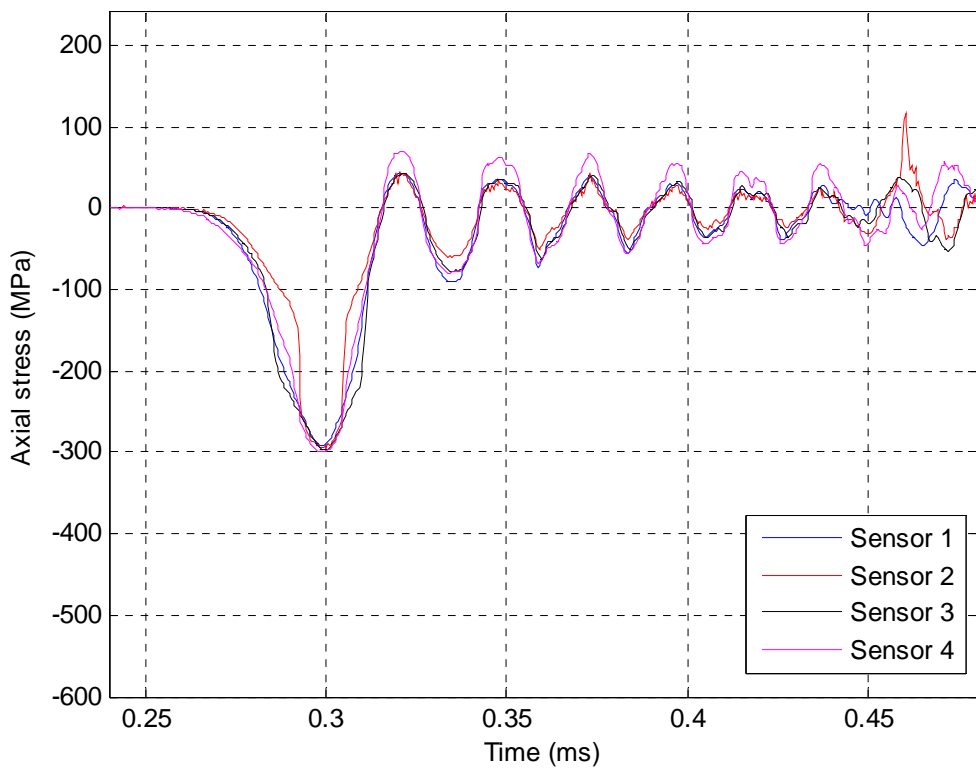
Shot #41 - Glasopor (0-4 mm) (100 mm)



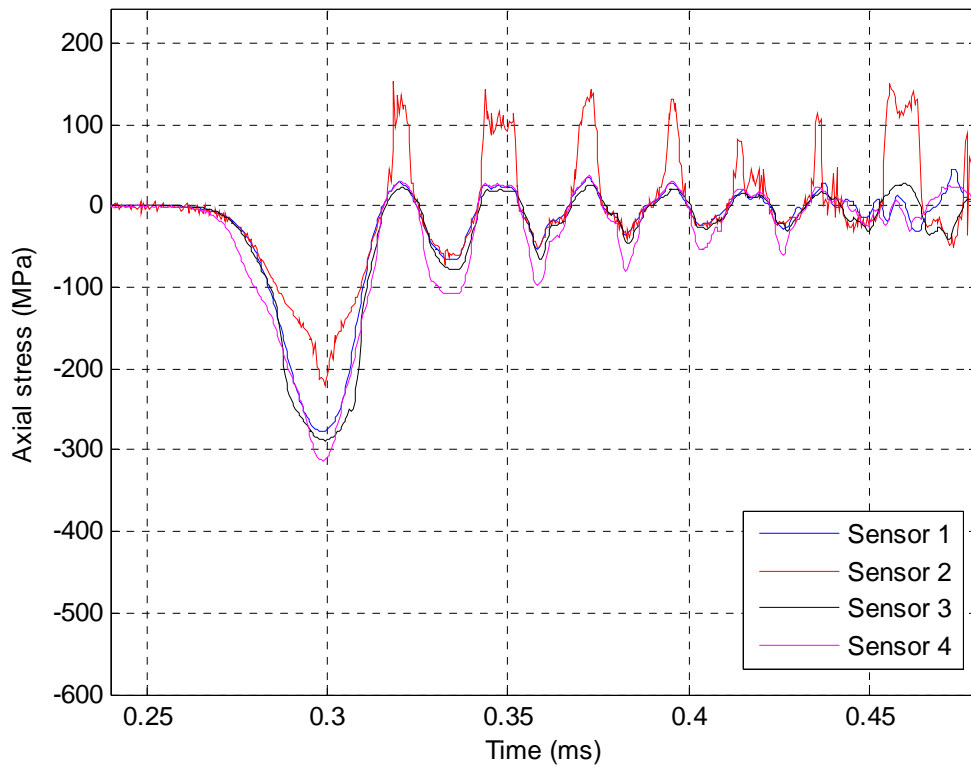
Shot #42 - Glaspor (4-14 mm) (100 mm)



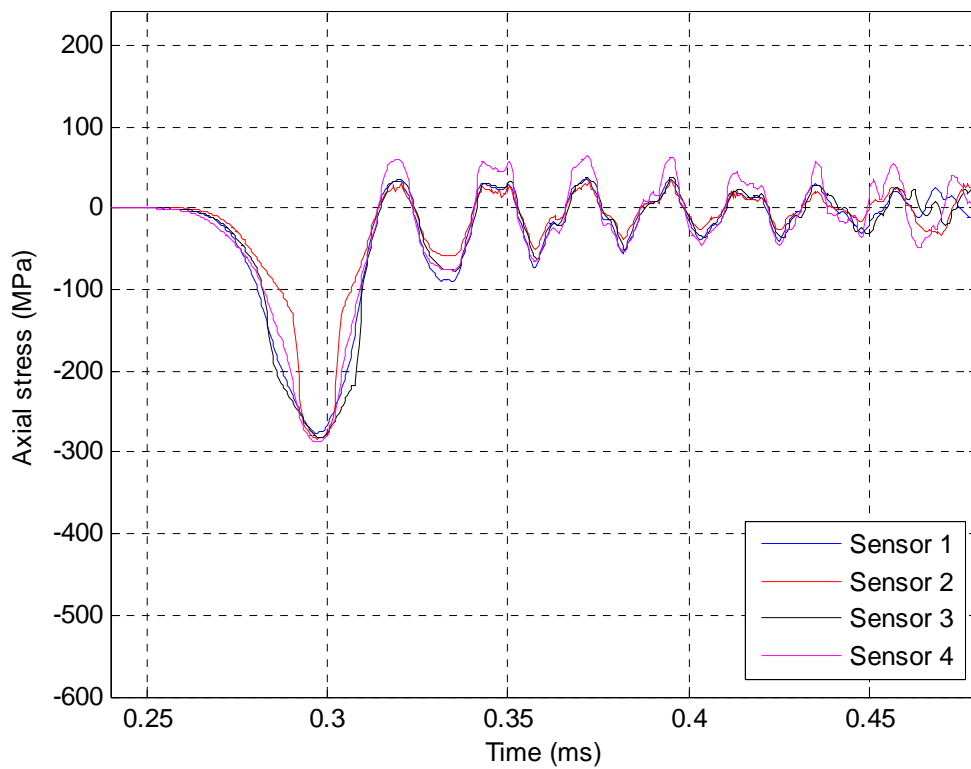
Shot #43 - Glaspor (4-14 mm) (100 mm)



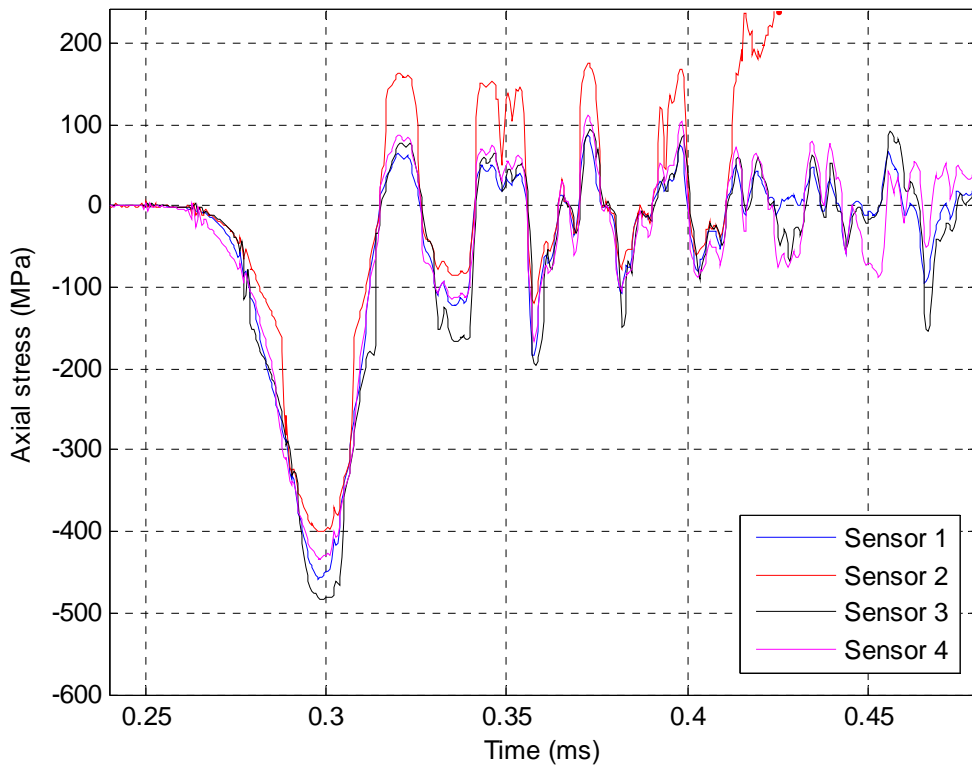
Shot #44 - Glaspor (14-22 mm) (100 mm)



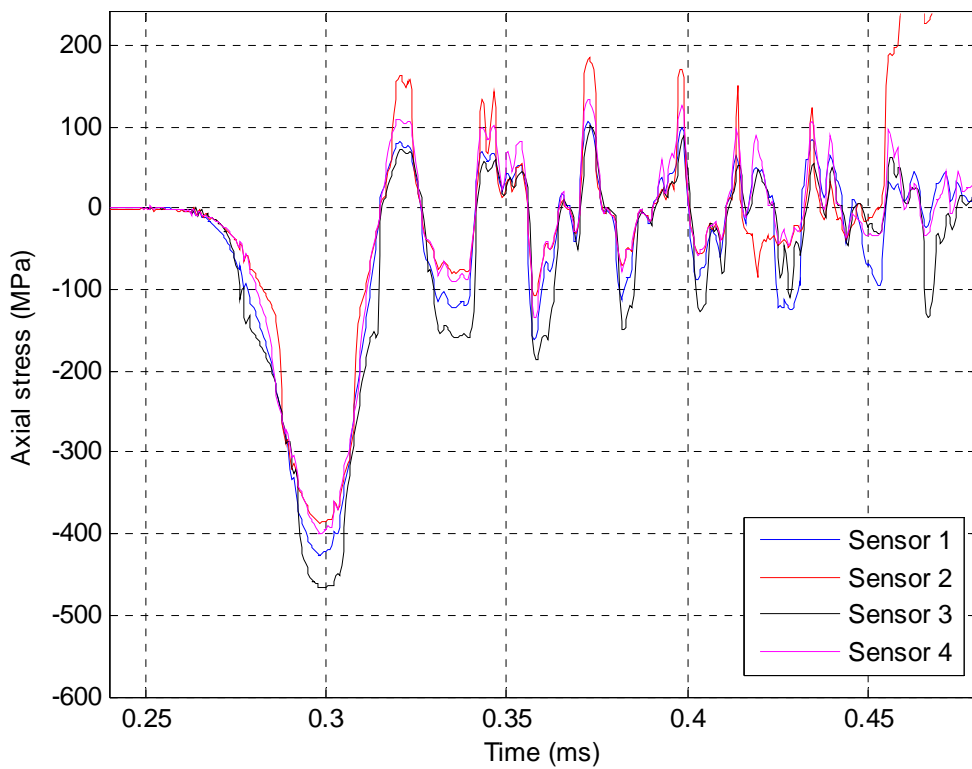
Shot #45 - Glaspor (14-22 mm) (100 mm)



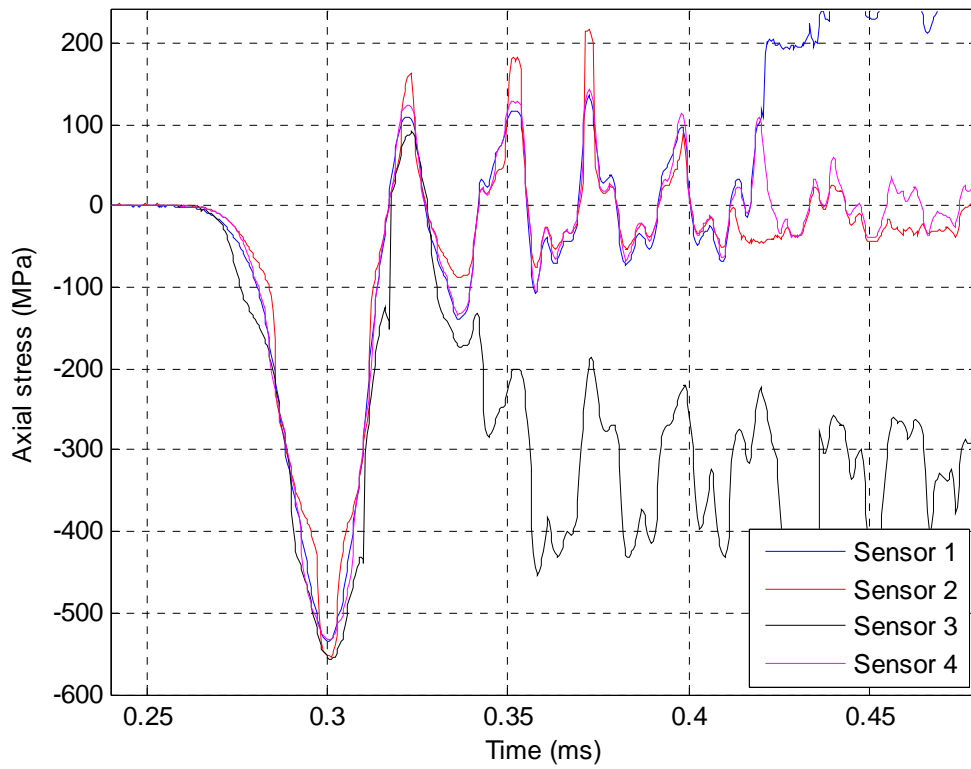
Shot #46 - Siporex (80 mm)



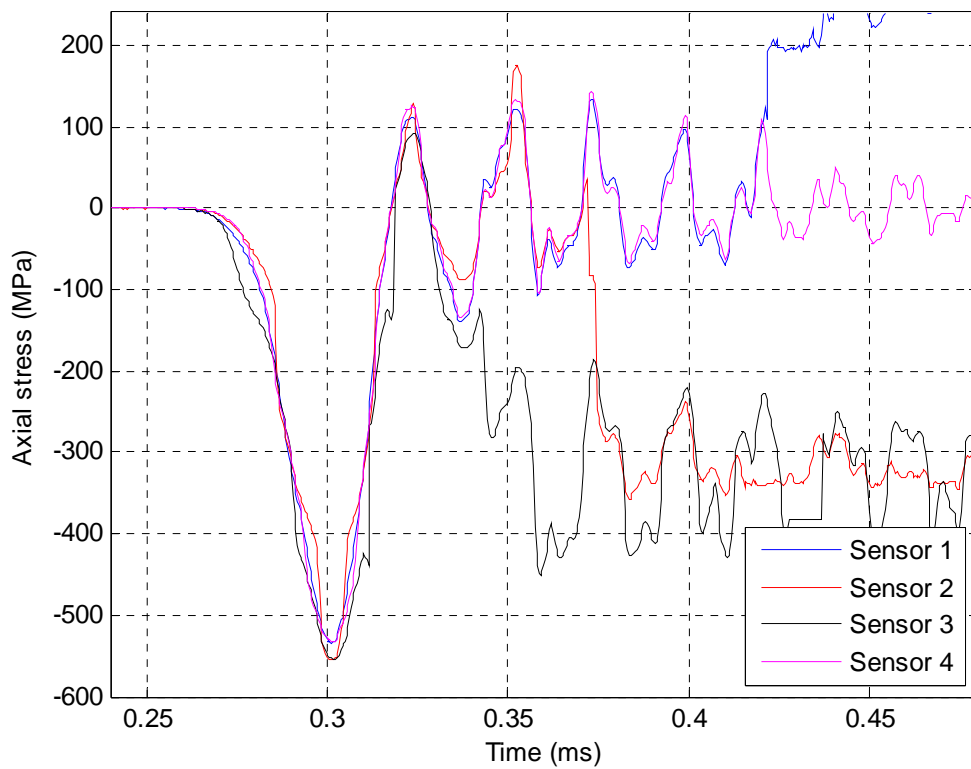
Shot #47 - Siporex (80 mm)



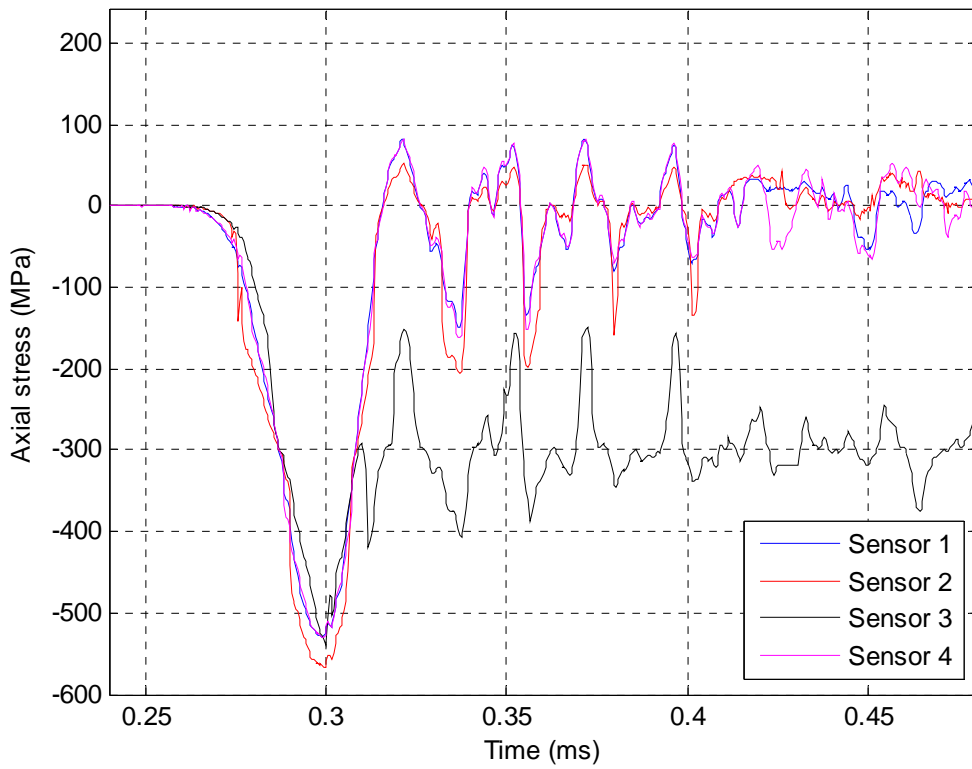
Shot #48 - Brick (80 mm)



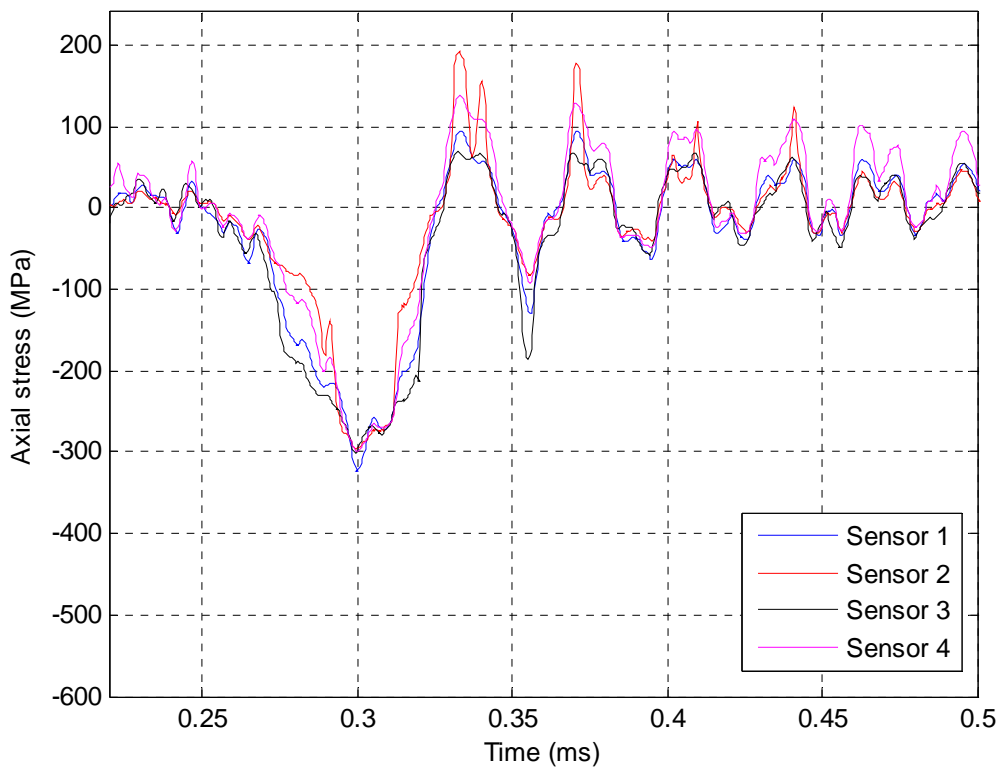
Shot #49 - Brick (80 mm)



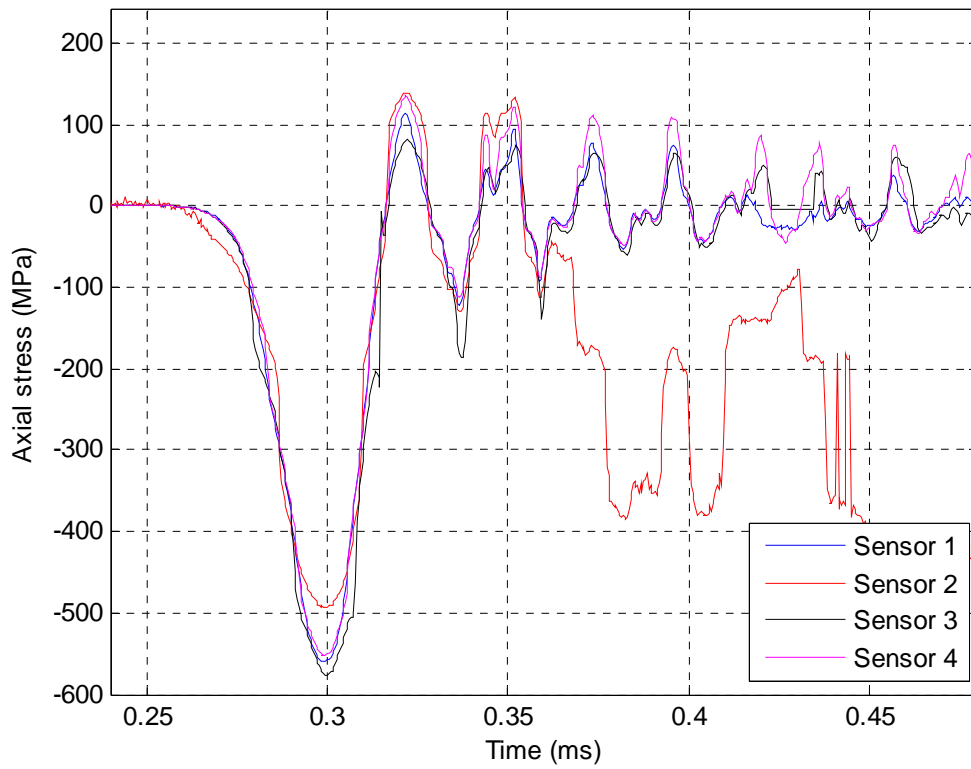
Shot #50 - No material (100 mm)



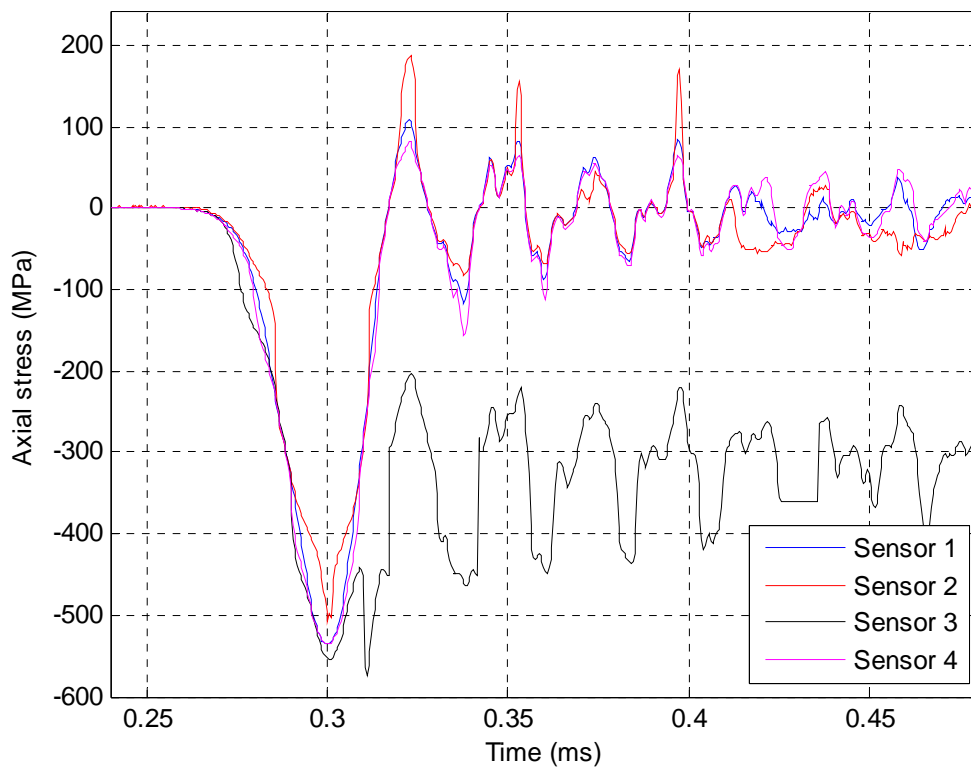
Shot #51 - No material (100 mm)



Shot #52 - No material (100 mm)

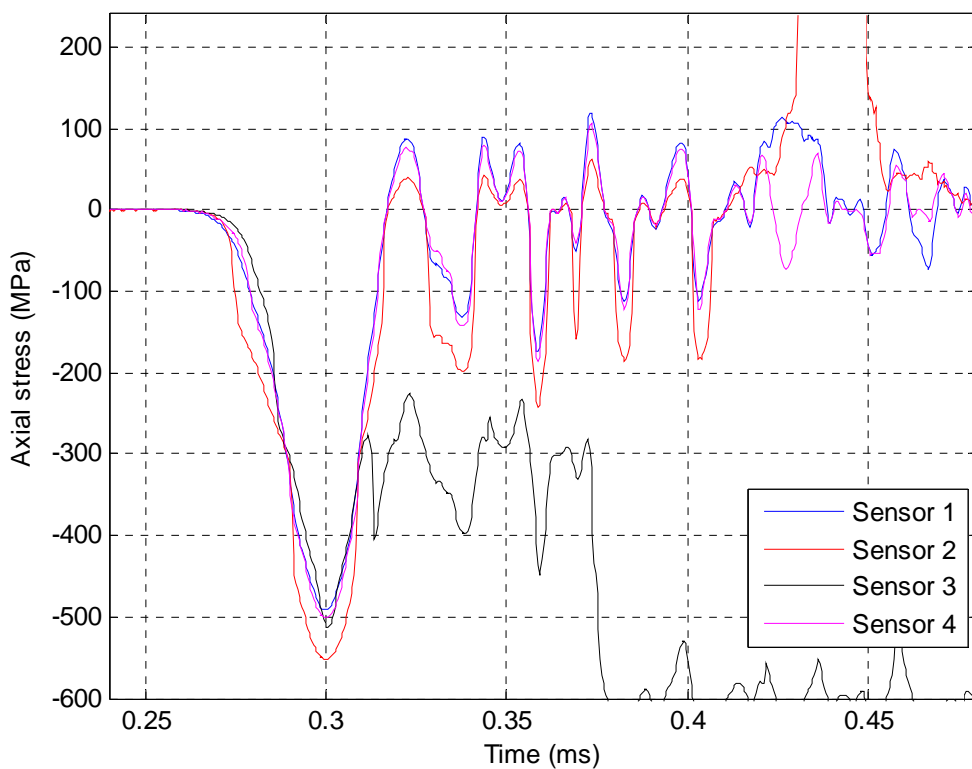


Shot #53 - No material (100 mm)

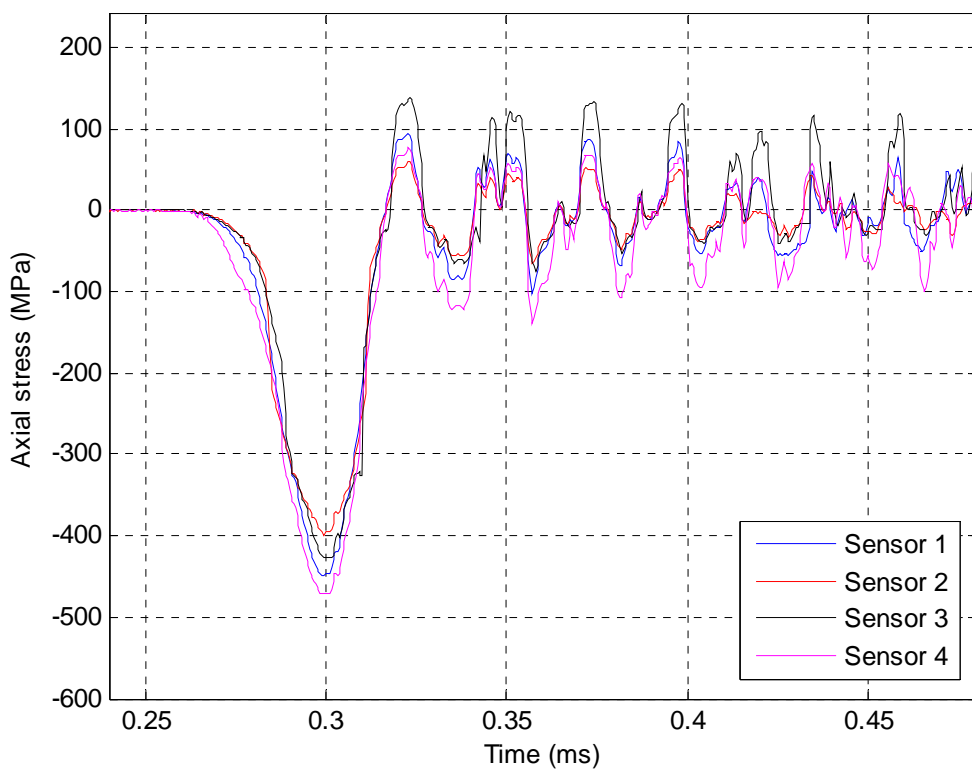




Shot #54 - No material (140 mm) (no cardboard)



Shot #55 - No material (140 mm)



## Appendix C Data analysis software

In this chapter we briefly describe the software used for analysis of the data from the strain sensors.

### C.1 Introduction

As mentioned, the measurements are done using fibre Bragg gratings. Each Bragg grating reflects a certain known wavelength. The grating constant is changed due to strain; hence the reflected wavelength is shifted. By measuring the change in wavelength, the strain can be calculated. A schematic view of the “measurement chain” is shown in Figure C.1.

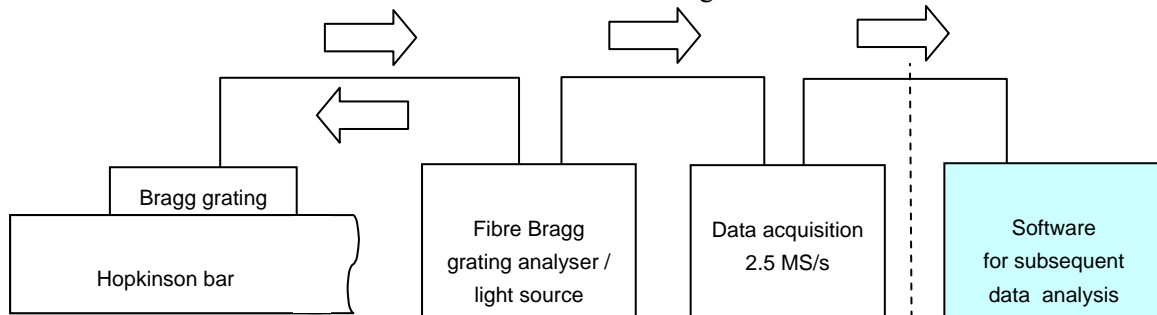


Figure C.1 Schematic outline of the signal flow.

To increase the accuracy of the measurement, the reflected wavelength is converted into a phase dependent function of time. The phase variation is caused by an interferometer, found within the grating analyser. After passing the interferometer, the signal is split into three separate but dependent signals, all  $120^\circ$  ( $2\pi/3$  radians) out of phase using different path lengths. This method is often referred to as a wavelength to phase conversion.

The files generated contain information of the measured intensities (interpreted as voltage), and therefore information of the phase dependency. The phase change will be proportional to the strain within the Bragg grating, and hence the steel bar. The proportionality constant between the phase change and the strain is found by calibration.

The software used to calculate the phase change is proprietary to Lightstructures AS, and beyond the scope of this report. However, in order to do the full analysis, a few technical (and practical) issues are described.

### C.2 Data analysis

The data is evaluated in four steps. First, the data is converted by Matlab into an appropriate format. Next, the data is evaluated using software made by Lightstructures AS. This software evaluates the phase change based on the measured intensity. In the third step, the phase data is translated into strain using the calibration data. Finally, the strain is represented in suitable plots.

In order to utilize the equipment (having in mind that other users than the authors should be able to perform measurements), the file formats and procedures are described shortly in the next subsections.

### C.2.1 Data conversion

The raw data contains a heading, and a matrix (n x 12) numbers. There are three columns for each Bragg grating and 4 gratings; in total twelve columns. Example is shown below. (Don't be fooled by the apparently eight columns resulting from the limited paper size.)

```

Example; raw data

LabVIEW Measurement
Writer_Version 0.92
Reader_Version 1
Separator Tab
Multi_Headings No
X_Columns No
Time_Pref Absolute
Operator Administrator
Date 2008/09/17
Time 13:21:46,161875
***End_of_Header***

Channels 12

Samples 25000 25000 25000 25000 25000 25000 25000 25000
Date 2008/09/17 2008/09/17 2008/09/17 2008/09/17 2008/09/17 2008/09/17 2008/09/17 2008/09/17
Time 14:11:08,03125 14:11:08,03125 14:11:08,03125 14:11:08,03125 14:11:08,03125 14:11:08,03125 14:11:08,03125 14:11:08,03125
Y_Unit_Label Volts Volts Volts Volts Volts Volts Volts Volts
X_Dimension Time Time Time Time Time Time Time Time
X0 0.0000000000000000E+0 0.0000000000000000E+0 0.0000000000000000E+0 0.0000000000000000E+0 0.0000000000000000E+0 0.0000000000000000E+0 0.0000000000000000E+0 0.0000000000000000E+0
Delta_X 4.000000E-7 4.000000E-7 4.000000E-7 4.000000E-7 4.000000E-7 4.000000E-7 4.000000E-7 4.000000E-7
***End_of_Header***

X_Value CH_1A CH_1B CH_1C CH_2A CH_2B CH_2C CH_3A
CH_3B CH_3C CH_4A CH_4B CH_4C Comment
0.344238 0.742187 0.836182 0.236206 0.220337 0.165405 3.735962
0.463867 0.819092 2.154541 0.499268 0.692749 0.217285 0.164185
0.344238 0.737305 0.829468 0.235596 0.217285 0.164185 3.746338
0.462646 0.827026 2.135620 0.490723 0.687256

```

In order to analyse these data, the heading has to be removed, and the voltages ( $V$ ) has to be converted according to the following formula:

$$\left(\frac{V}{5} + 1\right) * 32768, \tag{C.1}$$

and written to a text file (\*.lvm). The data must be comma separated as shown below:

```

Example; Input file

35024,37632,38248,34316,34212,33852,57252,35808,38136,46888,36040,37308
35024,37600,38204,34312,34192,33844,57320,35800,38188,46764,35984,37272
35032,37644,38228,34324,34212,33848,57488,35840,38200,46964,36000,37412
35016,37656,38244,34312,34200,33844,57572,35844,38228,47000,36024,37356
35032,37648,38256,34320,34188,33860,57720,35864,38236,46640,35960,37252

```

```
35032,37616,38244,34332,34200,33844,57244,35792,38152,46792,35980,37364
35040,37624,38240,34312,34212,33868,57528,35852,38192,46860,36012,37312
```

```
35024,37652,38252,34312,34196,33844,57396,35792,38156,46856,35992,37288
35048,37652,38280,34308,34200,33848,57424,35844,38200,47020,36040,37364
35024,37620,38204,34312,34188,33844,57424,35840,38164,46852,36004,37296
35040,37592,38224,34316,34188,33860,57356,35816,38172,46652,35936,37284
```

...

## C.2.2 Analysing software; "FFIFRIMP"

To analyse the phase change, software proprietary to Lightstructures AS is used. The software is installed on the "mf048" FFI-PC. Detailed description of the procedure is found (on that computer) in the file "/usr/local/EO/config/readme.txt".

The output file contains a heading and five columns. The first (dummy) column contains information of the time, while the remaining columns contain phase information from the four Bragg gratings, see example below.

### Example; Output file containing phase information

```
# ASCII dump of data stream from localhost:5003
# Data saved on man des 1 18:21:54 2008
# SourceID = 0
# Timeline = 1
# Data dimensions = 1
# Dimension0 (NoSensors) = 4
# Dimension1 = 0
# Dimension2 = 0
# Dimension3 = 0
# Data is Homogeneous type
# Datatype = 8
# Sensor 0 = FBG1
# Sensor 1 = FBG2
# Sensor 2 = FBG3
# Sensor 3 = FBG4
# File format = 1D (time D0 D1 D2 ...)
1228152114.632704 -3.369005e-01 -5.102404e+00 2.364631e+00 4.225158e+00
1228152114.639895 -3.796604e-01 -5.101829e+00 2.338170e+00 4.260056e+00
1228152114.649678 -3.988350e-01 -5.112758e+00 2.324364e+00 4.276546e+00
1228152114.659651 -4.055460e-01 -5.091474e+00 2.324364e+00 4.266384e+00
1228152114.691023 -4.061216e-01 -5.065205e+00 2.331076e+00 4.269069e+00
```

As the software is written for a continuously data stream application, the data input file is looped until the software is manually terminated. This means that the output file will contain more than one sequence of the measured data (the number is dependent on the time the software is terminated). Therefore, a Matlab code has been written in order to post process the data.

## C.2.3 Post processing

Post processing is done using Matlab codes. First the output from the analysing software is reduced in size, having only one sequence corresponding to the original measurements. This is done more or less manually. The next operation is converting the phase ( $\varphi$ ) into strain ( $\varepsilon$ ). If the subscripts  $i$  refer to a certain vector element and the subscripts  $j$  refer to the Bragg gratings, the equation is

$$\varepsilon_j(i) = \frac{\varphi_j(i) - \varphi_j(1)}{K_j}. \quad (\text{C.1})$$

The coefficients  $K_j$  are found by calibration. By manually inspecting the results from each Bragg grating, the obviously erroneous measurements are omitted. The remaining measurements are used to find the mean strain, calculated by the following relation:

$$\bar{\varepsilon} = \frac{1}{J_{\max}} \sum_{j=1}^{J_{\max}} \varepsilon_j. \quad (\text{C.2})$$